8-2013

Modeling, Control, and Motion Analysis of a Class of Extensible Continuum Manipulators

Apoorva Kapadia
Clemson University, apoorvak@gmail.com

Modeling, Control, and Motion Analysis of a Class of Extensible Continuum Manipulators

---

A Dissertation
Presented to
the Graduate School of
Clemson University

In Partial Fulfillment
of the Requirements for the Degree
Doctor of Philosophy
Electrical Engineering

---

by
Apoorva Kapadia
August 2013

Accepted by:
Dr. Ian Walker, Committee Chair
Dr. Darren Dawson
Dr. Timothy Burg
Dr. John Wagner
Dr. Enver Tatlicioglu

Abstract

In this dissertation, the development of a kinematic model, a configuration-space controller, a master-slave teleoperation controller, along with the analysis of the self-motion properties for redundant, extensible, continuous backbone (continuum) "trunk and tentacle" manipulators are detailed. Unlike conventional rigid-link robots, continuum manipulators are robots that can bend at any point along their backbone, resulting in new and unique modeling and control issues. Taken together, these chapters represent one of the first efforts towards devising model-based controllers of such robots, as well as characterizing their self-motion in its simplest form.

Chapter 2 describes the development of a convenient set of generalized, spatial forward kinematics for extensible continuum manipulators based on the robot's measurable variables. This development, takes advantage of the standard constant curvature assumption made for such manipulators and is simpler and more intuitive than the existing kinematic derivations which utilize a pseudo-rigid link manipulator.

In Chapter 3, a new control strategy for continuum robots is presented. Control of this emerging new class of robots has proved difficult due to the inherent complexity of their dynamics. Using a recently established full Lagrangian dynamic model, a new nonlinear model-based control strategy (sliding-mode control) for continuum robots is introduced. Simulation results are illustrated using the dynamic model of a three-section, six Degree-of-Freedom, planar continuum robot and an ex-

periment was conducted on the OctArm 9 Degree-of-Freedom continuum manipulator. In both the simulation and experiment, the results of the sliding-mode controller were found to be significantly better than a standard inverse-dynamics PD controller.

In Chapter 4, the nature of continuum manipulator self-motion is studied. While use of the redundant continuum manipulator self-motion property (configuration changes which leave the end-effector location fixed) has been proposed, the nature of their null-spaces has not previously been explored. The manipulator related resolved-motion rate inverse kinematics which are based on the forward kinematics described in Chapter 2, are used. Based on these derivations, the self-motion of a 2-section, extensible redundant continuum manipulator in planar and spatial situations (generalizable to n-sections) is analyzed. The existence of a single self-motion manifold underlying the structures is proven, and simple self-motion cases spanning the null-space are introduced. The results of this analysis allow for a better understanding of general continuum robot self-motions and relate their underlying structure to real world examples and applications. The results are supported by experimental validation of the self-motion properties on the 9 Degree-of-Freedom OctArm continuum manipulator.

In Chapter 5, teleoperation control of a kinematically redundant, continuum slave robot by a non-redundant, rigid-link master system is described. This problem is novel because the self-motion of the redundant robot can be utilized to achieve secondary control objectives while allowing the user to only control the tip of the slave system. To that end, feedback linearizing controllers are proposed for both the master and slave systems, whose effectiveness is demonstrated using numerical simulations and experimental results (using the 9 Degree-of-Freedom OctArm continuum manipulator as the slave system) for trajectory tracking as well as singularity avoidance subtask.

Acknowledgments

I would like to express gratitude to Dr. Ian Walker for allowing me to work with the OctArm, which quickly became the focal point of this dissertation. I am also indebted to him for his patience. I have always looked forward to our conversations because of his ability to explain complicated concepts in unique and straightforward ways.

I would like to thank Dr. Darren Dawson for his constant guidance and encouragement, for the opportunity to work on so many different research projects, and supporting my teaching inclinations. I appreciate him including me in various teaching-related projects in Clemson University's Electrical & Computer Engineering Department, for classes as well as laboratories. His drive, leadership skills and teaching ability has been an inspiration and template for my approach to work.

I would like to thank Dr. John Wagner for letting me to work on the thermal projects. His insight and guidance were very useful towards understanding how to approach tackling problems with patience.

Thanks also goes to Dr. Enver Tatlicioglu, who despite being in Turkey, helped immeasurably with a lot of the research problems and math that went into this dissertation.

I would also like to thank my labmates and colleagues, David Braganza, Nitendra Nath, Erhun Iyasere, Jessica Merino, Ninad Pradhan, Bryan Willimon, Alan

Bartow, and Paul Yanik, all of whom provided much needed help, encouragement and advice. A big thank you to Katelyn Fry, whose hard work, assistance with the experimental validation and *joie de vivre* and was invaluable. Thanks to Tony Threatt who competitiveness and drive ensured I did not stray too far from the straight and narrow myself.

Last but not least, a big thank you to my mother for always projecting her composure, perseverance, and tenacity my way. This would not have been possible without your support.

Table of Contents

List of Tables

List of Figures

Chapter 1

Introduction

1.1 Literature Review

Robots with continuous backbones, more formally known as continuum robots, are receiving greater consideration for use by the robotics community. These robots are able to bend at any point along their structure. This distinguishes them from their rigid-link counterparts by their ability to execute tasks and achieve objectives that conventional robots find too complicated or are unable to perform. Continuum manipulators draw their design inspirations from members of the animal kingdom such as octopus arms, squid tentacles, and elephant trunks, as detailed in [1], [2], and [3]. An example of an extensible continuum manipulator, the OctArm (Octopus Arm) [4] is shown in Figure 1.1. The OctArm is a 3-section manipulator which has 9 Degrees-of-Freedom (DOFs); each section can bend with constant curvature about two axes as well as extend its backbone. The desire to design and use biomimetic continuum robots is due to the inherent structural compliance and ability to bend at any point along their length, affording them the potential to perform operations not feasible with conventional robots, such as:

- Manipulation of objects having arbitrary and *a priori* unknown shapes;
- Navigation through complex, cluttered, or unstructured environments (especially in search and rescue operations);
- On-sea refueling; and
- whole-arm grasping[1] shown in Figure 1.2.

Because of their novel capabilities, continuum robots can interact with an assortment of objects of highly variable shapes, sizes, and physical properties.

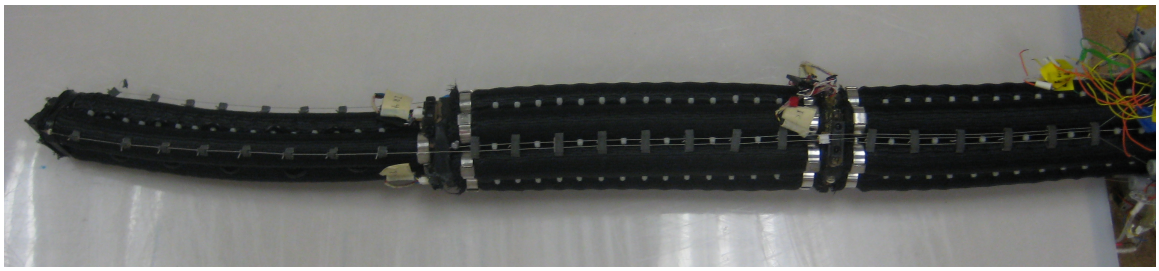

Figure 1.1: The 9-Degree-of-Freedom OctArm Continuum Manipulator.

While the general idea and basic set of desired properties remain the same, numerous continuum manipulator designs have been proposed. Several pneumatically-actuated designs are described in [2], [5], [6], [7], and [8]. Continuum robots based on a vertebrate design have been proposed by [9], while [10] demonstrated a continuum manipulator with tuneable stiffeness. Tendon-driven models were described in [11], [12] and [13] while manipulator mechanics where described in [14]. Continuum robots based on the concentric-tube paradigm and that had the ability to be used in a medical environment were proposed in [15], [16], and [17]. Other continuum manipulators proposed as medical devices were presented in [18], [19], [20], and [21]. Combinations

[1] As the name suggests, whole-arm grasping is where the arm curls around an object and uses its body to leverage and manipulate it, as opposed to the use of a set of parallel-jaw grippers by conventional robots

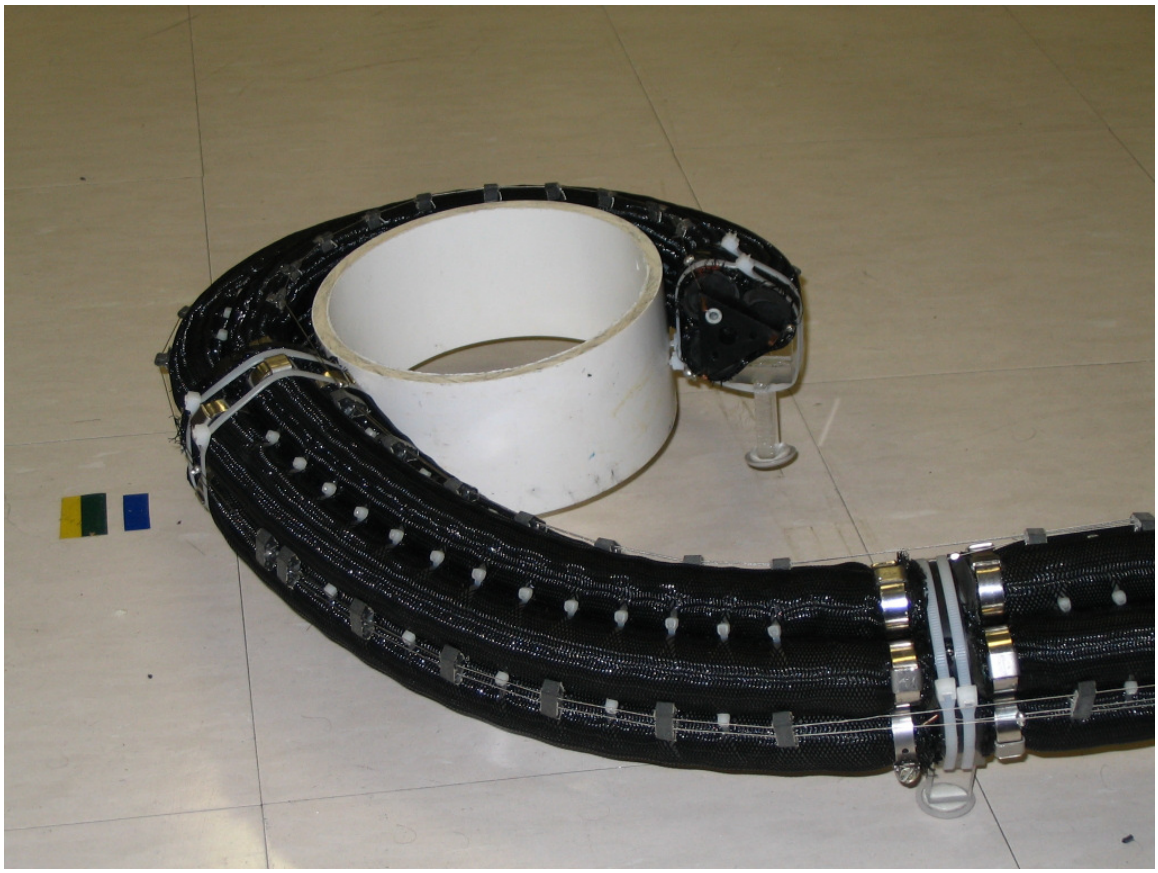

Figure 1.2: An Example of Whole-Arm Grasping

of continuum manipulators which could be used as fingers were proposed in [22], [23] and [24]. Applications have also been discussed: [25] proposed continuum manipulators be used as force sensors, [26] suggested their use for environmental interaction, while [15], [16], and [27] discussed motion planners for continuum manipulators.

To better understand and utilize such manipulators, the development of sophisticated mathematical models is essential. Kinematic models for various types of continuum robots have been developed and proposed. Chirikjian and Burdick [28] developed kinematics for a general hyper-redundant manipulator which restricted the manipulator curve-shaping functions to a 'modal' form, allowing for quick computation of the inverse kinematic solution. This method is hindered in practice by the ability of manipulators to shape themselves as the curve- functions require. Chen *et al.* [29] developed manipulator kinematics based on similar previously-designed models for a pneumatic kinematically-redundant manipulator with a silicone rubber tip which could be used for colonoscopy. Jones and Walker [30] extended the early kinematic developments by Hannan and Walker [31], to arrive at a general closed-form solution based on standard Denavit-Hartenberg techniques. The same authors added actuator length limits into the kinematic solutions derived previously [32], resulting in more practical but more complex shapes and solutions for continuum robot applications. Additionally, Gravagne and Walker developed kinematics using wavelet decomposition to derive novel kinematics for continuum robots in [33] and [34]. At this stage, the kinematics for continuum robots is considered to be well understood. However, the performance of continuum manipulators based on kinematic controllers have been shown to be poor.

Unlike the kinematic model development, the dynamic modeling of continuum robots is still an open and active area of research. Chirikjian, who was one of the first to develop dynamics for a continuum robot proposed an infinite degree of freedom

dynamic model [35]. Khalil *et al.* [36] and [37], developed dynamics for an eel-like robot using a recursive version of the Newton-Euler equation and the Cosserat beam model, along with Navier-Stokes equations for fluid interaction in underwater environments. However, this model required zero initial accelerations regardless of the initial joint positions. In [38], Matsuno and Sato developed a dynamic model for a snake-like robot having n-links. However while the model could be considered applicable to a hyper-redundant manipulator, the links were assumed to be rigid and thus the model was not appropriate for true continuous backbone continuum robots. In [39], Li *et al.* proposed another dynamic model for a snake-like robot with rigid links. Closed form dynamics were developed in [40], whose work was extended to include extensibility by Tatlicioglu *et al.* in [41] and [42]. These dynamics are based on the kinematic models developed in [30].

Having developed kinematic and dynamic models, the next logical step is to apply them towards the development of model-based controllers to improve the performance of the hardware. Some of the first known configuration-space controllers for continuum robots were proposed by Ivanescu et al. [43], [44], and [45]. A highly specific set-point tracking variable-structure controller was developed in [44] for a tentacle arm whose physical model was based on composite materials consisting of electrorheostatic fluids. An obstacle-avoidance controller based on the artificial potential field method with the goal of a desired final end-effector position was proposed in [43], using the dynamic model developed in [44]. In [45], a sliding-mode controller was developed along with a fuzzy controller for two cooperating hyper-redundant robots. In [46], Braganza *et al.* described a controller which included neural-network feedforward components to compensate for the robot's unknown dynamic model terms. In [47], Penning *et al.* described two task-space controllers to precisely control the tip of small-scale continuum manipulators prevalent in the medical field. All these works

except [46] have been restricted to simulations.

While the aforementioned controllers regulate the shape of the manipulators or the location of the tip (with or without any additional subtasks), they are not able to utilize, or do not exploit, the structure of the robot's self-motion. Self-motion of a robotic manipulator is defined as the ability of the tip (or end-effector) of the manipulator to maintain it's position in space while allowing the other parts of the robot to move (allowing the robot to change shape). Self-motion is a key property of redundant robots. Burdick [48] analyzed the underlying structure of the self-motion of rigid-link redundant manipulators and revealed it to be a set of distinct manifolds based on the sets of possible configurations reflecting the redundant robot's self-motion ability. However, this characterization does not apply to continuum manipulators due to the inherent structural differences between rigid-link manipulators and continuum ones.

Despite the numerous possible applications of continuum arms and the extensive work in teleoperation of robot manipulators, the teleoperation of continuum arms is still an active research problem. A teleoperation system enables a user to execute a task using an output system (*i.e.* a slave) while manipulating an input system (*i.e.* a master) in a remote environment. Teleoperation of robotic systems has been invaluable for numerous applications such as handling unstructured or hazardous materials, maneuvering underwater vehicles, search and rescue, and most recently in assisting medical procedures [49], [50].

Due to the relative rarity of continuum arms as compared to more conventional robots, teleoperation of such robots has the disadvantage of not always having a kinematically similar system to serve as a master, as shown in Figure 1.3. In such instances, and where only a non-redundant system might be available to serve as a master, a solution might be found in the task-space of both systems. Such solutions however would require that an additional control element be designed to achieve

secondary objectives such as obstacle or singularity avoidance with no user input necessary, relieving the master system of any duties beyond controlling the end-effector trajectory of the non-redundant master.

Related literature focuses on a similar problem of the master and slave systems having dissimilar kinematics. The literature primarily deals with rigid-link structures, and not continuum arms, as focused on in this dissertation. Kim *et al.* [51] classified the dissimilar kinematics teleoperation problem by comparing the DOFs of master and slave systems. Herndon *et al.* [52] were the first to use kinematically redundant robot manipulators in a dual-arm teleoperator system to avoid obstacles in space applications. Nguyen *et al.* [53] developed an adaptive joint-space controller for a dual arm system where both slave arms were kinematically redundant robot manipulators; however, kinematic redundancy was not considered in the control development. Jansen *et al.* [54] designed a stiffness controller for a teleoperator system with a 7 DOF slave and a 6 DOF master that utilized extended task-space techniques for redundancy resolution and Euler parameters to avoid artificial singularities. Those results were expanded in [55] by adding passivity to the overall system. Hwang *et al.* [56] outlined the performance of a teleoperator system with a kinematically redundant slave system, but did not provide robustness when the robot operated close to its kinematic singularities or for high joint velocities. Nanayakkara *et al.* [57] utilized neural networks to compensate for the uncertain master system and environmental dynamics. Goel *et al.* [58] demonstrated experimental results where a planar 3 DOF robot manipulator was considered as the slave system. Kinematic control was utilized and the kinematic redundancy was used to maintain control even with joint failures. Stanczyk *et al.* [59], [60], [61], [62] considered experimental verification of haptic teleoperation with a kinematically redundant slave system. In [63], Hayakawa *et al.* used a 7 DOF manipulator for the slave system while the master system had 6 DOF. The

redundancy in the slave system was utilized to move the robot away from its singular configurations but only with the help of the user. Gosselin *et al.* [64] demonstrated experimental results with a kinematically redundant haptic device: however the work in [64] did not make use of the redundancy resolution. Recently, Nath *et al.* [65] discussed teleoperation with kinematically redundant master and slave systems and utilized the redundancy in both systems to achieve secondary objectives where the master and slave systems were kinematically similar. Most of the aforementioned works focused on experimental verification [63] - [65] while others such as [53], [56], [64], and [66] did not take advantage of all the properties of kinematically redundant manipulators, especially for control design. Thus, a control framework is required for teleoperation with dissimilar kinematics, particularly for a kinematically redundant continuum arm as the slave system.

Thus, based on the existing literature it can be argued that there exists a need for a better mathematical understanding of the structure of continuum robots as well as their control. This dissertation aims to address these issues regarding continuum robots by devising a new set of kinematics along with a dynamic model-based nonlinear configuration space controller. Additionally, the self-motion of continuum robots is characterized in its most basic form, along with its occurrences in nature and potential uses. Finally, the task-space teleoperation of redundant continuum manipulator by a non-redundant, kinematically-dissimilar, rigid-link master, which exploits the self-motion property of the continuum manipulator, is discussed.

1.2 Dissertation Organization

This dissertation deals with research problems associated with the class of redundant, extensible continuum manipulators. The development is strongly motivated

by improving the accuracy and range of functionality of the OctArm. The Octarm was built by Pennsylvania State University and Clemson University, to closely resemble an octopus arm or an elephant trunk. The ability to extend as well as bend is significant and a key advantage of continuum robots over traditional rigid-link manipulators. This ability was highlighted by Walker *et al.* in [67] and detailed the increased workspace afforded by the OctArm due to its planar extension capabilities. A basic non model-based controller for the OctArm was developed and implemented in [46]. However, it was designed to compensate for the unknown dynamic model (subsequently, a kinematic model for the OctArm was proposed in [30], while the Lagrangian dynamics for the OctArm were developed later in [41] and [42]).

Most of the controllers previously proposed in the literature were found to not be suitable for practical application on the OctArm, due to either the design of the controller or specific assumptions regarding the manipulator design, and thus the dynamic model. Performance was found to be slow in response, subject to oscillatory motions, or both. In Chapter 3, the application of a standard sliding mode controller developed for manipulators whose models are based on the Lagrangian dynamics is proposed. However the controller was modified so as to fit the structure of the OctArm's continuum dynamics. A Lyapunov-type proof is utilized for the stability analysis of the proposed controller, with numerical simulations and experimental results shown to highlight the effectiveness of the proposed controller in comparison to a standard inverse-dynamics PD controller (which was the previously best performing controller on the OctArm hardware).

However, the development of a controller to regulate the shape of continuum manipulators does not exploit one of the main advantages of such devices, their self-motion. Before attempting to utilize this capability, an argument can be made for gaining a better understanding of the self-motion of continuum manipulators and

characterizing it. Thus in Chapter 4, the work in [68] is fully described and built upon by expanding and generalizing the self-motion analysis results of extensible continuum manipulators from the planar case to the spatial case. Building on the work in [48] for redundant rigid-link robots, the focus here is the analysis of the self-motion of continuum manipulators. This is done to better understand the structure of the redundant continuum manipulator self-motion and to exploit its capabilities by taking advantage of the Jacobian null-space with the tip position being arbitrarily fixed. In a fashion similar to [48], some initial studies of the null-space of continuum manipulators were conducted in [68]. These studies focus on the capabilities of 2-section, redundant, extensible continuum manipulators working in a plane. Based on the method first proposed in [69], the velocity kinematics are described and used to further describe and better understand the continuum manipulator null-space. The inherent structural differences between the self-motion manifolds for rigid-link redundant manipulators and their continuum manipulator counterparts are discussed. The importance of the analysis for numerous applications is discussed along with experimental demonstrations of self-motion on the OctArm continuum manipulator.

Knowledge of the self-motion capabilities of extensible continuum manipulators allows for its utilization towards achieving objectives and solving open research problems in the task-space. With that in mind, Chapter 5 focuses on the teleoperation control of a continuum manipulator slave system, specifically the OctArm [5], using a non-redundant, revolute, rigid-link robot as the master, and shown schematically in Figure 1.3. Due to the kinematic redundancy in the slave system, explicit control of the shape of the continuum manipulator by the user via the non-redundant master system is not possible. Thus, it is useful to develop a controller that makes use of the redundancy resolution by automatically satisfying secondary objectives while allowing the user to focus on control of the slave system's tip resulting in a

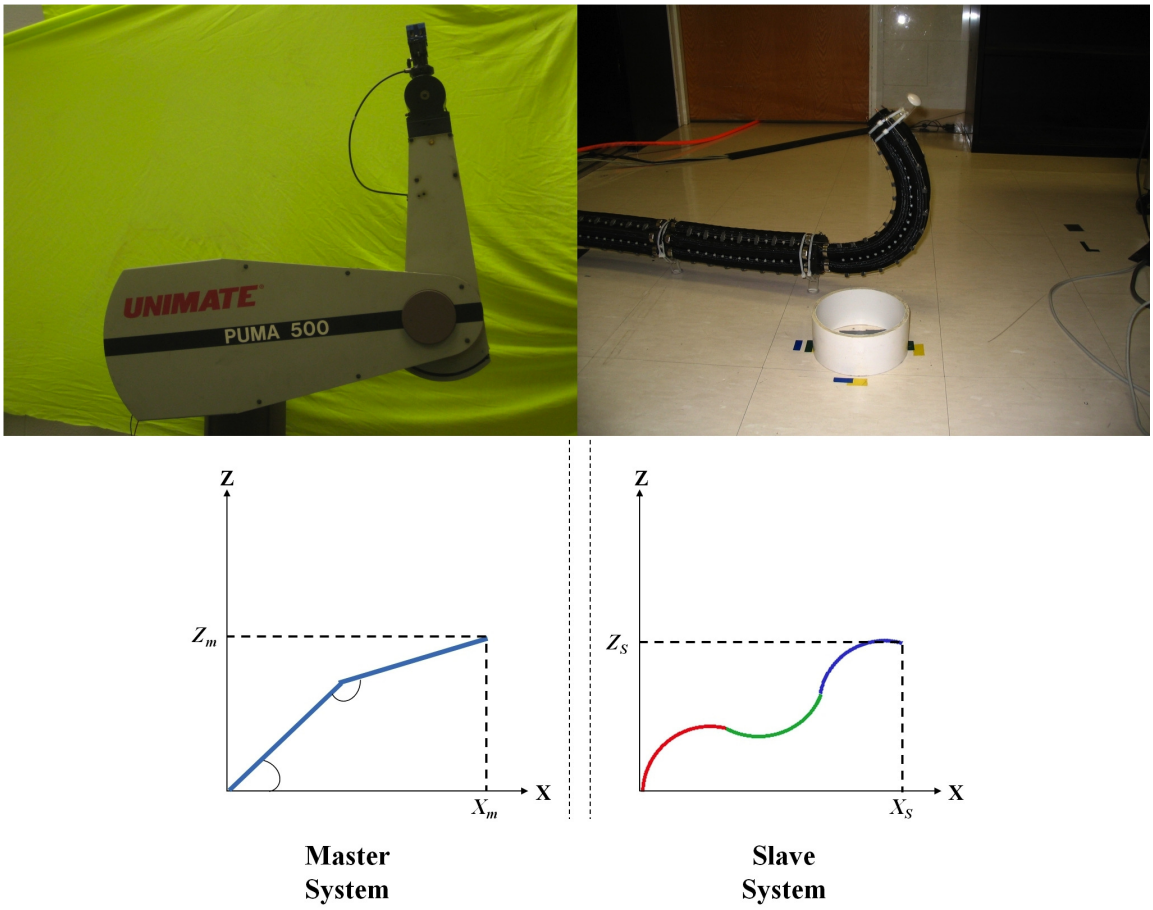

Figure 1.3: Example of a non-redundant, rigid-link master controlling a redundant, continuum slave system and a general representation of the proposed teleoperation system

reduced workload for the user. In the subsequent control development, dynamic and kinematic models and the interaction forces acting on both master and slave systems are assumed to be measurable. Based on the exact model knowledge, feedback linearizing controllers are designed for both master and slave systems. The designed controllers ensure that the desired trajectory tracking errors for both the master and slave systems are driven to zero exponentially fast. Additionally the slave system controller allows the integration of a null-space controller to make use of the redundancy resolution via the design of a null-space velocity tracking error [70]. The null-space velocity tracking error is shown to go to zero monotonically. To that end, the general sub-task controller developed in [71] is extended to integrate secondary control objectives. Numerical simulations are performed to highlight the proposed controller with experimental verification demonstrated on the OctArm.

The existing kinematic model for the OctArm in [30] is based on the standard Denavit-Hartenberg technique used for most rigid-link robots. As a result, Jones and Walker used a rigid-link equivalent of an OctArm section and related variables and parameters from the Denavit-Hartenberg table to the continuum manipulator shape variables. Thus, the kinematic equations do not intuitively reflect the shape of the manipulator, especially when multiple sections are involved. To solve this problem, Chapter 2 introduces a new and convenient kinematic model of extensible continuum manipulators based on the measurable variables of the OctArm and thus easier to correlate to the manipulator configuration. The full derivation for a 2-section manipulator, which is utilized in the developments of the subsequent chapters of this dissertation, is shown while an extension to $n-$sections is also provided.

1.3 The OctArm Manipulator

The OctArm is a 9-DOF pneumatically-actuated, extensible, continuum manipulator capable of motion in 3 dimensions. It is comprised of 3 serially-connected sections as seen in Figure 1.1 which are referred to (from right to left in Figure 1.1) as the base section ("the base"), the middle section ("the mid"), and the tip section ("the tip"). Each manipulator section is comprised of McKibben actuators in parallel. A McKibben actuator is a rubber tube within a mesh sleeve which determines if the tube will extend or contract upon actuation, a phenomenon detailed in [5]. Each section has a set of McKibben actuators connected together at the apexes of an imaginary equilateral triangle. The base- and mid- sections have 2 McKibben actuators at each apex to provide more lifting power, though at the expense of manipulability. The tip-section has only 1 such actuator at each apex resulting in greater manipulability as compared to the base- and mid- sections. Because of this type of construction, varying the pressures sent to each actuator or set of actuators in a section, will allow the section to bend in any cardinal direction. Providing the same pressure to all the actuators in a section will result in extension. Because there are 3 independent actuators for each of the 3 independent sections of the Octarm, it has 9 Degrees-of-Freedom. The length of each actuator is measured by a string encoder, a linear cable position transducer, which can measure the extension of a device as a function of encoder counts.

As discussed in sections 1.1 and 1.2, the controllers available for continuum manipulators either do not account for the OctArm's manipulability or are inaccurate because they deal with the manipulator at a kinematic level and do not incorporate the system nonlinearities and dynamics. Thus, experiments for the dynamic model-based approach discussed in this thesis are conducted on the OctArm to highlight

their effectiveness and accuracy as controllers, and to highlight the capabilities of the manipulator.

Chapter 2

Kinematics of a Two-Section Extensible Continuum Manipulator

In this chapter, a new, comparatively more intuitive method of kinematics development for serially-connected extensible, continuum manipulators is described. Jones and Walker [30], [32] used a rigid-link equivalent of an extensible continuum manipulator to develop a Denavit-Hartenberg based homogenous transformation matrix. However, this was not the most intuitive method to understand the shape of continuum manipulators, especially when multiple sections are serially connected as it required an understanding of how the rigid-link variables and parameters of the rigid-link equivalent related to the continuum shape variables. To provide a more intuitive solution, the kinematics developed in this chapter are based on the measurable variables of the 9-DOF OctArm manipulator. It should be noted that these kinematics only provide the position of any point along the manipulator backbone, unlike that of [30] and [32] which provided position and orientation information in a standard homogeneous transformation matrix. The lack of information regarding the orientation of the manipulator tip could be a hindrance if it needs to be controlled.

However, an application specifically regulating manipulator tip orientation, to the best of this author's knowledge, has not been found.

The general forward kinematics for a manipulator with $n-$degrees of freedom (DOF) are given by

$$x = f(\psi), \tag{2.1}$$

where $x(t) \in \mathbb{R}^m$ represents the task-space coordinates of the manipulator tip, $f(\cdot) : \mathbb{R}^m \rightarrow \mathbb{R}^n$ represents the manipulator forward kinematics, and $\psi(t) \in \mathbb{R}^n$ is the set of configuration-space variables (determining each internal degree of freedom) for the manipulator. When $n > m$, the manipulator is considered to be kinematically redundant.

Continuum manipulators are flexible and compliant robots that can theoretically bend in any direction at any point along their length. However, continuum backbones, which theoretically have infinite degrees of freedom, need to practically be realized robotically using a small (finite) number of actuators. The degrees of freedom not directly controlled must be constrained in the design in order to produce predictable behavior. In all continuum robots to date, this design constraint results in the robot being a series of serially connected "sections", which can bend (typically in 2 dimensions) and often extend/contract. Numerous physical instantiations of continuum robots have appeared [23], [72], [4], [36]. However, in all but one case [73], these designs result in sections which are constrained to approximately constant curvature (instantaneously, the curvatures vary with time, as the sections bend) [1], [2], [3]. Thus, constant curvature section continuum robots are analyzed in this dissertation.

Physical artifacts consist of serially-connected continuum sections allowing for bending in multiple directions to accomplish more complex tasks. Unlike rigid-link

redundant robots where the kinematics are based on the joint angles between links ($\theta(t)$) or their extensibility ($d(t)$), continuum manipulators are represented by the length of the arc each section subtends ($s(t)$), the curvature of the arc ($\kappa(t)$), and the angle of curvature ($\phi(t)$).

Consider a two-section extensible continuum robot in a plane as shown in Figure 2.1. There, $X_i(t)$, and $Z_i(t) \in \mathbb{R}$ represent the coordinates of the tip of each

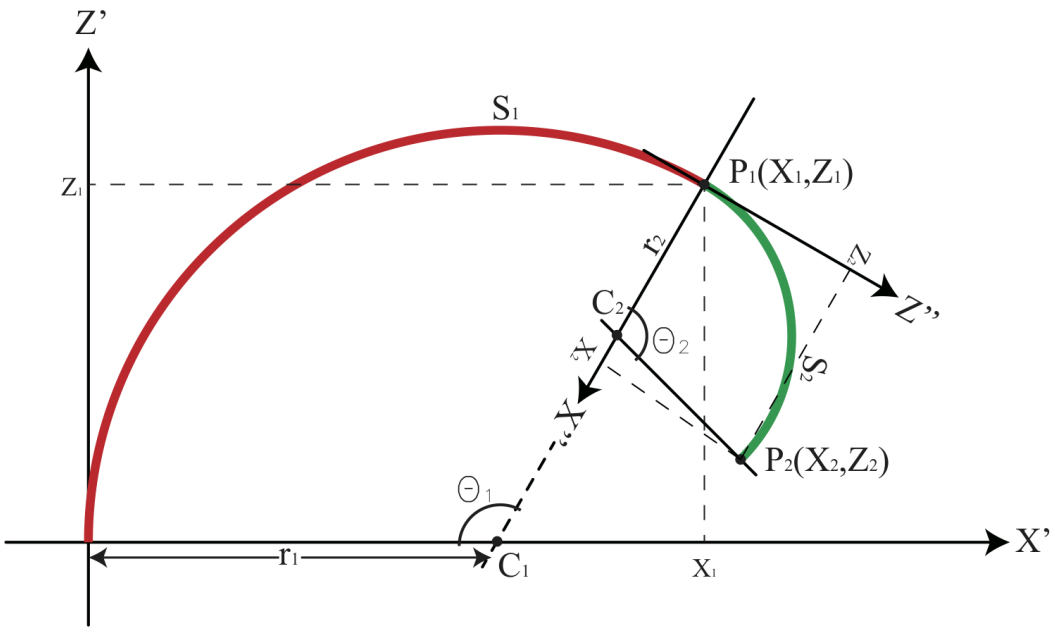

Figure 2.1: Planar Schematic of Two-Section Continuum Robot

of the robot sections in the local frame[1] and are collectively referenced as $P_i(t) \in \mathbb{R}^2$. The terms $s_i(t)$ and $\kappa_i(t) \in \mathbb{R}$ represent the section length and curvature, respectively. $C_i(t) \in \mathbb{R}$ represents the center of the circle that section i is a part of, in the local frame and is always on the local $X-axis$. The angle subtended by the section arc in the local frame is defined as $\theta_i \in \mathbb{R}$. The local coordinate frames are $\boldsymbol{X'Y'Z'}$ for the

[1]In this chapter, $i = 1, 2$ represents the first or second sections of the continuum robot, respectively

fixed base section and $X''Y''Z''$ for the tip section respectively. It can be seen that

$$\begin{aligned} \kappa_i &= r_i(t)^{-1} \\ \theta_i(t) &= s_i(t)\kappa_i(t). \end{aligned} \tag{2.2}$$

Remark 1 *It is assumed throughout this dissertation that the variables $s_i(t)$ and $\kappa_i(t)$ are measureable and each section bends with uniform curvature, resulting in the arcs being parts of circles with radius $r_i(t) = \kappa_i(t)^{-1}$.*

Remark 2 *For the kinematic analysis, the coordinate axes are set up at the base of each section such that each manipulator section curves tangentially to one of the local coordinate axes. This constraint is inherited directly from the implementation of physical continuum robots [5] which must bend about an initial (locally fixed) tangent.*

2.1 Planar Single Section Kinematics

Figure 2.1 shows a continuum robot in the $X'Z'$ plane (quadrant 1, in which the first section lies entirely). In that figure, consider the $\triangle C_1P_1X_1$, where it can be seen that $\angle P_1C_1X_1 = (\pi - \theta_1)$ and $\angle P_1X_1C_1 = \frac{\pi}{2}$. Also, $\bar{C_1P_1} = r_1$ and $\bar{C_1X_1} = X_1 - r_1$, which can be utilized to give

$$cos\,(\pi - \theta_1) = \frac{X_1 - r_1}{r_1}. \tag{2.3}$$

The expression in (2.3) can be rewritten as

$$X_1 = r_1 - r_1 cos\,(\theta_1)\,, \tag{2.4}$$

and using the expression in (2.2) in (2.4) results in

$$X_1 = \frac{1 - cos\,(\theta_1)}{\kappa_1}. \tag{2.5}$$

Similarly, the trigonometric expression that can be used from the same triangle results in

$$\frac{Z_1}{r_1} = sin\,(\pi - \theta_1)\,, \tag{2.6}$$

which can be rewritten as

$$Z_1 = \frac{sin\theta_1}{\kappa_1}. \tag{2.7}$$

2.1.1 Generalizing the Planar Kinematics

It should be noted that as stated in Remark 2, the single section kinematics developed for motion in the 1^{st} quadrant in equations (2.5) and (2.7), is tangential to the local Z- axis, and thus needs to be rotated by π radians (clockwise or counterclockwise) about the local X-axis to compute the section kinematics in the 4^{th} quadrant. Thus, the resulting kinematics become

$$P_{quadrant\ 4} = \begin{bmatrix} X_1 \\ Z_1 \end{bmatrix} = \begin{bmatrix} 1 & 0 \\ 0 & -1 \end{bmatrix} \begin{bmatrix} \frac{1-cos(\theta_1)}{\kappa_1} \\ \frac{sin(\theta_1)}{\kappa_1} \end{bmatrix} = \begin{bmatrix} \frac{1-cos(\theta_1)}{\kappa_1} \\ -\frac{sin(\theta_1)}{\kappa_1} \end{bmatrix}. \tag{2.8}$$

Similarly, the 1^{st} quadrant equations, (2.5) and (2.7), have to be rotated by π radians (clockwise or counterclockwise) about the local Z-axis to compute the section

kinematics in the 2^{nd} quadrant with the resulting kinematics being

$$P_{quadrant\ 2} = \begin{bmatrix} X_1 \\ Z_1 \end{bmatrix} = \begin{bmatrix} -1 & 0 \\ 0 & 1 \end{bmatrix} \begin{bmatrix} \frac{1-cos(\theta_1)}{\kappa_1} \\ \frac{sin(\theta_1)}{\kappa_1} \end{bmatrix} = \begin{bmatrix} -\frac{1-cos(\theta_1)}{\kappa_1} \\ \frac{sin(\theta_1)}{\kappa_1} \end{bmatrix}. \tag{2.9}$$

To calculate the kinematics of the manipulator in the 3^{rd} quadrant, the first quadrant kinematics have to be rotated by π radians first about the local Z-Axis and then about the local X-Axis. Thus the kinematics take the form

$$P_{quadrant\ 3} = \begin{bmatrix} X_1 \\ Z_1 \end{bmatrix} = \begin{bmatrix} 1 & 0 \\ 0 & -1 \end{bmatrix} \begin{bmatrix} -1 & 0 \\ 0 & 1 \end{bmatrix} \begin{bmatrix} \frac{1-cos(\theta_1)}{\kappa_1} \\ \frac{sin(\theta_1)}{\kappa_1} \end{bmatrix} = \begin{bmatrix} -\frac{1-cos(\theta_1)}{\kappa_1} \\ -\frac{sin(\theta_1)}{\kappa_1} \end{bmatrix}. \tag{2.10}$$

2.2 Planar Two Section Kinematics

In the local frame, the kinematic derivation of the second section is identical to that of the base section by considering $\triangle P_2C_2X_2$. In the local frame, this results in

$$\begin{bmatrix} X_2 \\ Z_2 \end{bmatrix} = \begin{bmatrix} \frac{1-cos(\theta_2)}{\kappa_2} \\ \frac{sin(\theta_2)}{\kappa_2} \end{bmatrix}. \tag{2.11}$$

In order to represent the coordinates of the second section tip in the world reference frame, the second section coordinates have to be rotated clockwise by an angle $\theta_1(t)$

about the Y'-axis before being added to the coordinates of the base section, giving

$$\begin{bmatrix} X \\ Z \end{bmatrix} = \begin{bmatrix} X_1 \\ Z_1 \end{bmatrix} + \begin{bmatrix} cos\theta_1 \ sin\theta_1 \\ -sin\theta_1 \ cos\theta_1 \end{bmatrix} \begin{bmatrix} X_2 \\ Z_2 \end{bmatrix}, \tag{2.12}$$

which results in

$$\begin{gathered} X = \tfrac{1}{k_1} - \tfrac{1}{k_1} cos\theta_1 + \tfrac{1}{k_2} cos\theta_1 - \tfrac{1}{k_2} cos\theta_1 cos\theta_2 + \\ \tfrac{1}{k_2} sin\theta_1 sin\theta_2; \\ Z = \tfrac{1}{k_1} sin\theta_1 - \tfrac{1}{k_2} sin\theta_1 + \tfrac{1}{k_2} sin\theta_1 cos\theta_2 + \\ \tfrac{1}{k_2} cos\theta_1 sin\theta_2. \end{gathered} \tag{2.13}$$

These results represent the configurations of the manipulator where both sections lie in their local first quadrants. Consequently, applying the appropriate rotations from Section 2.1.1, we can generate the kinematics for the 8 possible configurations for a two-section manipulator.

2.3 Spatial Single Section Kinematics

When a single section is rotated counterclockwise about the Z_1-axis by an angle $\phi_1(t) \in \mathbb{R}$, such that $\phi \neq 0$ or $\phi \neq \pi$, as shown in Figure 2.2, the manipulator motion is no longer restricted to the $X_1 - Z_1$ plane. Thus the 2D (X_1, Z_1) coordinates in (2.5) and (2.7) are converted to 3D (X_1, Y_1, Z_1) as shown in Figure 2.2 and resulting

in the following equation

$$P_{1-3D} = \begin{bmatrix} cos\phi_1 & -sin\phi_1 & 0 \\ sin\phi_1 & cos\phi_1 & 0 \\ 0 & 0 & 1 \end{bmatrix} \begin{bmatrix} \frac{1-cos(\theta_1)}{\kappa_1} \\ 0 \\ \frac{sin(\theta_1)}{\kappa_1} \end{bmatrix}, \tag{2.14}$$

where the matrix represents the 3D Z-axis rotation, resulting in

$$P_{1-3D} = \begin{bmatrix} X_1 \\ Y_1 \\ Z_1 \end{bmatrix} = \frac{1}{\kappa_1} \begin{bmatrix} cos\left(\phi_1\right)\left(1 - cos\left(\theta_1\right)\right) \\ sin\left(\phi_1\right)\left(1 - cos\left(\theta_1\right)\right) \\ sin\left(\theta_1\right) \end{bmatrix}. \tag{2.15}$$

Given the constraint of the initial tangent coinciding with Z_1, it should be noted

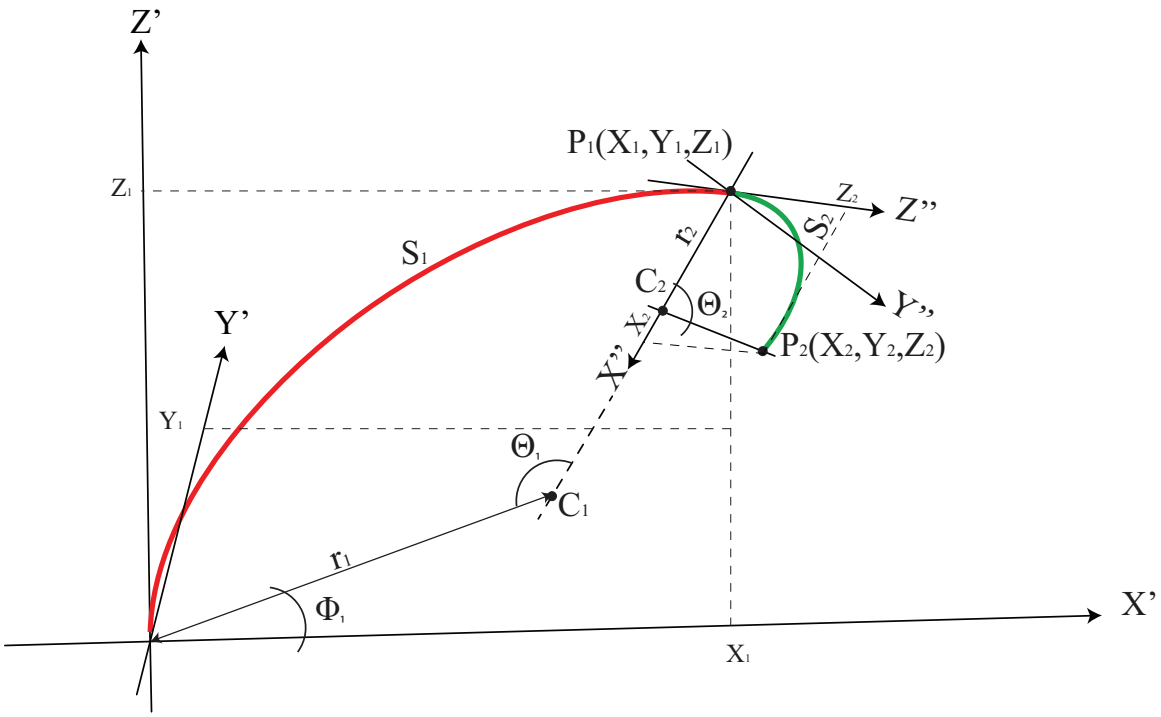

Figure 2.2: 3-Dimensional Schematic of a Two-Section Continuum Robot

that the forward kinematics in (2.15) are unique for a single section in either the

spatial or planar (when $\phi(t) = 0$, see Figure 4.1(b)) cases. The implications of this are discussed in further detail in Section 4.1.

2.3.1 Generalizing the Spatial Kinematics

For the general spatial case, the model needs to account for the situation where the manipulator section can reside in any of the eight octants of the Cartesian coordinate system. To calculate the spatial coordinates from the planar coordinates, X-Axis and Z-Axis kinematics from the appropriate starting quadrant are rotated about the local Z-Axis, clockwise or counterclockwise depending on the desired octant (the spatial coordinates for a section in the 1^{st} octant were calculated in (2.15)).

For example, the 4^{th} octant coordinates can be calculated by modifying (2.14) to represent clockwise rotation around the Z_1-Axis by an angle ϕ_1. This results in

$$P_{1(O4)} = \begin{bmatrix} cos\phi_1 & sin\phi_1 & 0 \\ -sin\phi_1 & cos\phi_1 & 0 \\ 0 & 0 & 1 \end{bmatrix} \begin{bmatrix} \frac{1-cos(\theta_1)}{\kappa_1} \\ 0 \\ \frac{sin(\theta_1)}{\kappa_1} \end{bmatrix}, \tag{2.16}$$

with the resulting coordinates having the form

$$P_{1(O4)} = \begin{bmatrix} X_1 \\ Y_1 \\ Z_1 \end{bmatrix} = \frac{1}{\kappa_1} \begin{bmatrix} cos\left(\phi_1\right)\left(1 - cos\left(\theta_1\right)\right) \\ -sin\left(\phi_1\right)\left(1 - cos\left(\theta_1\right)\right) \\ sin\left(\theta_1\right) \end{bmatrix}. \tag{2.17}$$

Thus the spatial coordinates for each octant can be similarly calculated and are tabulated in Table 2.1 and various configurations are shown in Figure 2.3:

Starting Quadrant	Rotation Direction	Angle of Rotation	Resulting Octant
1	Counterclockwise	ϕ	1
1	Clockwise	ϕ	4
2	Clockwise	ϕ	2
2	Counterclockwise	ϕ	3
3	Counterclockwise	ϕ	6
3	Clockwise	ϕ	7
4	Counterclockwise	ϕ	8
4	Clockwise	ϕ	5

Table 2.1: List of rotations required for various manipulator orientations

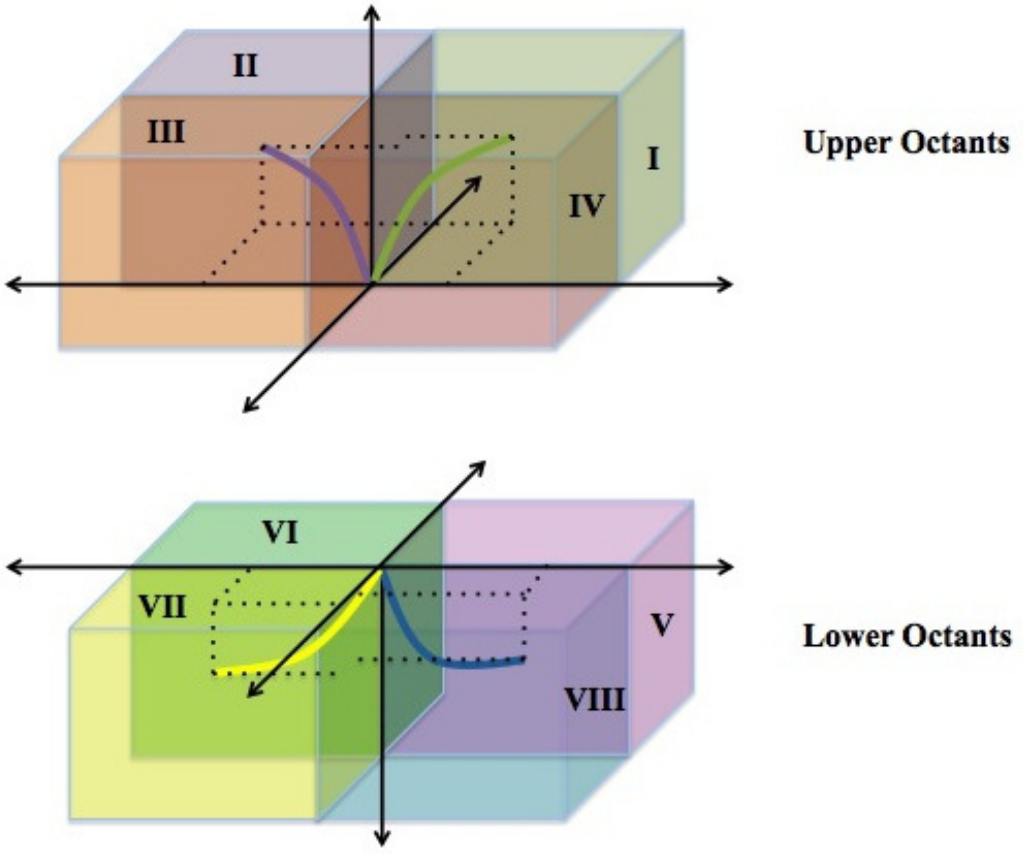

Figure 2.3: Continuum Robot Configurations in Various Octants

2.4 Spatial Two Section Kinematics

In the local frame, the kinematics derivation of the second section is identical to that of the base section by considering $\triangle C_2 P_2 X_2$ in Figure 2.2. This results in the local frame coordinates of the tip of the second section having the form

$$P_{2-3D} = \begin{bmatrix} X_2 \\ Y_2 \\ Z_2 \end{bmatrix} = \frac{1}{\kappa_2} \begin{bmatrix} cos\left(\phi_2\right)\left(1 - cos\left(\theta_2\right)\right) \\ sin\left(\phi_2\right)\left(1 - cos\left(\theta_2\right)\right) \\ sin\left(\theta_2\right) \end{bmatrix}. \tag{2.18}$$

In order to represent the coordinates of the second section tip in the world frame, the second section coordinates have to be first rotated clockwise by the angle $\theta_1(t)$ about the Y_1-axis, rotated again (counterclockwise) by the angle $\phi_1(t)$ about the Z_2 axis and finally added to the coordinates of the first section tip. Thus the 3D coordinates of a two-section continuum manipulator are given by

$$\begin{bmatrix} X \\ Y \\ Z \end{bmatrix} = \begin{bmatrix} X_1 \\ Y_1 \\ Z_1 \end{bmatrix} + \begin{bmatrix} cos\phi_1 & -sin\phi_1 & 0 \\ sin\phi_1 & cos\phi_1 & 0 \\ 0 & 0 & 1 \end{bmatrix} \begin{bmatrix} cos\theta_1 & 0 & sin\theta_1 \\ 0 & 1 & 0 \\ -sin\theta_1 & 0 & cos\theta_1 \end{bmatrix} \begin{bmatrix} X_2 \\ Y_2 \\ Z_2 \end{bmatrix}. \tag{2.19}$$

This results in the coordinates of the tip in the base frame represented as

$[X(t)\ Y(t)\ Z(t)]^T$, in which

$$\begin{aligned}
X = &\tfrac{1}{k_1}cos\phi_1 - \tfrac{1}{k_1}cos\theta_1 cos\phi_1 + \tfrac{1}{k_2}cos\theta_1 cos\phi_1 cos\phi_2 \\
&-\tfrac{1}{k_2}cos\theta_1 cos\theta_2 cos\phi_1 cos\phi_2 - \tfrac{1}{k_2}sin\phi_1 sin\phi_2 \\
&+\tfrac{1}{k_2}cos\theta_2 sin\phi_1 sin\phi_2 + \tfrac{1}{k_2}sin\theta_1 sin\theta_2 cos\phi_2; \\
\\
Y = &\tfrac{1}{k_1}sin\phi_1 - \tfrac{1}{k_1}cos\theta_1 sin\phi_1 + \tfrac{1}{k_2}cos\theta_1 sin\phi_1 cos\phi_2 \\
&-\tfrac{1}{k_2}cos\theta_1 cos\theta_2 sin\phi_1 cos\phi_2 + \tfrac{1}{k_2}cos\phi_1 sin\phi_2 \\
&-\tfrac{1}{k_2}cos\theta_2 cos\phi_1 sin\phi_2 + \tfrac{1}{k_2}sin\theta_1 sin\theta_2 sin\phi_2; \\
\\
Z = &\tfrac{1}{k_1}sin\theta_1 - \tfrac{1}{k_2}sin\theta_1 cos\phi_2 + \tfrac{1}{k_2}sin\theta_1 cos\theta_2 cos\phi_2 \\
&+\tfrac{1}{k_2}cos\theta_1 sin\theta_2.
\end{aligned} \tag{2.20}$$

While these results represent a manipulator in the first octant, choosing the appropriate starting octant and applying the necessary rotation will establish the kinematics for the 32 possible configurations. If $\phi_1(t) = \phi_2(t) = 0$, in (2.20), the manipulator motion is restricted to the X-Z plane, as shown in Figure 2.1, and discussed in Section 2.2.

2.5 Spatial $n-$Section Kinematics

The forward kinematic equation providing the tip location of a 2-section extensible continuum manipulator developed in (2.19) can be recursively generalized to $n-$sections first by the clockwise rotation of the n^{th} section about the $Z_{n-1}-$Axis by an angle of of θ_{n-1} and then by the rotation of the same section about the (2.19) can be generalized to $n-$sections first by the clockwise rotation of the same section about the $Z_{n-1}-$Axis by an angle of ϕ_{n-1}. Thus the resulting recursive formula to generate

the kinematics of an $n-$section serially-connected extensible continuum manipulator can be given by

$$\begin{bmatrix} X \\ Y \\ Z \end{bmatrix} = \begin{bmatrix} X_{n-1} \\ Y_{n-1} \\ Z_{n-1} \end{bmatrix} + \begin{bmatrix} cos\phi_{n-1} & -sin\phi_{n-1} & 0 \\ sin\phi_{n-1} & cos\phi_{n-1} & 0 \\ 0 & 0 & 1 \end{bmatrix} \begin{bmatrix} cos\theta_{n-1} & 0 & sin\theta_{n-1} \\ 0 & 1 & 0 \\ -sin\theta_{n-1} & 0 & cos\theta_{n-1} \end{bmatrix} \begin{bmatrix} X_n \\ Y_n \\ Z_n \end{bmatrix}. \tag{2.21}$$

As stated previously, this kinematic development provides a more instinctive understanding of the shape of the manipulators when provided with their shape variables. Because of this, these forward kinematic equations (in their 3-section form) are utilized in the developments of the subsequent chapters, especially towards the generation of the velocity Jacobian, self-motion characterization, and teleoperation control.

Chapter 3

A Sliding-Mode Configuration-Space Controller for Extensible Continuum Manipulators

In this chapter, a standard sliding-mode controller is developed for continuum manipulators whose models are based on the Lagrangian dynamics. Specific modifications have been made to ensure the control algorithm fits the structure of the OctArm's continuum dynamics. Sliding-mode controllers are a class of variable-structure controllers which alter the dynamics of a system with the application of a discontinuous high-frequency switching control signal. The control signal is of a high frequency because it is not a continuous function of time and switches from one continuous state to another depending on the current position of the system in the state-space. Thus, the control signal and subsequently the system is forced to "slide" along cross-sectional boundaries of their respective structures. Because of a lack of

model-based controllers for continuum robots, a sliding-mode controller was a natural choice for the following reasons:

- Sliding-mode controllers exhibit relatively low sensitivity to uncertainty in robot dynamic model parameters,
- the robot dynamic model does not need to have higher-order terms.
- and because it is discontinuous, finite-time convergence can be achieved with the appropriate choice of gain values.

A Lyapunov-type proof is utilized for the stability analysis of the proposed controller, while numerical simulations and experimental results are demonstrated to highlight the effectiveness of the proposed controller in comparison to a standard inverse dynamics PD controller.

Based on the general forward kinematics equation given in (2.1), the forward kinematics for the 3-section OctArm can be represented by

$$x = f(q), \tag{3.1}$$

where $x(t) \in \mathbb{R}^3$ represents the $[X(t)\ Y(t)\ Z(t)]^T$ coordinates of the manipulator tip in space, while the $q(t) \in \mathbb{R}^9$ represents the manipulator section lengths, curvatures, and angles-of-orientation, defined as

$$q \triangleq \begin{bmatrix} s_1\ \kappa_1\ \phi_1\ s_2\ \kappa_2\ \phi_2\ s_3\ \kappa_3\ \phi_3 \end{bmatrix}^T, \tag{3.2}$$

where $s_1(t)$, $s_2(t)$, and $s_3(t) \in \mathbb{R}^+$ are the section lengths, $\kappa_1(t)$, $\kappa_2(t)$, and $\kappa_3(t) \in \mathbb{R}$ are the section curvatures, and $\phi_1(t)$, $\phi_2(t)$, and $\phi_3(t) \in \mathbb{R}$ are the angles of orientation, of the 3 sections respectively. It can further be seen that since the number of

configuration-space terms (also system independent variables) are greater than the space in which it operates, the manipulator is considered to be kinematically redundant.

3.1 Dynamic Model

The model developed by Tatlicioglu *et al.* [41] [42] provides for the first time a closed form model, applicable to continuum robot extension as well as bending, which contains key properties (well established for conventional rigid- link robot structures) essential for nonlinear controller synthesis. In particular, the overall model takes the familiar form,

$$\tau = M(q)\ddot{q} + N\left(q, \dot{q}\right)\dot{q} + G(q) + B(q) + E(q), \tag{3.3}$$

where $q(t) \in \mathbb{R}^n$ represents the configuration-space variables, while $M(q)$, $N\left(q, \dot{q}\right) \in \mathbb{R}^{n \times n}$ represent the inertia matrix and Centripetal-Coriolis matrix respectively. The terms $G(q)$, $B(q)$, and $E(q) \in \mathbb{R}^n$ refer to vectors relating to the effects of gravity, potential energy due to bending, and potential energy due to extension, respectively, while $\tau(t) \in \mathbb{R}^n$ is the control input. The individual elements of the dynamic model developed in [41] and [42] can be found in Appendix D.

Remark 3 *The model has the following properties:*

1. *The inertia matrix $M(q)$ is symmetric and positive definite.*

2. *The matrix $\dot{M} - 2N$ is skew symmetric and satisfies the property,*

$$\xi^T \left(\dot{M} - 2N\right) \xi = 0 \ \forall \xi \in \mathbb{R}^n, \tag{3.4}$$

which will be exploited in the following controller synthesis.

3.2 Controller Synthesis

Here, the dynamic model described above is used to extend and adapt the nonlinear control approach in [74] to the case of extensible continuum robots. In [74], the authors designed a sliding-mode controller for rigid-link robot manipulators by exploiting their Euler-LaGrangian dynamic models.

To develop the controller, let the manipulator configuration-space tracking error, $e(t) \in \mathbb{R}^9$ be defined as

$$e \triangleq q_d - q \tag{3.5}$$

where $q_d(t) \in \mathbb{R}^9$ is the desired manipulator position. The first and second time derivatives of (3.5) are given by

$$\begin{aligned} \dot{e} &\triangleq \dot{q}_d - \dot{q} \\ \ddot{e} &\triangleq \ddot{q}_d - \ddot{q} \end{aligned} \tag{3.6}$$

in which $\dot{q}(t)$ and $\ddot{q}(t) \in \mathbb{R}^9$ respectively represent the manipulator configuration-space velocities and accelerations, while $\dot{q}_d(t)$ and $\ddot{q}_d(t) \in \mathbb{R}^9$ respectively represent the desired configuration-space velocities and accelerations. The desired position term, $q_d(t)$, should be chosen such that $q_d(t)$, $\dot{q}_d(t)$, $\ddot{q}_d(t) \in \mathcal{L}_\infty$.

Let $r(t) \in \mathbb{R}^9$ be the sliding surface and defined as the filtered tracking error such that

$$r \triangleq \alpha e + \dot{e}, \tag{3.7}$$

where $\alpha = I_9 \begin{bmatrix} \alpha_1 & \alpha_2 & \alpha_3 & \alpha_4 & \alpha_5 & \alpha_6 & \alpha_7 & \alpha_8 & \alpha_9 \end{bmatrix}^T$, in which $\alpha_i \in \mathbb{R}^+$ for $i = 1...9$.

Similar to (3.7), let the filtered trajectory, $\dot{q}_r(t) \in \mathbb{R}^9$ be defined as[1]

$$\dot{q}_r = \alpha e + \dot{q}_d. \tag{3.8}$$

Theorem 1 *Consider the controller*

$$\tau = \hat{M}(q)\ddot{q}_r + \hat{N}\left(q, \dot{q}\right)\dot{q} + \hat{G}(q) + \hat{B}(q) + \hat{E}(q) + Ksgn(r), \tag{3.9}$$

in which $\hat{M}(q)$, $\hat{N}\left(q, \dot{q}\right) \in \mathbb{R}^{9\times 9}$, $\hat{G}(q)$, $\hat{B}(q)$, $\hat{E}(q) \in \mathbb{R}^9$ *are estimates of* $M(q)$, $N\left(q, \dot{q}\right)$, $G(q)$, $B(q)$, *and* $E(q)$ *respectively, and* $K \in \mathbb{R}^{9\times 9}$ *is a diagonal matrix with positive entries.*

Using this controller, the error reaches the sliding surface described in (3.7) in finite time. In addition, once on the surface, $q(t)$ *will converge to* $q_d(t)$ *exponentially fast.*

Proof. The dynamic model of the manipulator in (3.3) can be rewritten as

$$M(q)\ddot{q} = \tau - N\left(q, \dot{q}\right)\dot{q} - G(q) - B(q) - E(q), \tag{3.10}$$

in which the substitution of (3.6) results in

$$M(q)\left(\ddot{q}_d - \ddot{e}\right) = \tau - N\left(q, \dot{q}\right)\left(\dot{q}_d - \dot{e}\right) - G(q) - B(q) - E(q). \tag{3.11}$$

Substituting (3.8) and its time derivative in (3.11) yields

$$M(q)\left(\ddot{q}_r - \alpha\dot{e} - \ddot{e}\right) = \tau - N\left(\left(q, \dot{q}\right)\dot{q}_r - \alpha e - \dot{e}\right) - G(q) - B(q) - E(q). \tag{3.12}$$

[1]Throughout the dissertation, I_n and $0_{m\times r}$ will be used to represent an $n \times n$ standard identity matrix and an $m \times r$ zero matrix, respectively.

Using (3.7) and its time derivative in (3.12) results in

$$M(q)\left(\ddot{q}_r - \dot{r}\right) = \tau - N\left(q, \dot{q}\right)\left(\dot{q}_r - r\right) - G(q) - B(q) - E(q), \tag{3.13}$$

which, after expanding and moving terms around can be rewritten as

$$M(q)\dot{r} = M(q)\ddot{q}_r + N\left(q, \dot{q}\right)\dot{q}_r - N\left(q, \dot{q}\right)r + G(q) + B(q) + E(q) - \tau. \tag{3.14}$$

Consider the candidate Lyapunov function

$$V = \frac{1}{2} r^T M(q) r, \tag{3.15}$$

whose time derivative yields

$$\dot{V} = r^T M\dot{r} + \frac{1}{2} r^T \dot{M}(q) r. \tag{3.16}$$

Substituting (3.14) in (3.16) we obtain

$$\dot{V} = r^T\left[M\ddot{q}_r + N\dot{q}_r - Nr + G + B + E - \tau\right] + \frac{1}{2} r^T \dot{M}(q) r, \tag{3.17}$$

which can be rewritten as

$$\dot{V} = r^T\left[M\ddot{q}_r + N\dot{q}_r + G + B + E - \tau\right] - r^T Nr + \frac{1}{2} r^T \dot{M}(q) r. \tag{3.18}$$

Using Property 2 in Remark 3 it can be seen that

$$r^T Nr = \frac{1}{2} r^T \dot{M} r, \tag{3.19}$$

which when substituted in (3.18) yields

$$\dot{V} = r^T \left[M\ddot{q}_r + N\dot{q}_r + G + B + E - \tau \right] \tag{3.20}$$

Substituting the controller proposed in (3.9) in (3.20) yields

$$\dot{V} = r^T \left[\tilde{M}\ddot{q}_r + \tilde{N}\dot{q}_r + \tilde{G} + \tilde{B} + \tilde{E} \right] - \sum_{i=1}^{9} k_i \mid r_i \mid, \tag{3.21}$$

where $\tilde{M}(q) \triangleq M(q) - \hat{M}(q)$ and $\tilde{N} \triangleq N(q,\dot{q}) - \hat{N}(q,\dot{q}) \in \mathbb{R}^{9\times 9}$, $\tilde{G}(q) \triangleq G(q) - \hat{G}(q)$, $\tilde{B}(q) \triangleq B(q) - \hat{B}(q)$, and $\tilde{E}(q) \triangleq E(q) - \hat{E}(q) \in \mathbb{R}^9$. The term $k_i \in \mathbb{R}^+$ is chosen such that

$$k_i \geq \mid \left[\tilde{M}\ddot{q}_r + \tilde{N}\dot{q}_r + \tilde{G} + \tilde{B} + \tilde{E} \right]_i \mid + \eta_i, \tag{3.22}$$

in which $\left[\tilde{M}\ddot{q}_r + \tilde{N}\dot{q}_r + \tilde{G} + \tilde{B} + \tilde{E} \right]_i$ represents the i^{th} element of that vector, and $\eta_i \in \mathbb{R}^+$. Substituting (3.22) in (3.18) yields the following inequality

$$\dot{V}_r \leq -\sum_{i=1}^{9} \eta_i \mid r_i \mid, \tag{3.23}$$

from which it can be seen that $r(t) \to 0$ in finite time. Thus from (3.7), when $r(t) = 0$, $\dot{e}(t) = 0$ and $e(t) = 0$. Thus, once the system is in the sliding mode, $e(t) \to 0$ exponentially fast. ■

3.3 Controller Performance - Simulation

In this section we first present the results of the controller applied to a simulation of the OctArm manipulator to demonstrate the effectiveness of the control strategy introduced in the Section 3.2. In the following, all three sections of the robot

are actuated. For simplicity, the robot motions are restricted to the plane orthogonal to gravity, thus $G(q) = 0$ and $\phi_1(t) = \phi_2(t) = \phi_3(t) = 0$. because of this, the robot now has six degrees of freedom, three of extension/contraction (one for each link), and three for bending (again, one for each link).

The simulation was developed in the Matlab/Simulink ®environment which was hosted on an Dell®PC running on an Intel®i5 processor under the Windows 7®operating system. In the simulation, the robot is modeled using the dynamic model in Section 3.1. The nominal trajectories of the sections are an aggressive set of sinusoids given by

$$q_{d_{sim}} = \begin{bmatrix} s_{1_d} \\ k_{1_d} \\ s_{2_d} \\ k_{2_d} \\ s_{3_d} \\ k_{3_d} \end{bmatrix} = \begin{bmatrix} 0.35 + 0.01sin(2\pi t)\ [m] \\ 1 + 0.2sin(2\pi t)\ \left[\frac{1}{m}\right] \\ 0.35\ [m] \\ 2 + 0.2sin(2\pi t)\ \left[\frac{1}{m}\right] \\ 0.4 + 0.01sin(2\pi t)\ [m] \\ 3\ \left[\frac{1}{m}\right] \end{bmatrix}. \tag{3.24}$$

The ability of the controller proposed in this chapter to track the trajectories is compared with that of a conventional inverse dynamics controller, i.e. PD controller with an inner linearization loop [74]. The results for the standard (PD) controller are illustrated in Figures 3.1 and 3.2 respectively. Note that the inverse dynamics controller includes all the possible problems and caveats associated with system inversion. This includes the possible presence of non- minimum-phase zeros. Additionally, the gains required for optimal performance change depending on the nature of the performance objectives, while it should be ensured that the system is critically damped.

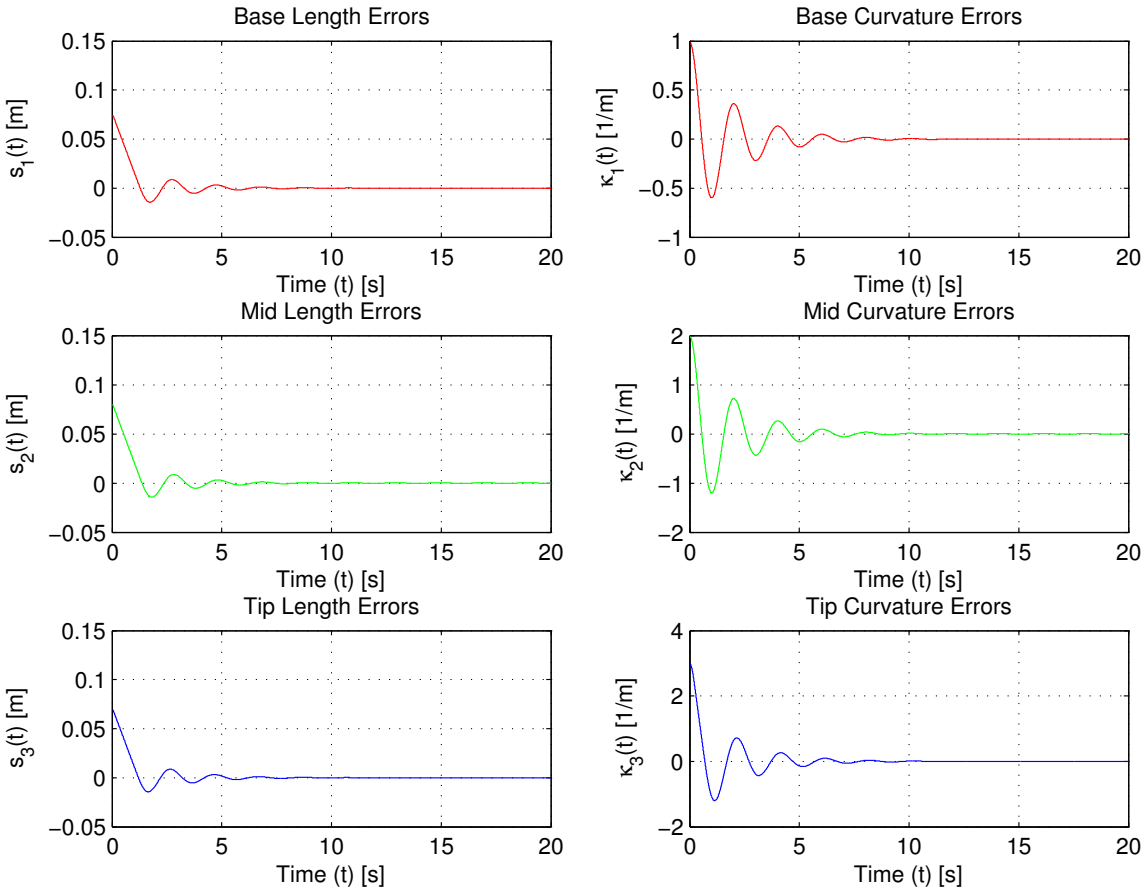

Figure 3.1: C-Space PD Controller Simulation: Tracking Errors

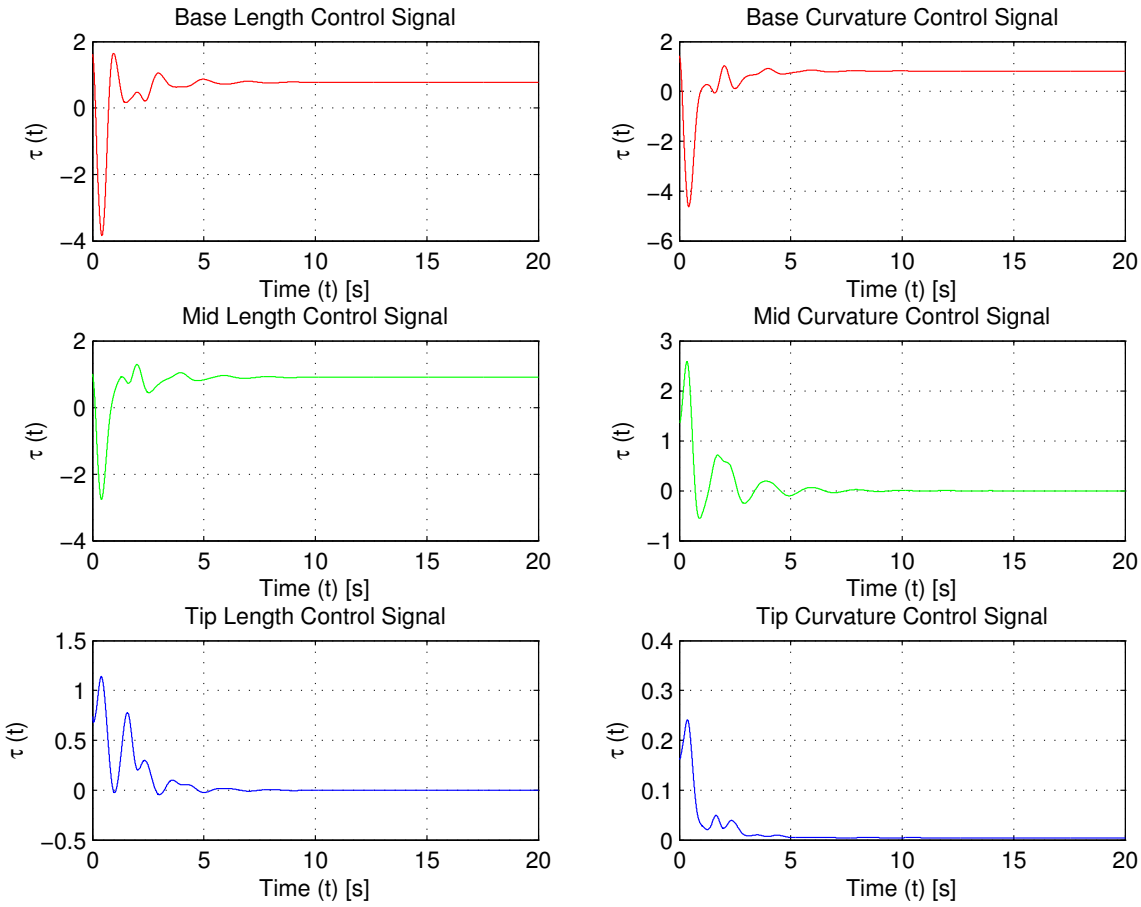

Figure 3.2: C-Space PD Controller Simulation: Control Signals

The results for the controller introduced in (3.9) are illustrated in Figures 3.3 and 3.4 respectively. The hallmark of the sliding- mode controller is that the error only needs to be driven to the switching surface, after which the system will not be affected by any modeling uncertainties or disturbances. Also, the additional caveats noted for the inverse dynamics controller do not apply in this case. A comparison of the plots in Figures 3.1 and 3.2 for the inverse dynamics PD controller, and Figures 3.3 and 3.4 reveal that the nonlinear controller successfully compensates for dynamic uncertainty.

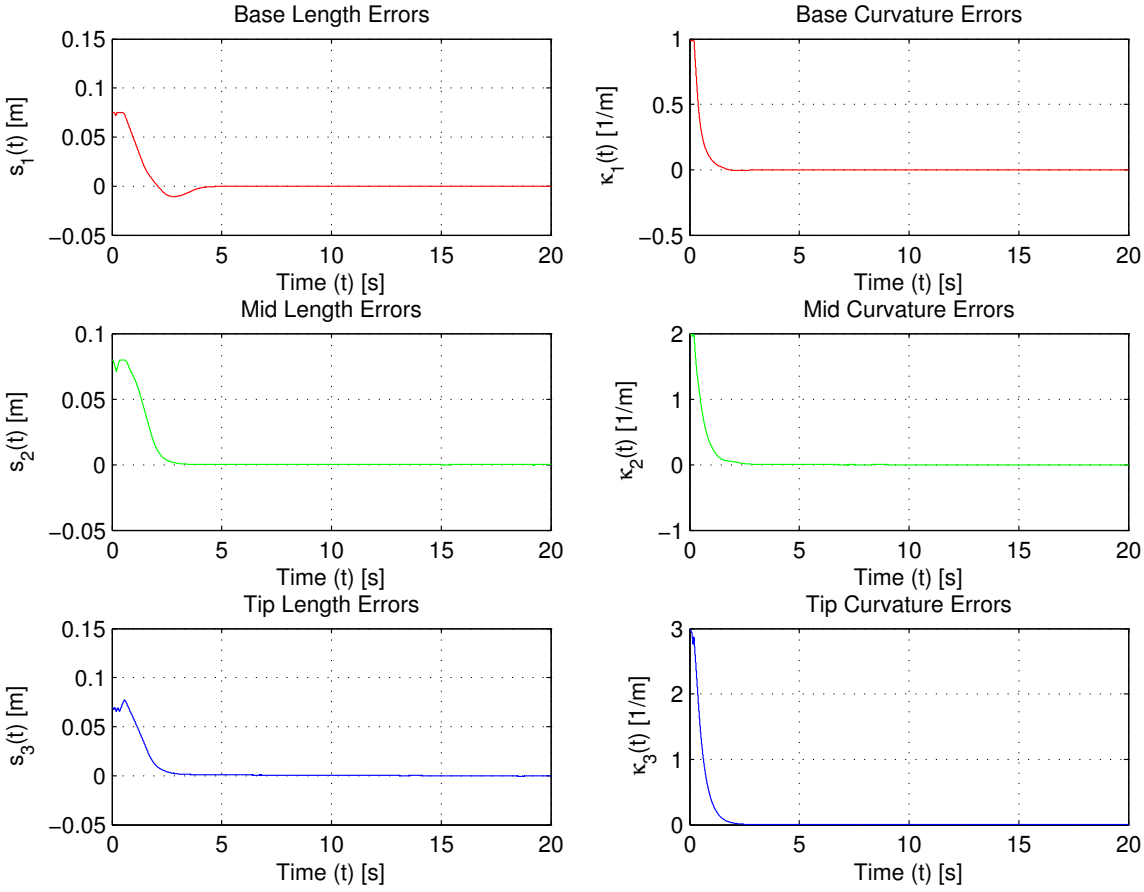

Figure 3.3: C-Space Sliding Mode Controller Simulation: Tracking Errors

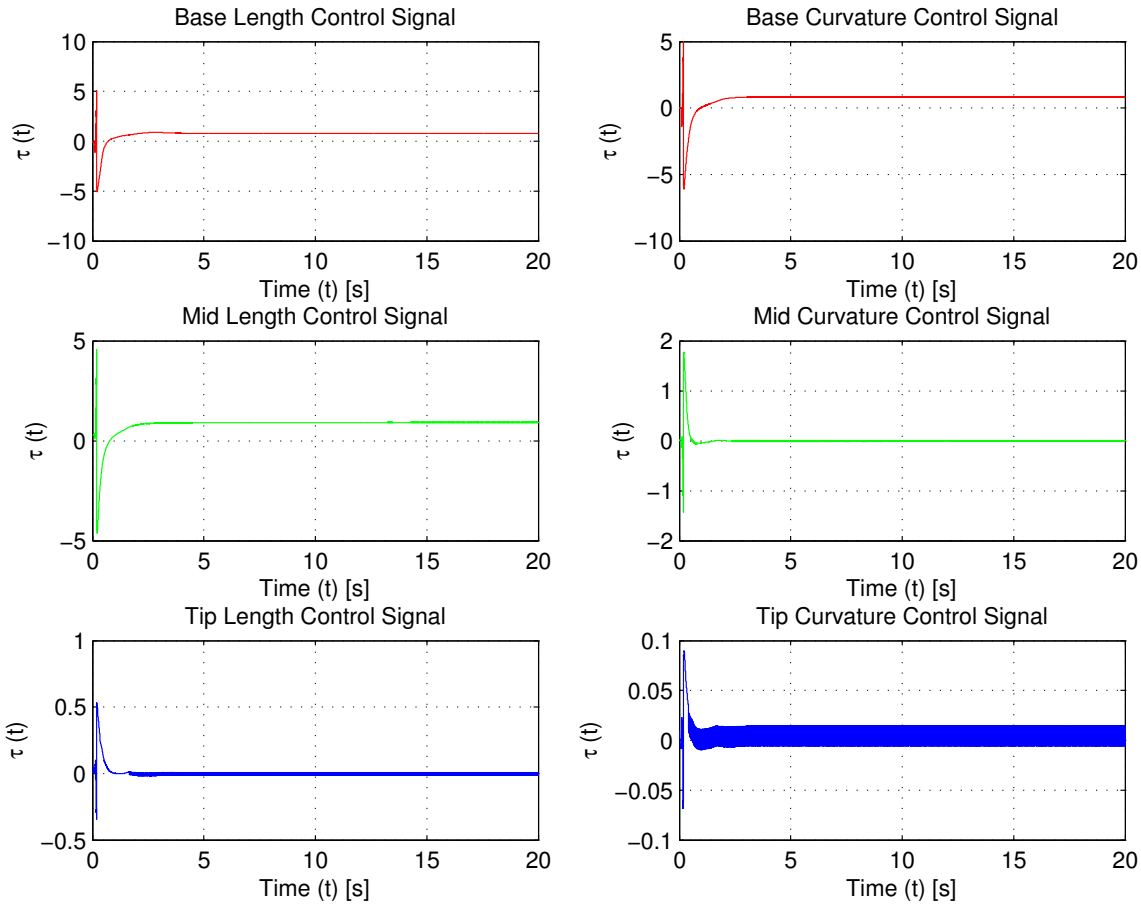

Figure 3.4: C-Space Sliding Mode Controller Simulation: Control Signals

3.4 Controller Performance - Experimental Validation

The controller described in (3.9) was implemented on the OctArm extensible continuum manipulator. The objective of the experiment was to verify the performance of the sliding-mode controller. Given that the available dynamic model developed in [41] and [42] is planar, the robot was placed on a horizontal surface. Because of this orientation, the gravitational terms in the model were unnecessary.

Similar to the simulation, the control algorithm was developed on a Dell® PC running on an Intel® i5 processor under the Windows 7® operating system. Additionally, Quanser® Q8 and Q2 data acquisition boards were used along with the QUARC® interface to connect to the OctArm hardware. The control signal from the algorithm was converted into voltages and sent to the 9 pressure regulators (one for each McKibben actuator on the OctArm) which give each section its length and curvature. The length of each actuator was measured using a string encoder from which the robot section lengths and curvatures were inferred using the conversions developed in [30] for the feedback. A schematic of the control loop is shown in Figure 3.5 and was run at 1 KHz.

As in Section 3.3, the performance of the proposed controller was measured

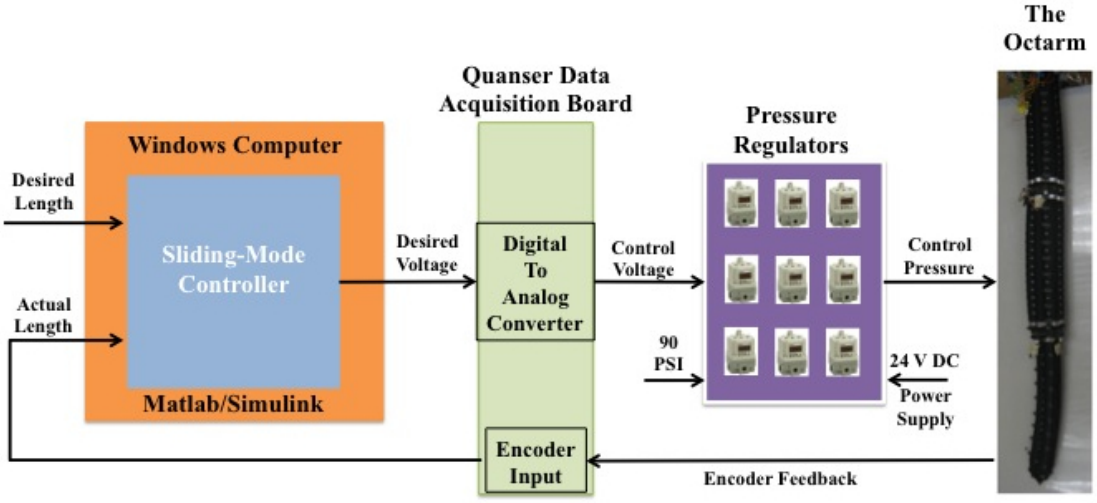

Figure 3.5: Experimental Control Loop Block Diagram

against a PD controller. The nominal desired trajectory was chosen to be:

$$q_{d_{exp}} = \begin{bmatrix} s_{1_d} \\ k_{1_d} \\ s_{2_d} \\ k_{2_d} \\ s_{3_d} \\ k_{3_d} \end{bmatrix} = \begin{bmatrix} 0.38 + 0.05sin\left(\frac{\pi}{4}t\right) \ [m] \\ 1.5 + 0.2sin\left(\frac{\pi}{4}t\right) \ \left[\frac{1}{m}\right] \\ 0.34 + 0.02cos\left(\frac{\pi}{4}t\right) \ [m] \\ 1.5 + 0.2sin\left(\frac{\pi}{4}t\right) \ \left[\frac{1}{m}\right] \\ 0.38[m] \\ 3.5 + 0.2sin\left(\frac{\pi}{4}t\right) \ \left[\frac{1}{m}\right] \end{bmatrix} \tag{3.25}$$

The PD controller results can be seen in Figures 3.6, 3.7, 3.8, and 3.9, while the Sliding-mode control voltages are shown in Figures 3.10, 3.11, 3.12, and 3.13. The control gains that provided the results for the PD controller are $K_p = diag\{10\ 100\ 10\ 100\ 500\ 100\}$ and $K_v = diag\{50\ 50\ 50\ 50\ 50\ 50\}$, while the gains for the sliding-mode controller are $\alpha = diag\{1.3\ 2.9\ 0.5\ 1.1\ 0.8\ 0.6\}$ and $\eta = diag\{1\ 2.5\ 0.15\ 1.1\ 0.7\ 3\}$. Comparing the results of the PD controller with those of the Sliding-mode controller, it can be seen that the Sliding-Mode controller tracking error converges slightly faster than that of

the PD controller while the Sliding-mode controller also ensure tighter oscillations about the desired tip location, as seen in Figures Figures 3.6 and 3.10. Additionally, the control voltages generated by the Sliding-mode controller are significantly lower than those of the PD controller, showing that better control is achieved with less energy being consumed, as seen in the control signal figures.

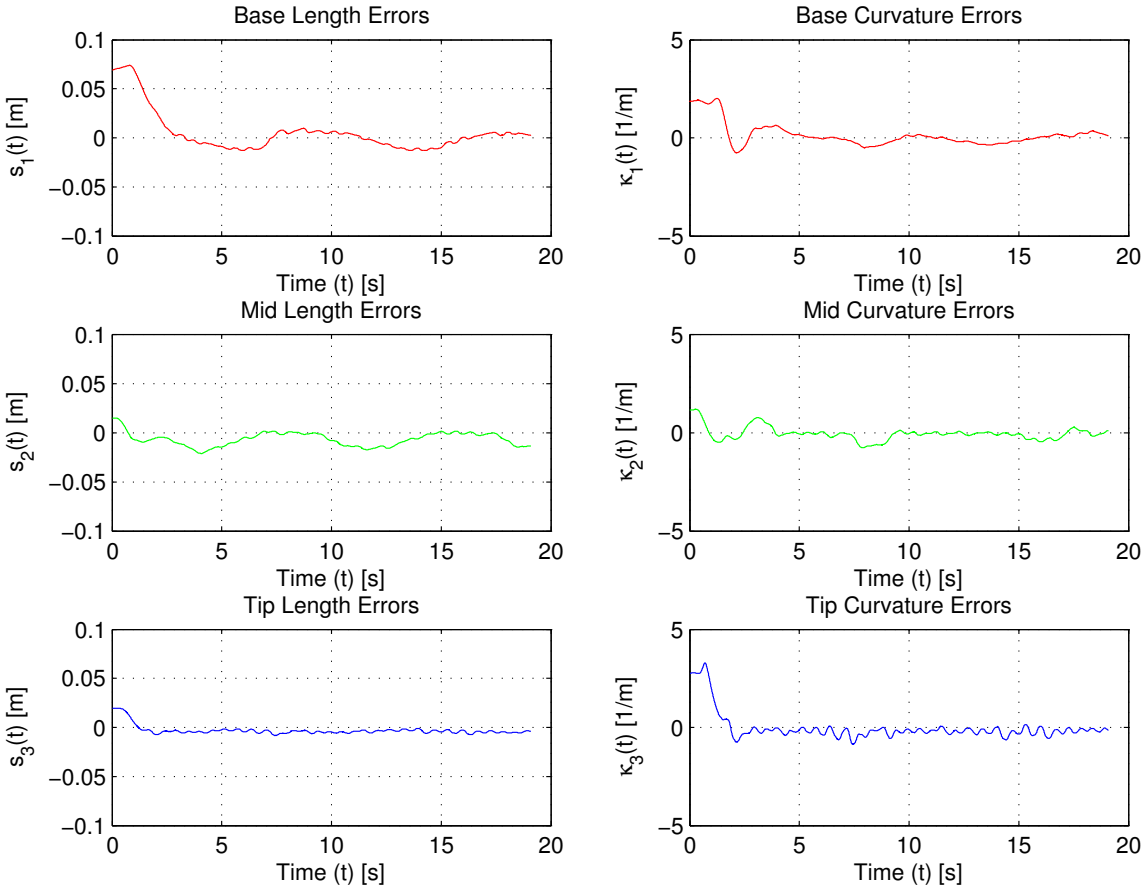

Figure 3.6: C-Space PD Controller Experiment: Tracking Error

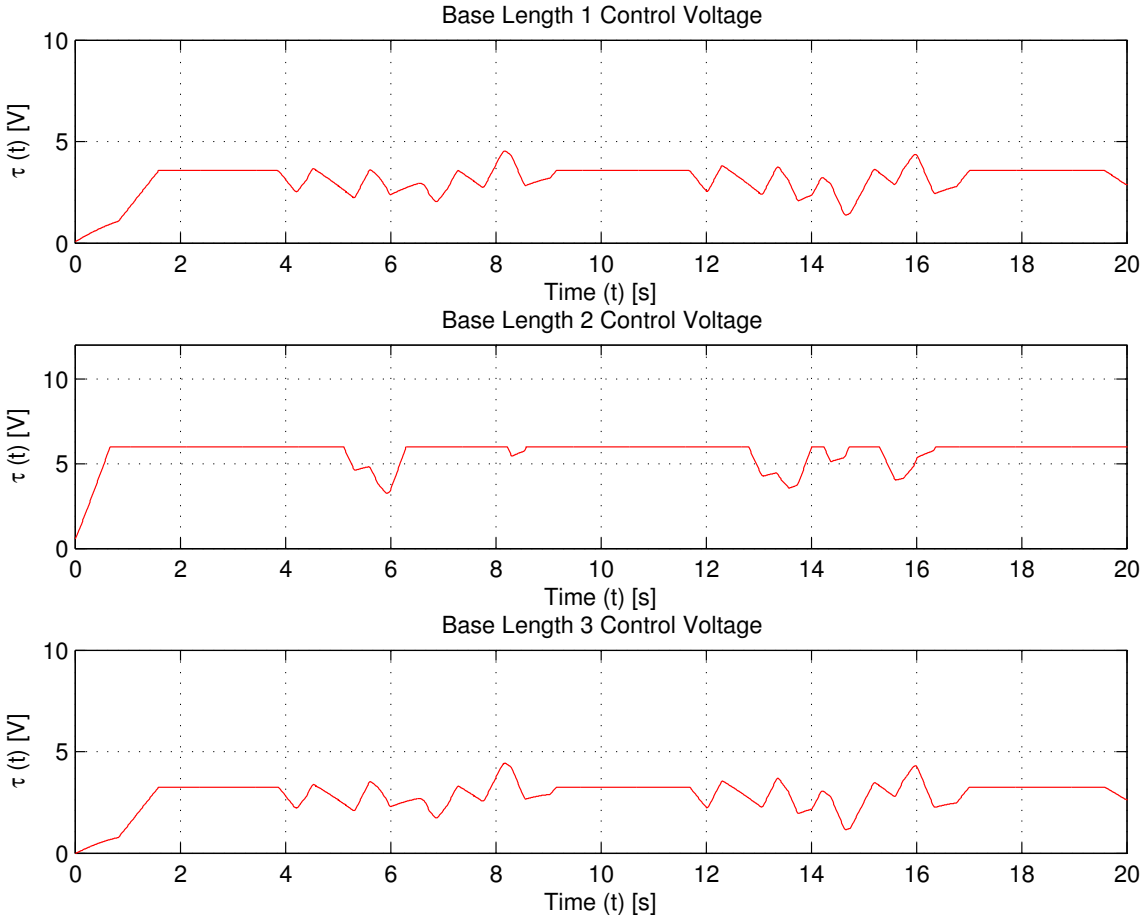

Figure 3.7: C-Space PD Controller Experiment: Base Actuators Control Voltage

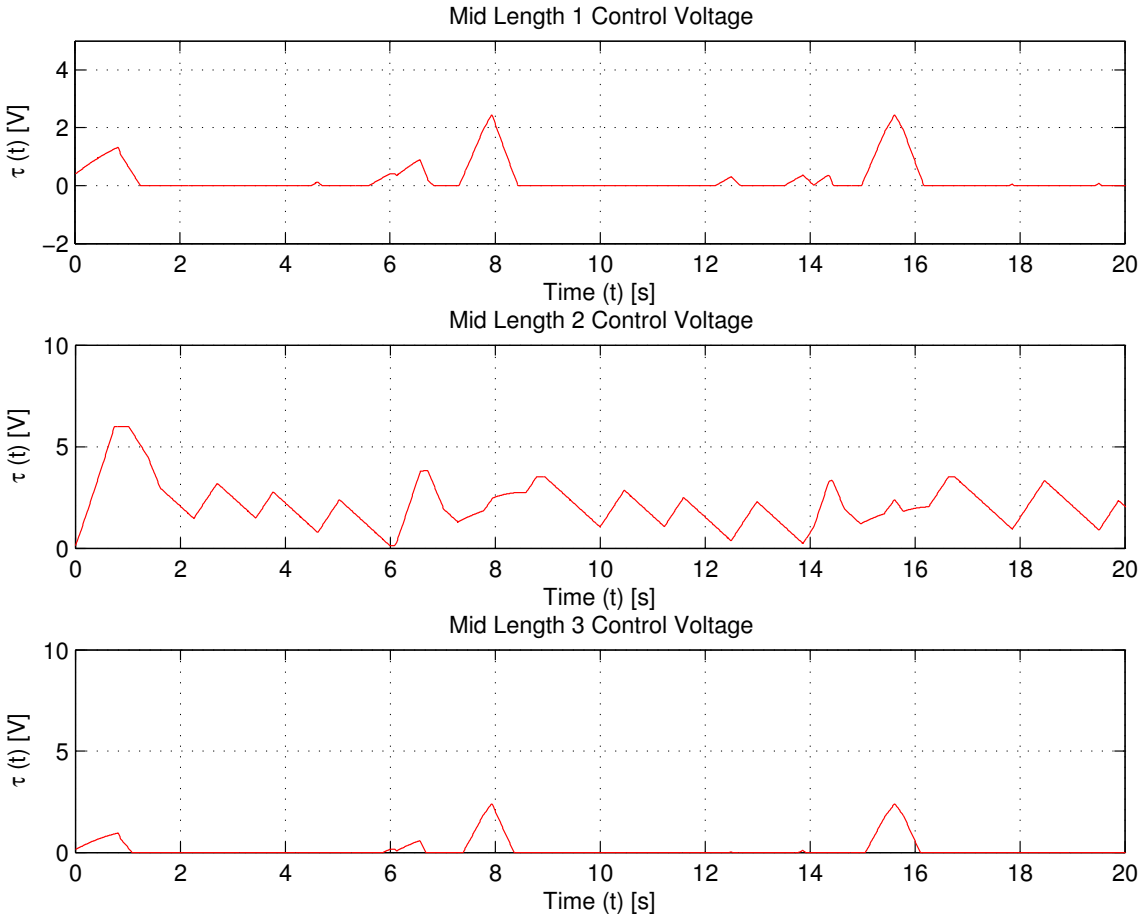

Figure 3.8: C-Space PD Controller Experiment: Mid Actuators Control Voltage

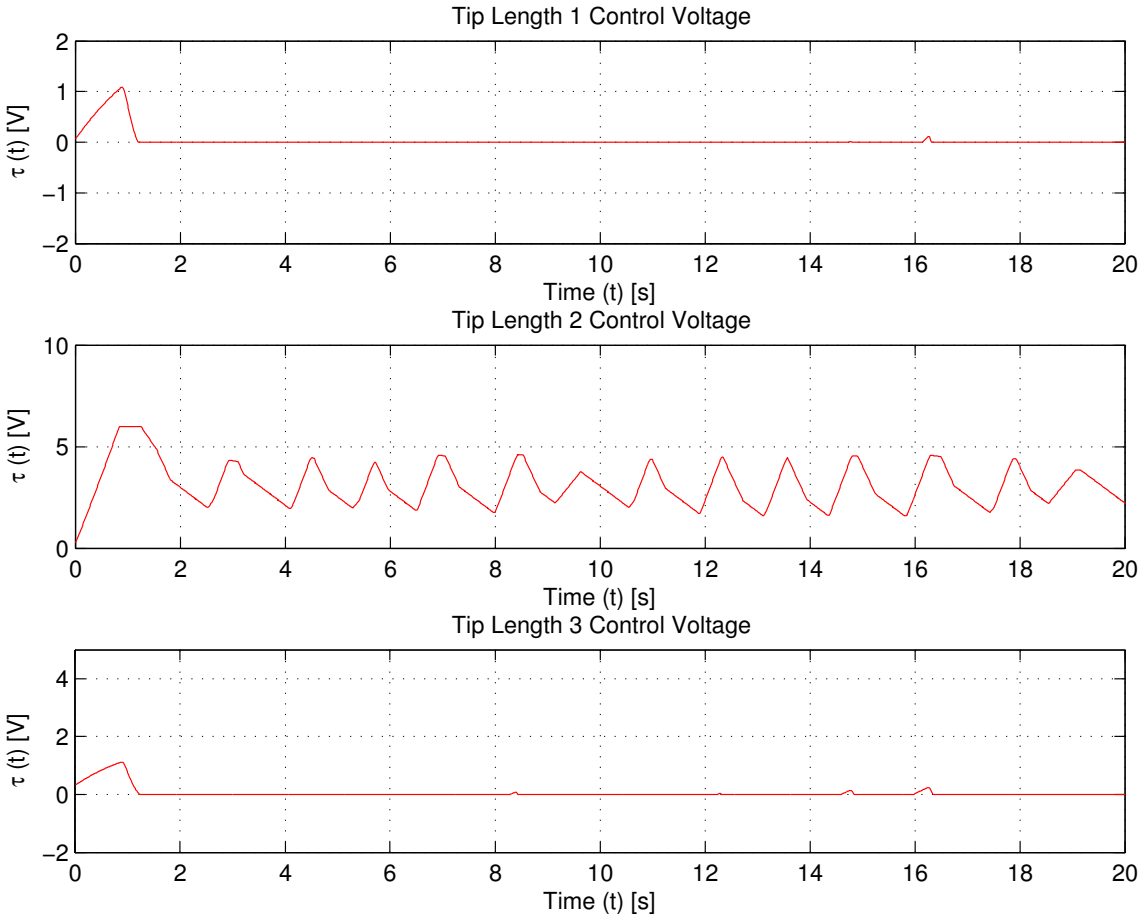

Figure 3.9: C-Space PD Controller Experiment: Tip Actuators Control Voltage

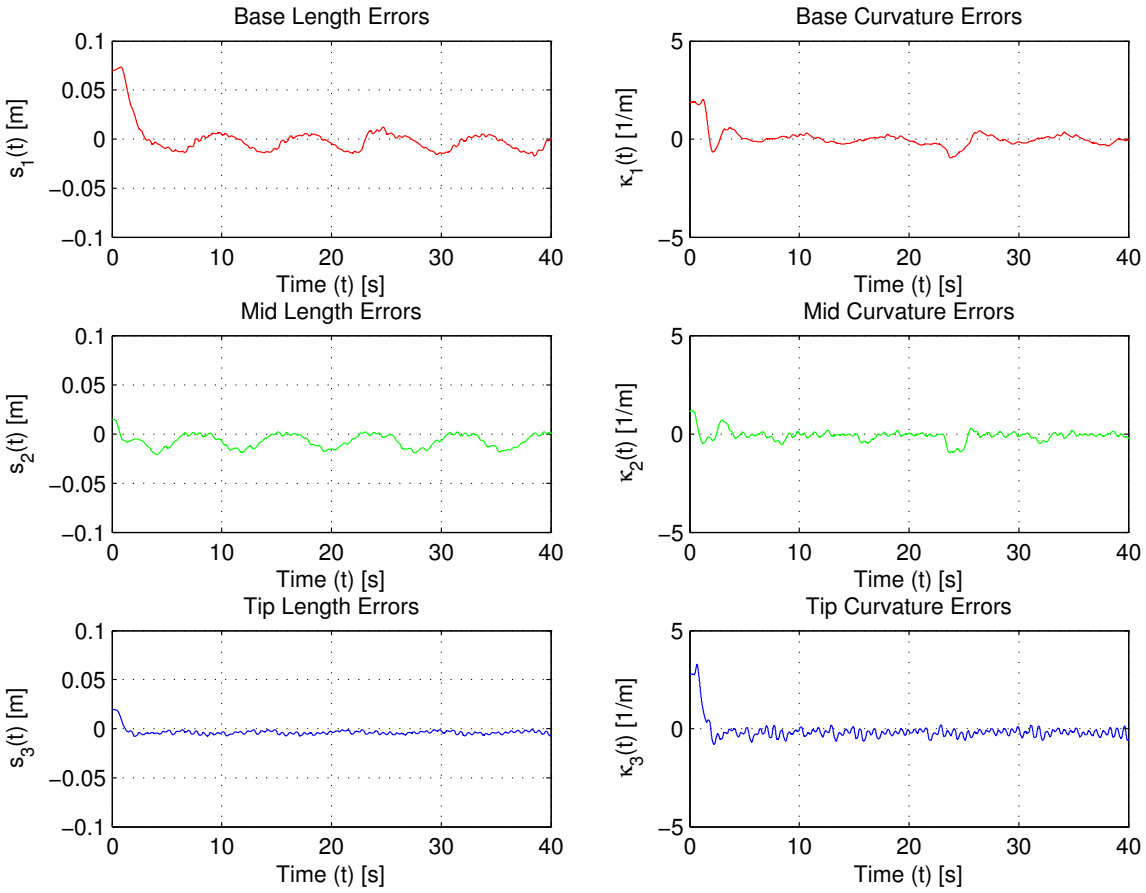

Figure 3.10: C-Space Sliding-Mode Controller Experiment: Tracking Error

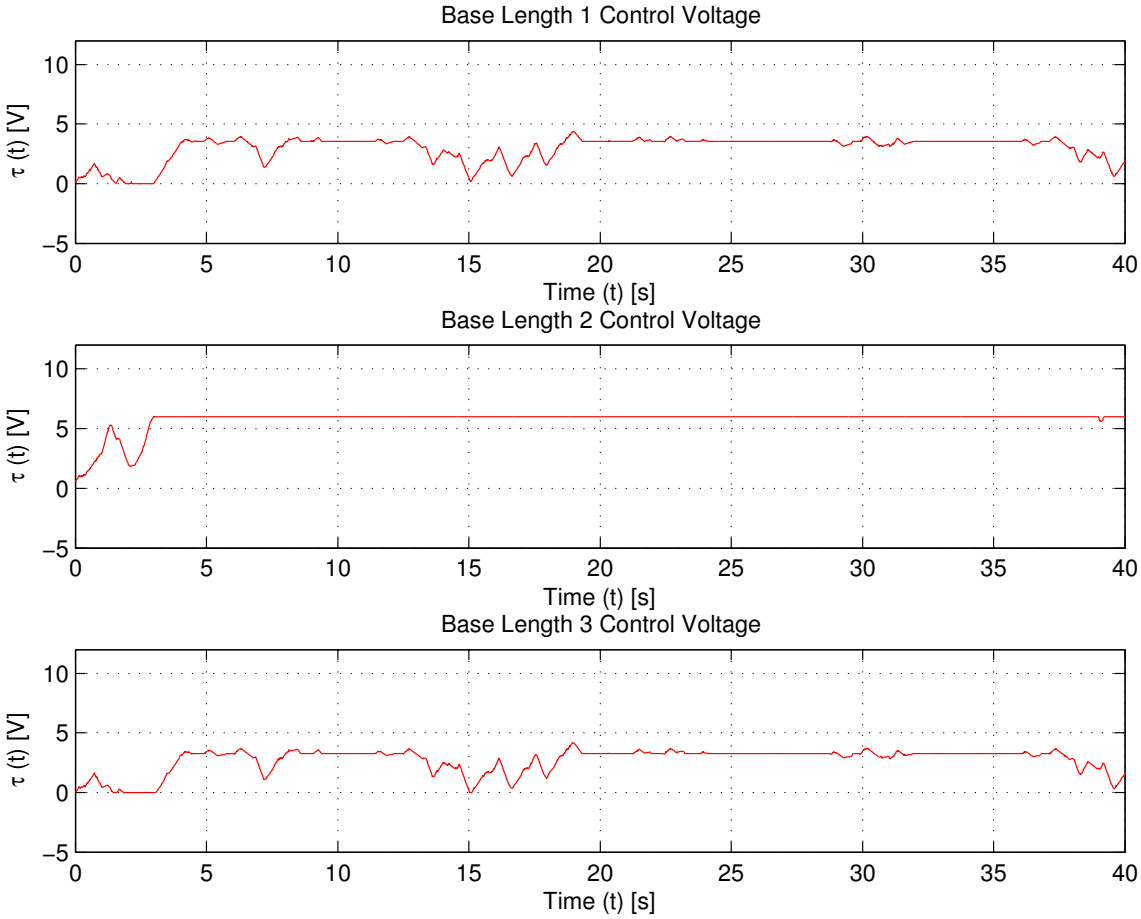

Figure 3.11: C-Space Sliding-Mode Controller Experiment: Base Actuators Control Voltage

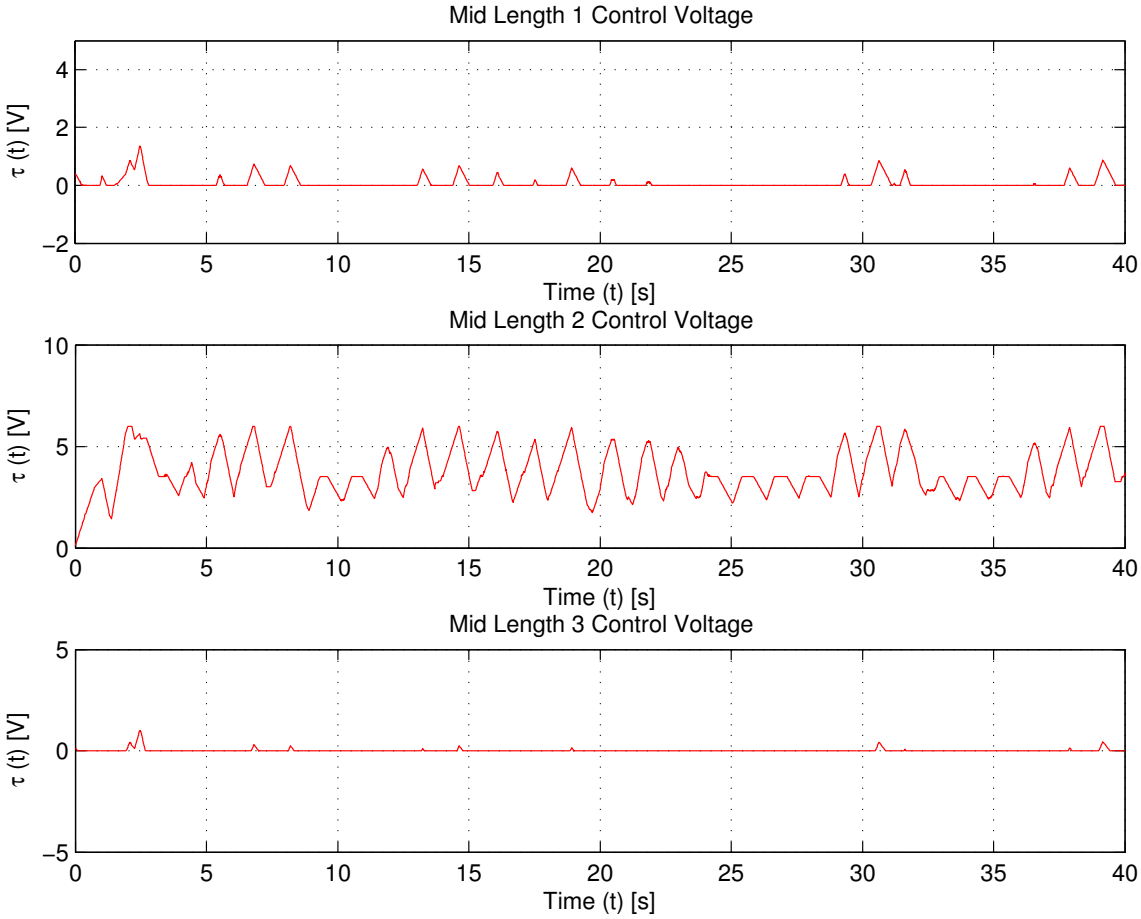

Figure 3.12: C-Space Sliding-Mode Controller Experiment: Mid Actuators Control Voltage

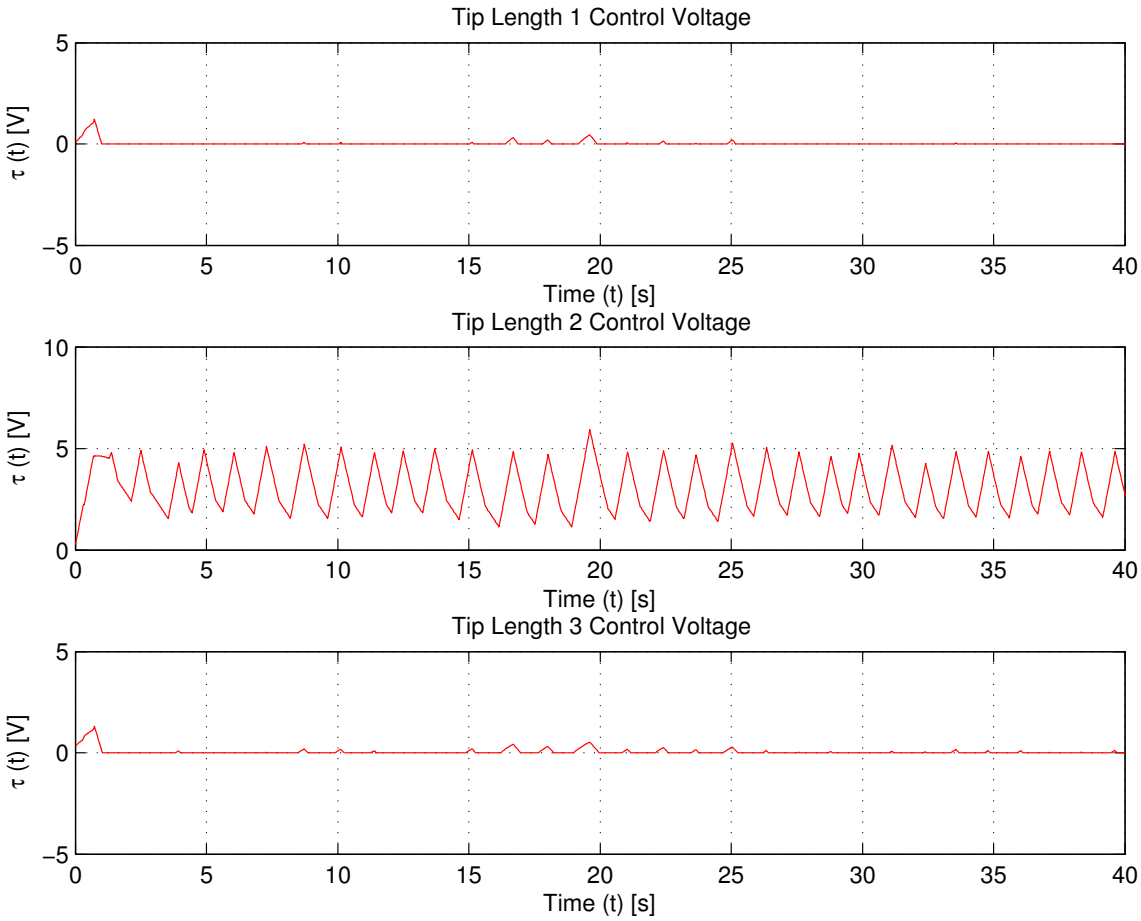

Figure 3.13: C-Space Sliding-Mode Controller Experiment: Tip Actuators Control Voltage

Chapter 4

A Study of the Self-Motion of Extensible Continuum Manipulators

In this chapter, we present the first work in categorizing the self-motion of continuum robots (*i.e.* the type and nature of internal movement where the tip remains at a fixed location). The underlying structures topologically describing the self-motion are described in [48] as self-motion manifolds. Self-motion manifolds group the infinite number of inverse kinematic solutions into a finite and bounded set of solutions. Gaining an understanding of these solutions enables practical exploitation of the manipulator self-motion. Here, we study and discuss the self-motion manifold inherent for continuum robots, analyze its null-space, characterize the self-motion, provide examples in nature or potential applications, and demonstrate the motion on the OctArm extensible continuum robot.

4.1 Self-Motion Manifolds

Self-motion manifolds of redundant manipulators have been categorized in [48]. However, the manipulators in question were rigid-link and revolute. For these manipulators, the analysis in [48] resolves the fundamental question of how many distinct self-manifolds exist (physically, how many distinct self-motions exist). In [48], it is shown that for serial rigid-link revolute manipulators, there are up to 16 potential distinct self-motion solutions. As the number of rigid links increase, the number of self motion solutions decrease, until they resemble "strings" having only one self-motion solution.

Serially-connected continuum sections bend to resemble "strings" more so than their rigid-link counterparts. However, the physical constraints continuum manipulators have in comparison to strings are significant. Thus since continuum manipulator physical motion capabilities lie in between that of redundant rigid-link robots and strings, a deeper understanding is motivated.

For rigid-link manipulators, it is shown in [48] that there exist two distinct types of pose-based self-motion manifolds. These manifolds physically corresponding to different self-motions from the "elbow up" and "elbow-down" configurations for the same position as shown in Figure 4.1(a). Multiple self-motion manifolds arise because, for some end-effector locations, there are disjoint "elbow-up" and "elbow-down" trajectories which cannot cross into each other. Such crossings occur at singular configurations. It is shown by induction in [48] that there is an upper limit (that number being 16) of distinct self-motions manifolds. However, for continuum robots the solution is quite different. In fact, the following result holds:

Theorem 2 *There is a single unique self-motion manifold for serially connected constant curvature section continuum manipulators.*

Proof. Consider a single section continuum robot. As noted in Remark 2, there exists the physical constraint that the initial tangent has to be fixed. This constraint, along with the constant curvature assumption implies that there is a unique configuration for any tip location. Thus, it can be seen that the "elbow up" and "elbow down" configurations of rigid-link robots (shown in Figure 4 (a)) do not have equivalent feasible inverse kinematic solutions for continuum manipulators. The "elbow down" equivalent of the continuum manipulator base section is possible only with a different initial mounting (π^c rotation about the $X-axis$ from that shown in Figures 2.1 and 2.2), and shown in Figure 4.1 (right). This is true for both planar and spatial sections (rotating Figure 4.1 (b) about the vertical axis still yields a unique solution given the initial vertical tangent).

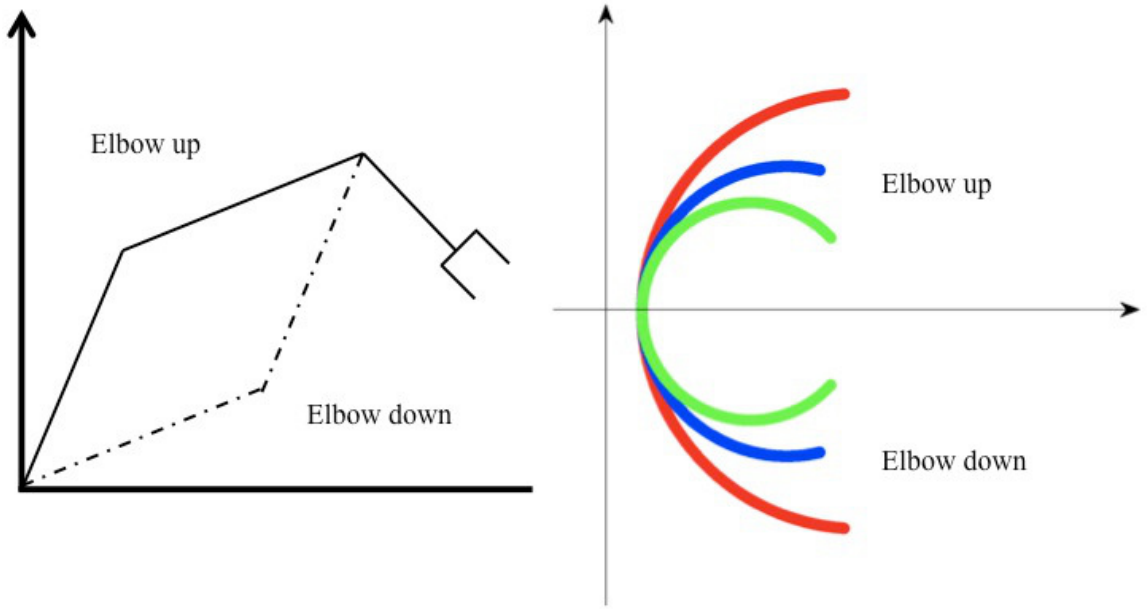

Figure 4.1: Left: The "Elbow-up" and "Elbow-down" Configurations for Rigid-Link Robots as Described in [48]. Right: The Equivalent for Continuum Robots is Only Possible For Opposite Initial Tangents, *i.e.* Physically Different Continuum Robots.

Now consider a two-section continuum manipulator. Let $\mathbb{C}$ denote the set of

locations formed by the point $\mathbb{D}$ connecting the two solutions when moving section 2 and keeping the tip fixed. Each point in $\mathbb{C}$ corresponds uniquely to a configuration of section 1 (base to $\mathbb{D}$) since that section has a unique $1-1$ kinematic map given its fixed initial tangent, as illustrated in Figures 4.2 and 4.3. Further, each point in $\mathbb{C}$ is associated with a unique tangent at the tip of section 1; this tangent connects section 1 and section 2 ($\mathbb{D}$ to tip) (the tip of each section has the physical constraint of being collinear with the initial tangent from base of the next section). This means that any point in $\mathbb{C}$ uniquely defines an initial tangent for section 2, implying a 1-1 kinematic map between section 2 configurations and the given section tip point (in planar or 3-Dimensional situations). The robot must inherit the unique tangent at the end of section 1. Because section 2 has to begin at the same point, with its own uniquely specified tangent, there exists a single unique configuration for section 2 for a given tip location. Thus, any self-motion trajectory corresponds to a unique self-motion trajectory, and hence there exists only a single self-motion manifold.

By induction, it can be seen that there is only one self-motion manifold for any serially connected, constant curvature, multi-section continuum robot. Given that any two sections have to be collinear at their intersection point, for 2 sections of a continuum manipulator, the angles-of-orientation for each section have a unique 1-1 kinematic map for a set of section lengths and curvatures corresponding to the subsequent fixed tip location. ■

The self-motion manifold for continuum manipulators, unlike its rigid-link counterparts, is also not hindered by singularities. This is because singular configurations exist only when each manipulator section is straight along the axis its base is tangential to, resulting in the curvature $k(t) = 0$. This lack of singularities within the rest of the configuration-space results in self-motion solutions easily "traveling into" one another as opposed to being divided by a loci of singularities in the rigid-link

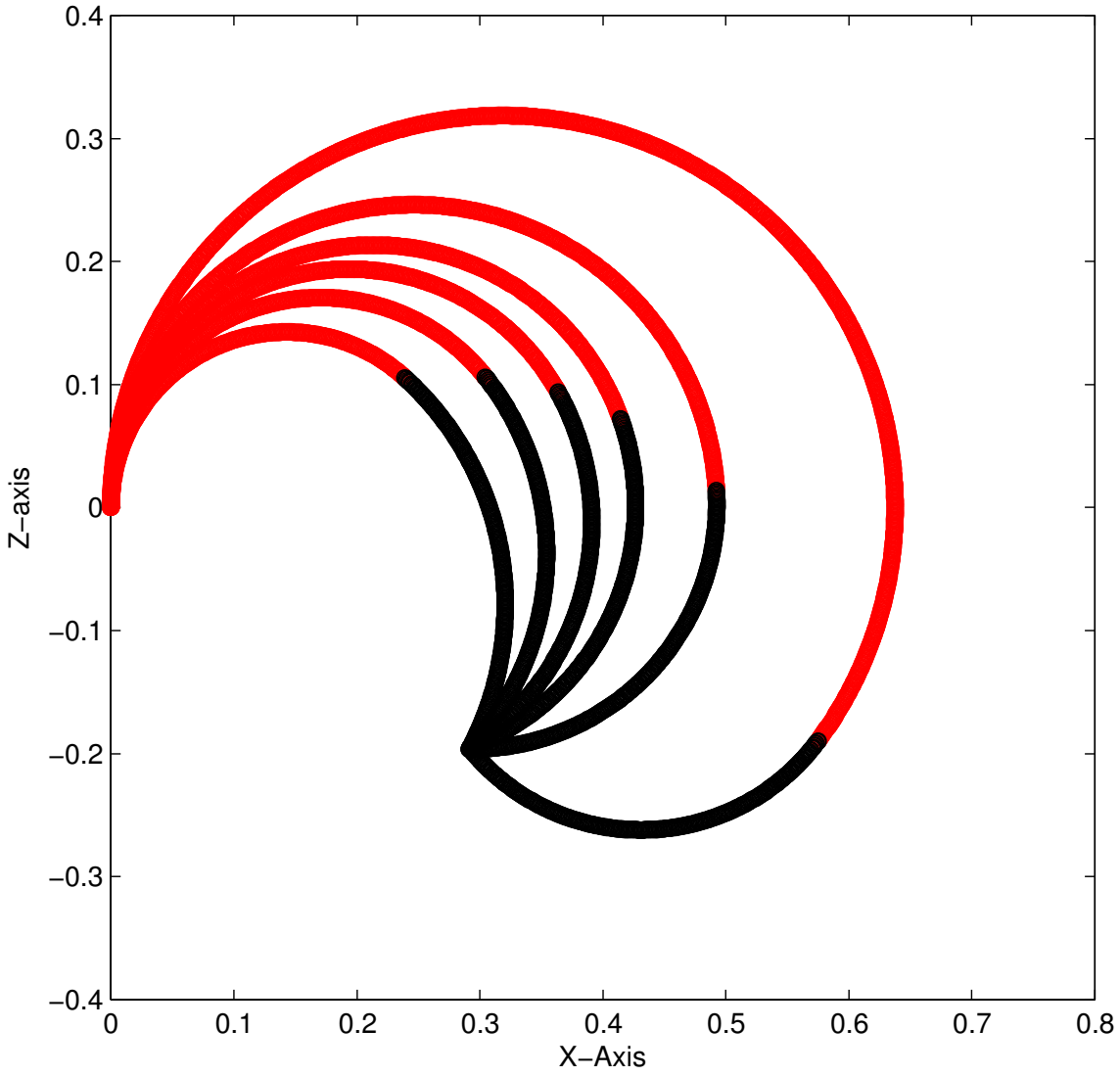

Figure 4.2: The 2-Section Continuum Manipulator, Showing a Planar $1-1$ Kinematic Map for the Point Connecting Sections 1 and 2.

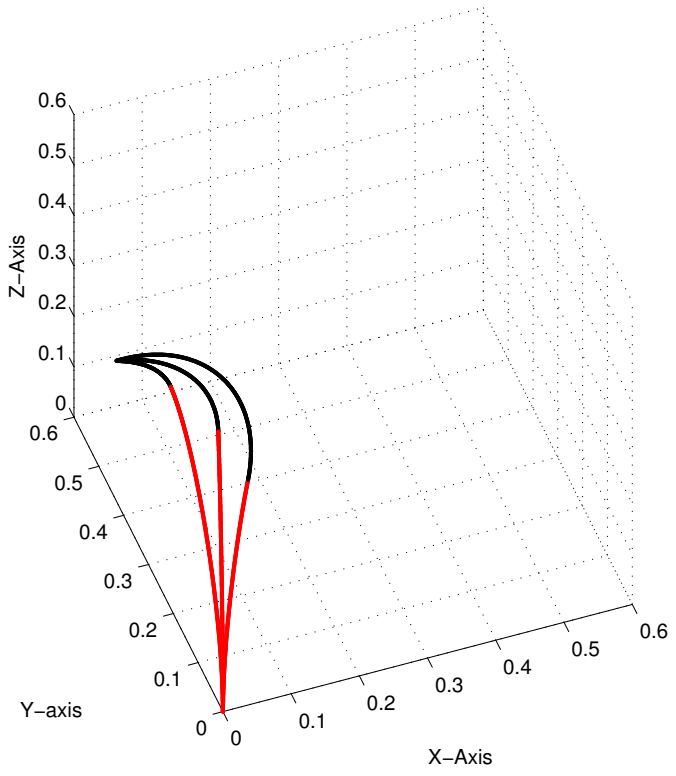

Figure 4.3: The 2-Section Continuum Manipulator, Showing a Spatial $1-1$ Kinematic Map for the Point Connecting Sections 1 and 2.

cases.

4.2 The Null-Space: Local Analysis

4.2.1 Velocity Kinematics

A two-section extensible continuum manipulator as seen in Figure 2.2 is kinematically redundant for 3D (X-Y-Z) positioning tasks in 3D space as it has 6 Degrees of Freedom (DOFs). Redundancy also exists for the XZ planar positioning case (by setting $\phi_1(t) = \phi_2(t) = 0$), since 4 DOFs still exist ($s_1(t)$, $k_1(t)$, $s_2(t)$, and $k_2(t)$).

Given that such manipulators are redundant, their inverse kinematics for the manipulator yield non-unique solutions. This means that there exist infinite manipulator configurations for the same position of the manipulator tip, the very property which produces the self-motion. Thus the manipulator configuration cannot be conveniently computed in closed form from positional inverse kinematics. Due to this, we next utilize the manipulator velocity kinematics.

The velocity kinematics for the extensible continuum manipulator can be obtained by taking the time derivative of the kinematic model in (2.1), and are given here by

$$\dot{x} = J(\psi)\,\dot{\psi}, \tag{4.1}$$

where $J(\cdot) \in \mathbb{R}^{m\times n}$ is the Jacobian matrix defined by

$$J = \frac{\partial f(\cdot)}{\partial \psi}, \tag{4.2}$$

in which $\dot{x}(t) \in \mathbb{R}^m$ represents the task-space velocity and $\dot{\psi} \in \mathbb{R}^n$ represents the

configuration-space velocity. Thus the spatial velocity Jacobian is found to be

$$J \triangleq \begin{bmatrix} \frac{\partial X}{\partial s_1} & \frac{\partial X}{\partial k_1} & \frac{\partial X}{\partial \phi_1} & \frac{\partial X}{\partial s_2} & \frac{\partial X}{\partial k_2} & \frac{\partial X}{\partial \phi_2} \\ \\ \frac{\partial Y}{\partial s_1} & \frac{\partial Y}{\partial k_1} & \frac{\partial Y}{\partial \phi_1} & \frac{\partial Y}{\partial s_2} & \frac{\partial Y}{\partial k_2} & \frac{\partial Y}{\partial \phi_2} \\ \\ \frac{\partial Z}{\partial s_1} & \frac{\partial Z}{\partial k_1} & \frac{\partial Z}{\partial \phi_1} & \frac{\partial Z}{\partial s_2} & \frac{\partial Z}{\partial k_2} & \frac{\partial Z}{\partial \phi_2} \end{bmatrix}, \tag{4.3}$$

whose elements are detailed in Appendix B.

4.2.2 Resolved Motion Rate Inverse Kinematics

To numerically solve the inverse kinematics problem for non-redundant manipulators in the velocity domain conceptually, given an initial configuration, an initial motion is fed on both sides of (4.1) to be multiplied by $J(\cdot)^{-1}$ (when $[J]^{-1}$ is defined and invertible) resulting in

$$\dot{\psi} = [J]^{-1} \dot{x}. \tag{4.4}$$

The expression in (4.4) can then be numerically integrated to obtain $\psi(t)$. This method of obtaining a robot configuration from the velocity kinematics is known as the "resolved-motion rate" approach [69].

However, for kinematically redundant manipulators, $J(\cdot)$ is never square, in which case matrix inversion is not directly possible. Thus the Moore-Penrose pseudoinverse of $J(\cdot)$, given by $J^{+}(\cdot) = J^{T}\left(JJ^{T}\right)^{-1} \in \mathbb{R}^{n \times m}$, is often utilized. The pseudoinverse $J^{+}(\cdot)$ satisfies the property $JJ^{+} = I_m$ where I_m is the $m \times m$ identity matrix. Further Moore-Penrose Pseudoinverse properties are provided in Appendix A. For kinematically redundant manipulators, the inverse kinematics solution in the

velocity space can be given by

$$\dot{\psi} = [J]^{+} \dot{x}. \tag{4.5}$$

Along with finding a specific inverse kinematic solution for redundant manipulators, it is important to characterize all the solutions. Thus, the pseudoinverse solution is modified, resulting in (4.5) to be rewritten as

$$\dot{\psi} = [J]^{+} \dot{x} + \left[I_n - J^{+}J\right] \epsilon, \tag{4.6}$$

where $I_n \in \mathbb{R}^{n \times n}$ is the $n \times n$ identity matrix and $\epsilon \in \mathbb{R}^{n \times 1}$ is an arbitrary vector. Both terms on the right side of (4.6) represent joint velocities and can be further denoted as

$$\dot{\psi} = \dot{\psi}_P + \dot{\psi}_N, \tag{4.7}$$

where $\dot{\psi}_P \in \mathbb{R}^{n \times 1}$ represents the particular solution and $\dot{\psi}_N \in \mathbb{R}^{n \times 1}$ (the null-space vector) represents the homogeneous solution. Furthermore

$$\begin{aligned} \dot{\psi}_P &= [J]^{+} \dot{x} \\ \dot{\psi}_N &= [I_n - J^{+}J] \, \epsilon. \end{aligned} \tag{4.8}$$

The homogeneous (null-space) solution has the property that $[J]\dot{\psi}_N = 0$, i.e. solutions $\dot{\psi}_N$ (parameterized by the arbitrary ϵ) are joint velocities that produce no tip motion, and thus generate the self-motion.

Thus, to better explore the self-motion of extensible continuum manipulators, we calculate the Jacobian null-space and analyze manipulator motion in that space. To that end, we begin with the spatial 2-section extensible continuum robot, for which

the null-space matrix, denoted by $\xi_N(t) \in \mathbb{R}^{6\times 6}$, is defined as

$$\xi_N \triangleq I_6 - J^+ J, \tag{4.9}$$

where $I_6 \in \mathbb{R}^{6\times 6}$ represents an identity matrix, and $J^+(\cdot) \in \mathbb{R}^{6\times 3}$ is the Moore-Penrose pseudoinverse of the Jacobian matrix, $J(\cdot)$. The columns (or rows) of $\xi_N(t)$ span the null space in $\mathbb{R}^6$.

4.3 Self-Motion Characterization

To better understand the self-motion behavior of continuum manipulators we consider 4 cases for 2-section extensible continuum robots:

1. Planar constant second section curvature case;
2. Planar constant second section length case;
3. Spatial constant second section orientation case;
4. General motion case.

In case 1 and case 2, the constant curvature and length respectively represent restrictions on curvature and length of the second section only. In these cases, because we are considering motion in the plane, $\phi_1(t) = \phi_2(t) = 0$ (these restrictions do not apply to cases 3 and 4). In all cases the first section is free to move without any constraints while the manipulator tip remains fixed at its initial point. No physical restrictions have been placed on the manipulator section lengths or curvatures except $s_i(t) > 0$ and $r_i(t) > 0$ (*i.e.* $k_i(t) < \infty$).

4.3.1 Planar Self-Motion Due To Extension

In this case, the first section has no constraints on its length or curvature while the length of the second section is free to change with its curvature being fixed, as seen in Figure 4.4. Further, it can be seen that the overall shape of the manipulator remains the same despite the changes in section lengths. This is probably the most intuitive self-motion case.

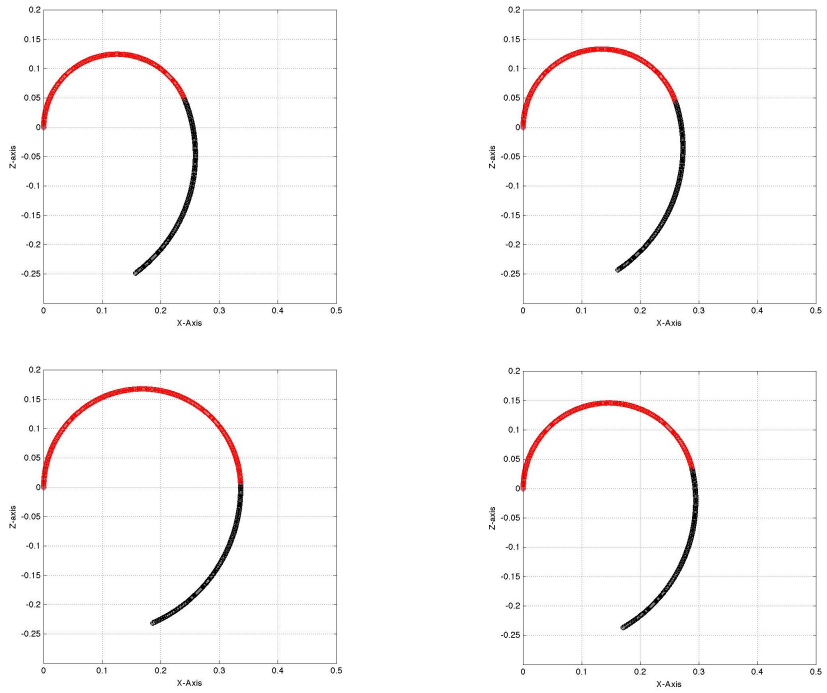

Figure 4.4: Time Lapse: Planar Self-Motion Due To Extension. The Time Lapse is Clockwise Starting from the Top Left.

Based on (4.6), the velocity kinematics for this case can be given by

$$\dot{\psi}_{cc} = \begin{bmatrix} \dot{s_1} \\ \dot{k_1} \\ 0 \\ \dot{s_2} \\ 0 \\ 0 \end{bmatrix} = [J_{cc}]^{+} \dot{x} + \left[I_6 - J_{cc}^{+} J_{cc}\right] \epsilon, \tag{4.10}$$

where $\dot{\psi}_{cc}(t) \in \mathbb{R}^6$ represents the configuration space velocity, $J_{cc}(t) \in \mathbb{R}^{3\times 6}$ is the Jacobian for the second section constant curvature case, $J_{cc}^{+}(t) \in \mathbb{R}^{6\times 3}$ is the pseudoinverse of $J_{cc}(t)$, and $\epsilon(t) \in \mathbb{R}^5$ is an arbitrary vector. Because this motion is planar, $\phi_1(t) = \phi_2(t) = \dot{\phi}_1(t) = \dot{\phi}_2(t) = 0$. Let the homogeneous solution in (4.10) be defined by the variable $\dot{\psi}_{cc_N} \in \mathbb{R}^3$ such that

$$\dot{\psi}_{cc_N} \triangleq \left[I_6 - J_{cc}^{+} J_{cc}\right] \epsilon, \tag{4.11}$$

The $\dot{k_2}(t)$ term in (4.10) is replaced by a zero because, due to constant curvature, $\dot{k_2}(t) = 0$.

4.3.2 Planar Self-Motion Due to Bending

In this case, the curvature of the second section is variable while its length is kept constant and there are no restrictions on the base section. Figure 4.5.

Based on (4.6), and parallel to (4.10) the velocity kinematics for this case can

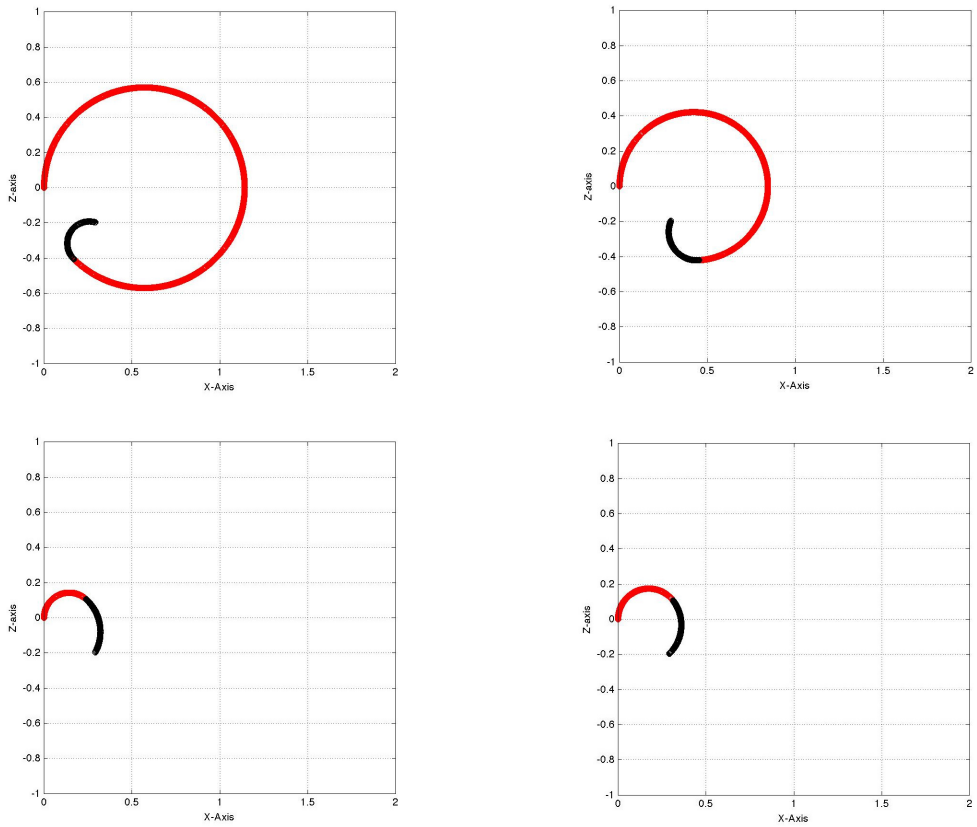

Figure 4.5: Time Lapse: Planar Self-Motion Due To Bending. The Time Lapse is Clockwise Starting from the Top Left.

be given by

$$\dot{\psi}_{cl} = \begin{bmatrix} \dot{s_1} \\ \dot{k_1} \\ 0 \\ 0 \\ \dot{k_2} \\ 0 \end{bmatrix} = [J_{cl}]^{+} \dot{x} + \left[I_6 - J_{cl}^{+} J_{cl}\right] \epsilon, \tag{4.12}$$

where $\dot{\psi}_{cl}(t) \in \mathbb{R}^6$ represents the configuration space velocity, $J_{cl}(t) \in \mathbb{R}^{3\times 6}$ is the Jacobian for the second section constant curvature case, $J_{cl}^{+}(t) \in \mathbb{R}^{6\times 3}$ is the pseudoinverse of $J_{cl}(t)$, and $\epsilon(t) \in \mathbb{R}^6$ is an arbitrary vector. Because this motion is planar, $\phi_1(t) = \phi_2(t) = \dot{\phi}_1(t) = \dot{\phi}_2(t) = 0$. Let the homogeneous solution in (4.12) be defined by the variable $\dot{\psi}_{cl_N} \in \mathbb{R}^6$ such that

$$\dot{\psi}_{cl_N} \triangleq \left[I_6 - J_{cl}^{+} J_{cl}\right] \epsilon, \tag{4.13}$$

The $\dot{s_2}(t)$ term in (4.12) is replaced by a zero because, due to constant length, $\dot{s_2}(t) = 0$.

4.3.3 Self-Motion Due to Constrained Angle-of-Orientation

In this case, neither section of the manipulator has any constraints on the variable section lengths and curvatures. However, while the base section angle-of-orientation is variable, the angle-of-orientation of the second section is kept constant. Figure 4.6 demonstrates this motion. Based on (4.6), the velocity kinematics for this

case can be given by

$$\dot{\psi}_{co} = \begin{bmatrix} \dot{s_1} \\ \dot{k_1} \\ \dot{\phi_1} \\ \dot{s_2} \\ \dot{k_2} \\ 0 \end{bmatrix} = [J_{co}]^{+} \dot{x} + \left[I_6 - J_{co}^{+} J_{co}\right] \epsilon, \tag{4.14}$$

where $\dot{\psi}_{co}(t) \in \mathbb{R}^6$ represents the configuration-space velocity, $J_{co}(t) \in \mathbb{R}^{3\times 6}$ is the Jacobian for the second section constant angle-of-orientation case, $J_{co}^{+}(t) \in \mathbb{R}^{6\times 3}$ is the pseudoinverse of $J_{co}(t)$ and $\epsilon(t)$ is an arbitrary vector. Let the homogeneous solution in (4.14) be defined by the variable $\dot{\psi}_{co_N} \in \mathbb{R}^6$ such that

$$\dot{\psi}_{co_N} \triangleq \left[I_6 - J_{co}^{+} J_{co}\right] \epsilon, \tag{4.15}$$

The $\dot{\phi_2}(t)$ term in (4.14) is replaced by a zero because, due to constant angle-of-orientation, $\dot{\phi_2}(t) = 0$.

4.3.4 The General Motion Case

We now consider the general self motion case allowing for the manipulator to be completely unrestricted in its self-motion.

Theorem 3 *The general self-motion of spatial 2-section extensible continuum manipulators is spanned by the constrained manipulator self-motion velocities defined above.*

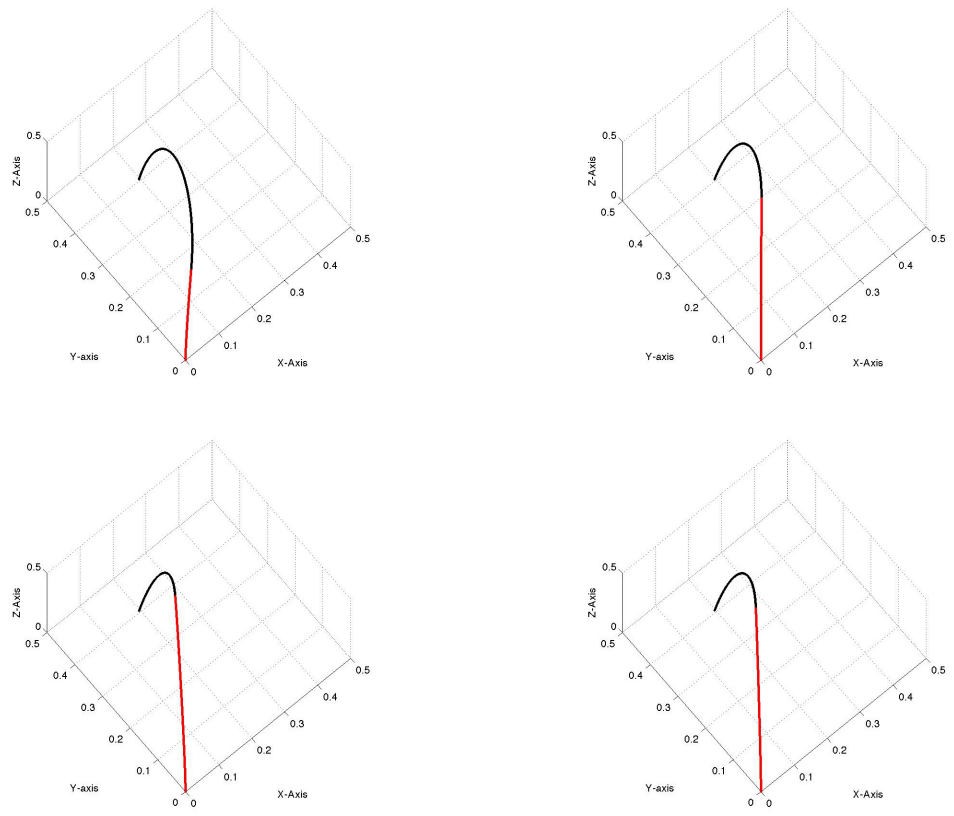

Figure 4.6: Time Lapse: Spatial Self-Motion Due To Fixed Angle-of-Orientation. The Time Lapse is Clockwise Starting from the Top Left.

Proof. The null-space vector in (4.10) can be viewed and expanded into $\mathbb{R}^6$ as

$$\dot{\psi}_{cc_N} = \begin{bmatrix} \dot{s}_{1_{cc_N}} \\ \dot{k}_{1_{cc_N}} \\ \dot{\phi}_{1_{cc_N}} \\ \dot{s}_{2_{cc_N}} \\ 0 \\ \dot{\phi}_{2_{cc_N}} \end{bmatrix} \in N\left[J\right]. \tag{4.16}$$

The 5^{th} element of ψ_{cc}, nominally $\dot{k}_2(t)$ does not exist for this case (constant second section curvature) and thus its position is padded with a zero. Note that (4.16) remains a self-motion velocity for the manipulator, (*i.e.* $[J]\psi_{ee} = 0$). Similarly, (4.12) can be expanded as,

$$\dot{\psi}_{cl_N} = \begin{bmatrix} \dot{s}_{1_{cl_N}} \\ \dot{k}_{1_{cl_N}} \\ \dot{\phi}_{1_{cl_N}} \\ 0 \\ \dot{k}_{2_{cl_N}} \\ \dot{\phi}_{2_{cl_N}} \end{bmatrix} \in N\left[J\right]. \tag{4.17}$$

As the $\dot{s_2}(t)$ term does not exist and therefore has no effect on the manipulator motion due the constant length second section case being considered, its position is thus padded by a zero. Similar to (4.16) and (4.17), the expression in (4.14) can be

expanded to give

$$\dot{\psi}_{co_N} = \begin{bmatrix} \dot{s}_{1_{co_N}} \\ \dot{k}_{1_{co_N}} \\ \dot{\phi}_{1_{co_N}} \\ \dot{s}_{2_{co_N}} \\ \dot{k}_{2_{co_N}} \\ 0 \end{bmatrix} \in N\left[J\right]. \tag{4.18}$$

The location of the $\dot{\phi}_2(t)$ term is padded with a 0 because it doesn't exist in that case.

From the general inverse kinematic solution in (4.6) (valid through the workspace except for the infinitesimally thin subspaces of the local X and Z axes, *i.e.* $k_i(t) = \sigma$), for $[J(t)]$ of full rank 3, it can be seen that $[I - J^{+}J]$ is also of rank 3, and thus the columns of $[I - J^{+}J]$ span the null-space [75]. The general null-space is thus 3-dimensional, and given that the vectors in (4.16), (4.17), and (4.18) are clearly in the null-space of $[J]$ and independent of each other, they form a basis for the null-space, resulting in

$$\dot{\psi} = \begin{bmatrix} \dot{s}_1 \\ \dot{k}_1 \\ \dot{\phi}_1 \\ \dot{s}_2 \\ \dot{k}_2 \\ \dot{\phi}_2 \end{bmatrix}. \tag{4.19}$$

Thus, we can see that (4.19) must result from a the linear combination of the vectors in (4.16), (4.17) and (4.18),

$$\dot{\psi} = K_{cc}\dot{\psi}_{cc_N} + K_{cl}\dot{\psi}_{cl_N} + K_{co}\dot{\psi}_{co_N}, \tag{4.20}$$

where K_{cc}, K_{cl} and $K_{co} \in \mathbb{R}$ are constants. ■

An example of the general self-motion, generated using (4.20), in Figure 4.7.

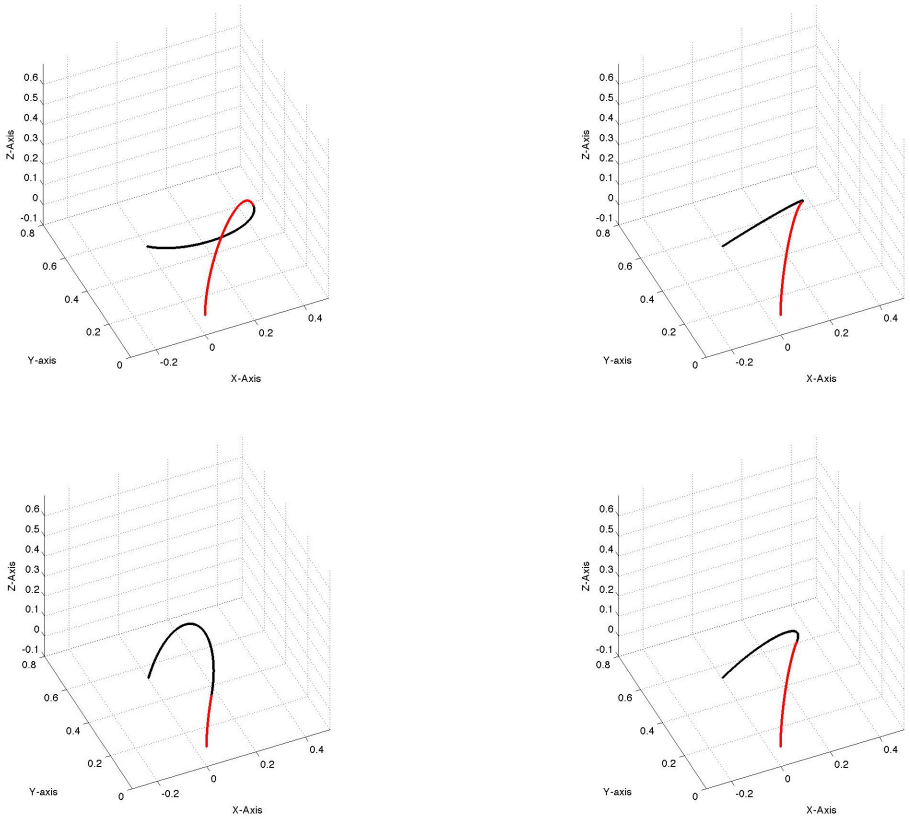

Figure 4.7: Time Lapse: Unconstrained Spatial Motion. The Time Lapse is Clockwise Starting from the Top Left.

It should be noted that in this case, the tip location was found to be at [0 0.5274 $-$ 0.0921], and as in all previous cases, the manipulator base is located at the origin, though the viewing angle could initially suggest otherwise.

4.3.5 Exploitation of Continuum Robot Self-Motion

Exposure of the underlying base structure of the continuum robot self-motion in the previous subsections yields new insight into how the self-motion could be

used innovatively in application scenarios. For example, the constant curvature base self-motion lends itself to construction and manipulation tasks. When the second section has a constant curvature constraint, it could potentially be used as a wrench-like device for large screws or bolts, with the curvature of the section matching the curvature of the bolt (or screw) head. With the curvature fixed, the base section length and curvature as well as the length of the second section can be changed so as to tighten or loosen the hold as required.

One application unique to continuum manipulators is that of rolling an object. Mobile hospital units often need help turning a patient over, especially in cases of rehabilitation. In this case, a 2-section continuum manipulator could maneuver around the patient with the tip's location setting up it's fixed point under the patient. Using self-motion, the tip section would increase it's curvature to leverage the patient while the base section reduces its length so as to pull the patient back. This motion would effectively roll the patient over. This is analogous to the way nurses utilize their hands and arms to roll a patient over. To do so, the nurse would leverage their hands around and under the patient while standing on the other side. The nurse then pulls their hands out and back while leveraging the patient with their elbows to avoid slip and thus rolling the patient over in their bed.

One potential application when the manipulator is unconstrained is on-sea refueling. The ships would line up next to each other and a continuum robot hose would be used for transmitting the fuel. Given that the ships are constantly in relative motion due to the active sea states and the high pressure with which the fuel is being transmitted, it is imperative that the "hose" not flail about in the event of a disconnection and that the configuration be compliant. Exploitation of the manipulator null-space is necessary in such situations.

A novel way to apply continuum manipulators is using two continuum sections

as a hand-finger equivalent with the hand and the finger distinguished from each other at the point where the sections join. The constant curvature paradigm could be used for the hand in order to set leverage a tip position similar to a lasso winding around an object. The constant length self-motion and/or base section motion can then change its shape to manipulate the object as required. For example, once the tip location is fixed at a point on the edge of an object (a circular wedge, as seen in Figure 4.8), the arm can ease itself into wrapping around the object by matching curvatures and adjusting lengths. Once the object is grasped, it can be manipulated by changing the shape of the base section as needed.

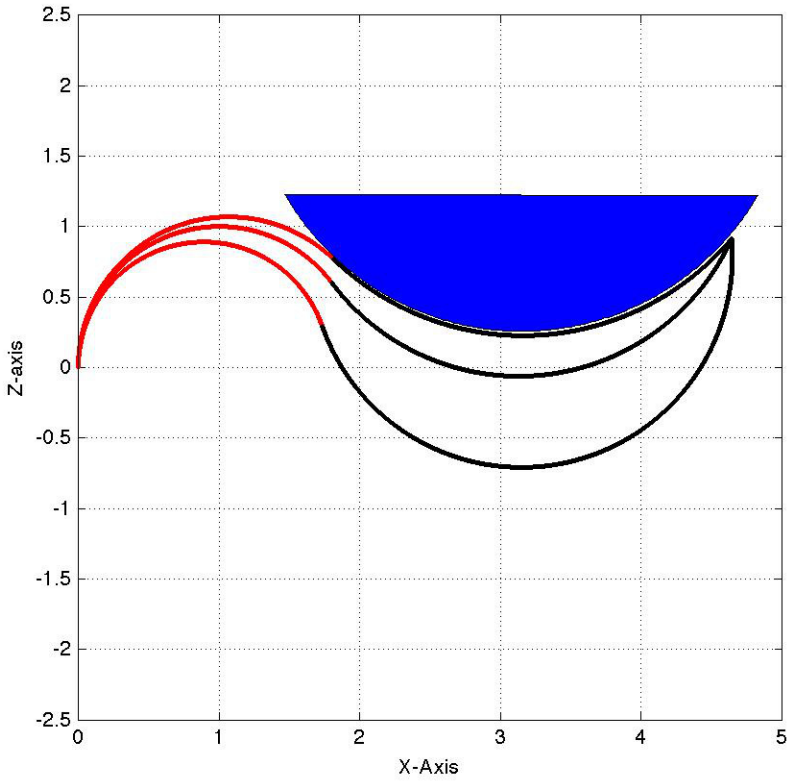

Figure 4.8: An example of a continuum manipulator (from bottom to top) grasping an object by matching curvatures.

Having grasped an object or a kitchen utensil, such as a mug, flask, bowl, or stock pot, varying angle-of-orientation for a fixed tip location allows for the arm to pour the contents out of the utensil as seen in Figure 4.9.

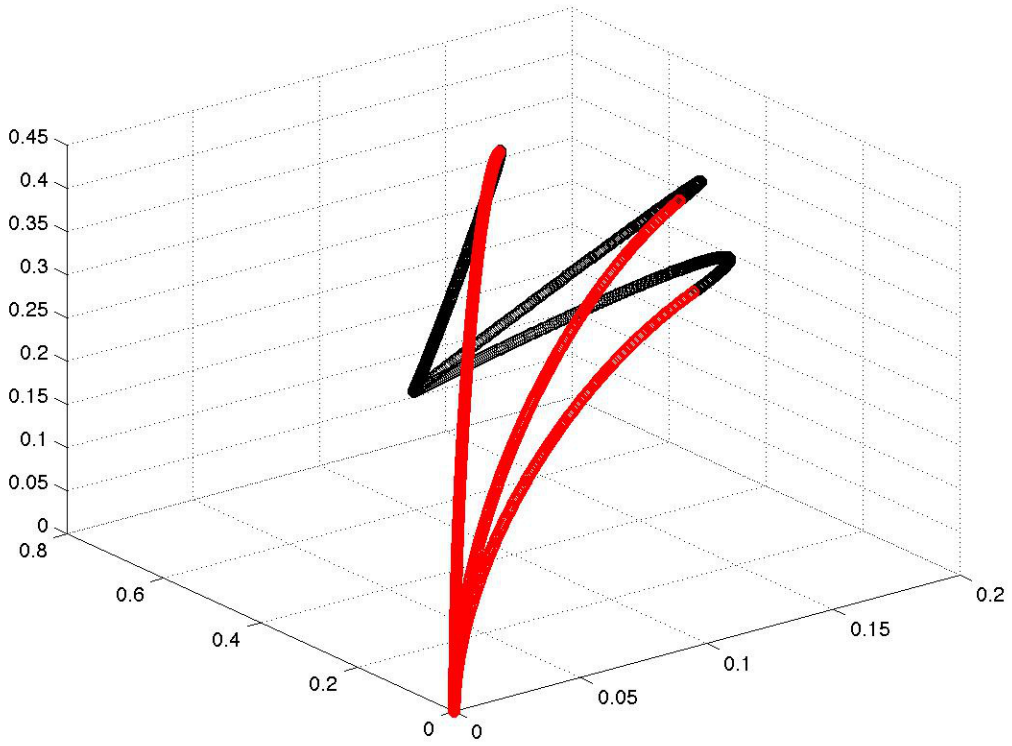

Figure 4.9: An example of changing angle of orientation (from right to left) demonstrating the effect of pouring material out of a utensil.

4.4 Experimental Validation

Experiments to further explore self-motion of extensible continuum manipulators were conducted on the 9-Degree-Of-Freedom OctArm continuum manipulator [5].

The pressure regulator signals that actuate the OctArm are generated using a

Matlab/Simulink^{TM}block diagram via a Quanser^{TM}data acquisition system. Figure 4.10 shows the ability of the OctArm to have different section lengths and curvatures for a single tip location demonstrating planar self-motion while Figure 4.11 demonstrating spatial self-motion. In both cases, the tip was loosely tied to metal bar allowing varying orientation for the same location.

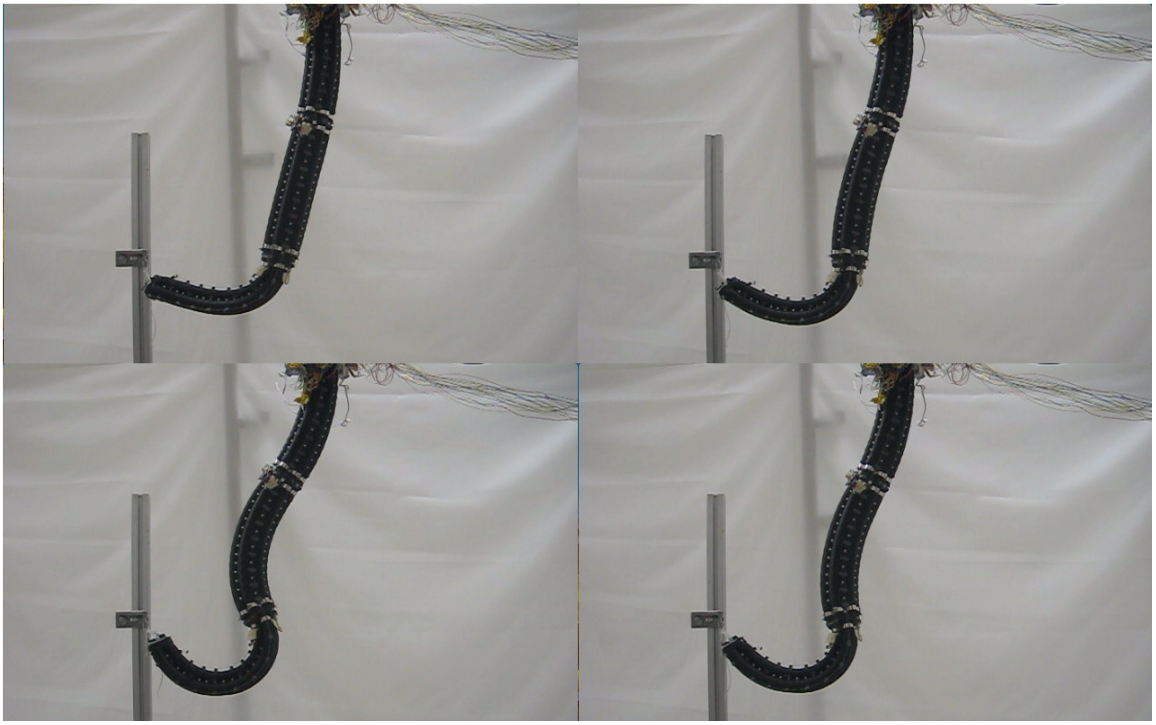

Figure 4.10: OctArm Planar Self-Motion starting at the top left and continuing clockwise.

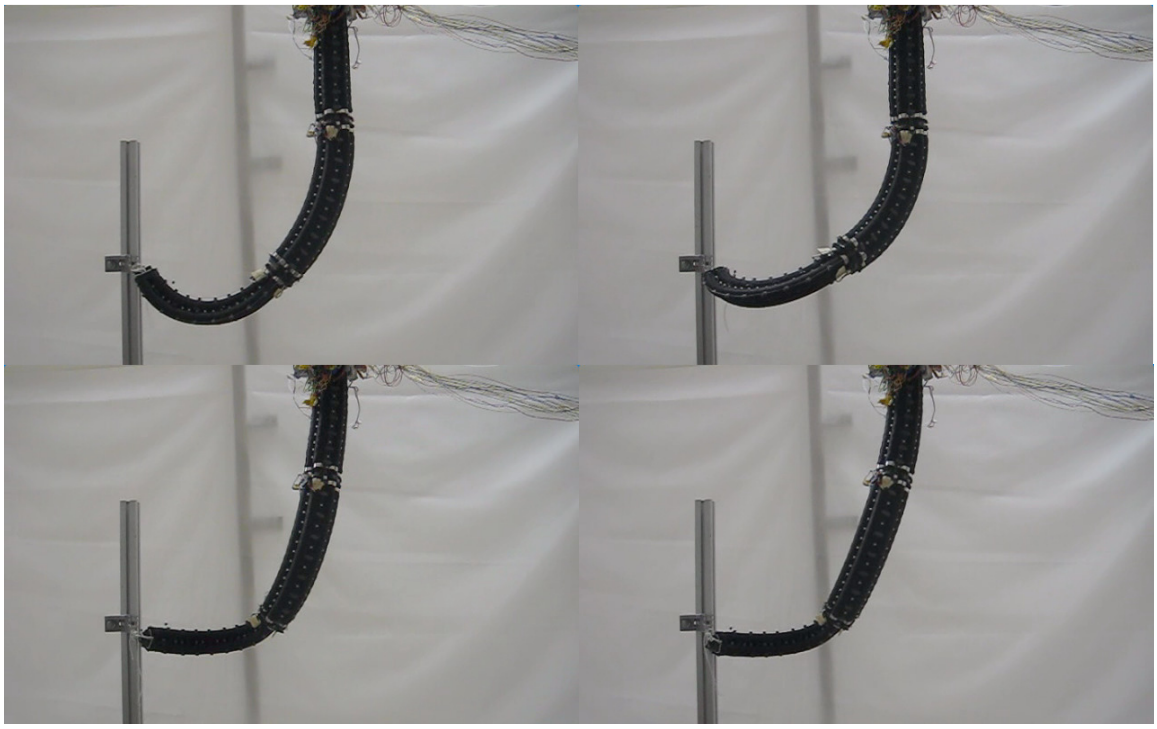

Figure 4.11: OctArm Spatial Self-Motion starting at the top left and continuing clockwise.

Chapter 5

Teleoperation Control of a Redundant Continuum Manipulator Using a Non-Redundant Rigid-Link Master

One of the most useful properties of redundant robots is their ability to change their shape without a change in the system tip (or end-effector) location. This is especially useful for performing tasks that require obstacle avoidance, or necessitates that the manipulator itself avoids motion limits and singularities. When required for teleoperation, one current disadvantage for extensible continuum manipulators is the lack of availability of other robots which are physically and kinematically similar. This issue requires that control solutions be found accordingly; where the master system would only regulate the tip of the slave continuum system with the slave system modifying its own shape based on the requirements of its local environment. A teleoperation controller addressing this question would be useful in a cluttered pick-

and-place environment in which the slave system might need to operate. Another use of such teleoperation could be for the on-sea refueling problem detailed in Chapter 4.3. Additionally, the insight into the self-motion of redundant, extensible, continuum manipulators gained in Chapter 4 can be utilized especially with the examples provided in Section 4.3.5.

Here, the teleoperation of a 9-DOF redundant extensible continuum manipulator (the slave) by a 2-section, planar, rigid-link, revolute robot (the master) is described. Despite the kinematic dissimilarity of the master and slave systems, the proposed controller ensures that the tip of the slave system tracks the end-effector of the master while the sub-task controller of the slave system ensures redundancy resolution (*e.g.* section length and limit avoidance, singularity avoidance etc.). A Lyapunov-type analysis proves stability while numerical simulation and experimental results highlight the ability of the proposed controller.

5.1 Mathematical Model

5.1.1 Dynamic Model

The dynamic models for both the master and slave systems are described by the standard Euler-Lagrangian form

$$M_i \ddot{q}_i + \tilde{N}_i = \tau_i + J_i^T F_i \tag{5.1}$$

where $i = 1$ represents the master system and $i = 2$ represents the slave system. The number of joints of the master system is denoted by n_1, whereas n_2 represents the number of slave system section lengths and curvatures.

The number of DOFs of master and slave systems are equal to $n_1 \in \mathbb{N}$ and

$n_2 \in \mathbb{N}$ respectively, where $n_2 > n_1$, highlighting the kinematic dissimilarity between the two systems. In (5.1), $q_1(t), \dot{q}_1(t), \ddot{q}_1(t) \in \mathbb{R}^{n_1}$ denote the position, velocity, and acceleration of the master system rigid-links. The terms $q_2(t), \dot{q}_2(t), \ddot{q}_2(t) \in \mathbb{R}^{n_2}$ represent the slave system section lengths and curvatures and their first- and second-order rates of change respectively. $M_i(q_i) \in \mathbb{R}^{n_i \times n_i}$ represents the inertia matrix, $\tilde{N}_i(q_i, \dot{q}_i) \in \mathbb{R}^{n_i}$ represents other dynamic effects (centripetal-Coriolis effects, gravitational forces, and other dynamic frictional effects), $\tau_i(t) \in \mathbb{R}^{n_i}$ represents the control input vector, $F_i(t) \in \mathbb{R}^{n_i}$ represents the task-space interaction forces, and $J_i(q_i) \in \mathbb{R}^{n_1 \times n_i}$ represents the Jacobian matrices for the master and slave systems[1]. The inertia matrix $M_i(\cdot)$ is symmetric and positive-definite, and satisfies the following inequalities [74]

$$m_{1i} \|\xi\|^2 \leq \xi^T M_i(\cdot) \xi \leq m_{2i} \|\xi\|^2 \qquad \forall \xi \in \mathbb{R}^{n_i} \tag{5.2}$$

where m_{1i}, $m_{2i} \in \mathbb{R}$ are positive constants and $\|\cdot\|$ denotes the standard Euclidean norm.

5.1.2 Kinematic Model

The kinematic models for the master and slave systems are defined as

$$x_i \triangleq f(q_i), \tag{5.3}$$

where $x_i(t) \in \mathbb{R}^{n_1}$ is the task-space position and $f(q_i) \in \mathbb{R}^{n_i}$ represents the forward kinematics of the manipulator. The first and second time derivatives of (5.3) are

[1]For the slave system, the $\tilde{N}_i(q_i, \dot{q}_i)$ term represents a catchall for the $N_i(q_i, \dot{q}_i)$, $G(q)$, $B(q)$, and $E(q)$ terms of the continuum manipulator dynamics in (3.3) from Chapter 3.

found to be

$$\begin{aligned} \dot{x}_i &= J_i \dot{q}_i \\ \ddot{x}_i &= \dot{J}_i \dot{q}_i + J_i \ddot{q}_i, \end{aligned} \tag{5.4}$$

where the first time derivative in (5.4) represents the velocity kinematics. For the redundant continuum slave system ($i = 2$), the Jacobian is similar to the one in (4.3) from Chapter 4 with terms added or removed depending on the configuration of the system involved in the teleoperation. Rearranging the terms in (5.4) results in

$$\ddot{q}_1 = J_1^{-1} \left(\ddot{x}_1 - \dot{J}_1 \dot{q}_1 \right) \tag{5.5}$$

$$\ddot{q}_2 = J_2^{+} \left(\ddot{x}_2 - \dot{J}_2 \dot{q}_2 \right) + \ddot{q}_N \tag{5.6}$$

where $\ddot{q}_N(t) \in \mathbb{R}^{n_2}$ is an auxiliary vector in the null-space of $J_2(\cdot)$ and $J_2^{+}(q_2) \in \mathbb{R}^{n_2 \times n_1}$ is the Moore-Penrose pseudo-inverse of the Jacobian of the slave system (more Moore-Penrose properties are found Appendix A).

Assumption 1 *The kinematic and dynamic terms for both the general revolute robot manipulator used as the master system, and the OctArm used as the slave system ($M_i(q_i)$, $N_i(q_i, \dot{q}_i)$, $J_i(q_i)$ and $J_2^{+}(q_2)$) are dependent on $q_i(t)$. Given $q_i(t)$ in both cases is a function of sinusoidal trigonometric terms, the kinematics and dynamics remain bounded for all possible $q_i(t)$. Thus it is assumed that if $x_i(t) \in \mathcal{L}_\infty$ then $q_i(t) \in \mathcal{L}_\infty$.*

5.1.3 The Task Space

The master system is represented by a 2-link, planar, revolute robot manipulator, thus $q_1(t)$ refers to the manipulator joint angles and $n_1 = 2$ thus also defining the planar task-space as $x = [X \;\; Z]^T$, where $X(t) \in \mathbb{R}$ and $Z(t) \in \mathbb{R}$ are the scalar

Euclidean coordinates of the master system end-effector.

Since the slave system is a continuum manipulator, $q_2(t) \in \mathbb{R}^{n_2}$ represents the manipulator section lengths and curvatures. For the 3-section OctArm used in the plane of motion of the master, to ensure redundancy $q_2(t) \in \mathbb{R}^6$ and $q_2(t) = [d_1, d_2, d_3, \kappa_1, \kappa_2, \kappa_3]^T$ are the extension lengths and curvatures for each of the three sections respectively.

5.2 Task-Space Controller Development

The primary design objective is to formulate a control input that ensures that the end-effector of the slave system tracks the end-effector of the master system while both of them track a desired task-space trajectory. The subsequent development is based on the assumption that the joint positions and velocities are measurable for both master and slave systems.

The task-space tracking error for the master system denoted by $e_1(t) \in \mathbb{R}^{n_1}$ is defined as follows

$$e_1 \triangleq x_d - x_1 \tag{5.7}$$

where $x_d(t) \in \mathbb{R}^{n_1}$ is the task-space desired trajectory[2]. Based on the exact model knowledge, the following feedback linearizing controller is designed for the master system

$$\tau_1 \triangleq M_1 u_1 + N_1 - J_1^T F_1 \tag{5.8}$$

$$u_1 \triangleq J_1^{-1}\left(\ddot{x}_d + k_1 \dot{e}_1 + k_2 e_1 - \dot{J}_1 \dot{q}_1\right) \tag{5.9}$$

[2]It is assumed that the desired trajectory and its first and second order time derivatives are bounded signals. It should also be noted that $x_d(t)$ is the task-space desired trajectory that the user of the master system will track.

where $u_1(t) \in \mathbb{R}^{n_1}$ is an auxiliary control input and $k_1 \in \mathbb{R}$, $k_2 \in \mathbb{R}$ are positive control gains. Substituting (5.8) and (5.9) into (5.1) for $i = 1$ and premultiplying with $M_1^{-1}(\cdot)$ results in the following

$$\ddot{q}_1 = J_1^{-1}\left(\ddot{x}_d + k_1\dot{e}_1 + k_2 e_1 - \dot{J}_1\dot{q}_1\right). \tag{5.10}$$

Substituting (5.5) into (5.10) and then premultiplying with $J_1(\cdot)$ results in the following closed-loop error system

$$\ddot{e}_1 + k_1\dot{e}_1 + k_2 e_1 = 0_{n_1\times 1} \tag{5.11}$$

from which it can be concluded that with appropriate choice of k_1 and k_2, $\|e_1(t)\|$ goes to zero exponentially fast.

The coordination error, denoted by $e_2(t) \in \mathbb{R}^{n_1}$, is the difference between the end-effector positions of the master and slave systems and is defined as follows

$$e_2 \triangleq x_1 - x_2. \tag{5.12}$$

The following feedback linearizing controller is designed for the slave system

$$\tau_2 \triangleq M_2 u_2 + N_2 - J_2^T F_2 \tag{5.13}$$

$$u_2 \triangleq J_2^{+}\left(\ddot{x}_d + k_1\dot{e}_1 + k_2 e_1 + k_3\dot{e}_2 + k_4 e_2 - \dot{J}_2\dot{q}_2\right) + \phi_N \tag{5.14}$$

where $u_2(t) \in \mathbb{R}^{n_2}$ is an auxiliary control input, $k_3 \in \mathbb{R}$, $k_4 \in \mathbb{R}$ are positive control gains and $\phi_N(t) \in \mathbb{R}^{n_2}$ is a vector in the null-space of $J_2(\cdot)$. Substituting (5.13) and

(5.14) into (5.1) for $i = 2$ and premultiplying with $M_2^{-1}(\cdot)$ results in the following

$$\ddot{q}_2 = J_2^+ \left(\ddot{x}_1 + k_3 \dot{e}_2 + k_4 e_2 - \dot{J}_2 \dot{q}_2 \right) + \phi_N \tag{5.15}$$

where (5.11) was utilized. The following expression is obtained after substituting (5.6) to the right-hand-side of (5.15)

$$\begin{aligned} J_2^+ \left(\ddot{x}_2 - \dot{J}_2 \dot{q}_2 \right) &= J_2^+ \left(\ddot{x}_1 + k_3 \dot{e}_2 + k_4 e_2 - \dot{J}_2 \dot{q}_2 \right) \\ &\quad + \phi_N - \ddot{q}_N. \end{aligned} \tag{5.16}$$

After premultiplying (5.16) with $J_2(\cdot)$ and rearranging, the following simplified error system is obtained

$$\ddot{e}_2 + k_3 \dot{e}_2 + k_4 e_2 = 0_{n_1 \times 1} \tag{5.17}$$

where (**??**) and the following facts were utilized

$$J_2 \phi_N = 0_{n_1 \times 1} \quad , \quad J_2 \ddot{q}_N = 0_{n_1 \times 1} \ . \tag{5.18}$$

From (5.17), it is clear that with appropriate choice of k_3 and k_4, $\|e_2(t)\|$ goes to zero exponentially fast.

5.3 Null-Space Velocity Tracking

In addition to the task-space tracking and coordination objectives, secondary or sub-task objectives may be required to successfully accomplish a particular task. In order to ensure the sub-task objective is achieved, an auxiliary null-space signal $g(t) \in \mathbb{R}^{n_2}$, is introduced. The integration of this signal into the controller is done by

designing a framework that places preferences on desirable slave configurations based on the corresponding sub-task objective. This auxiliary signal is designed to operate in the null-space of the slave continuum manipulator's Jacobian matrix $J_2(q_2)$.

As noted in [70], the null-space velocity tracking error is defined as

$$\dot{e}_N \triangleq \left(I_{n_2} - J_2^+ J_2\right)(g - \dot{q}_2), \tag{5.19}$$

where $g(t)$ is the auxiliary null-space term(yet to be designed). The time derivative of (5.19) is found to be

$$\ddot{e}_N = \left(I_{n_2} - J_2^+ J_2\right)(\dot{g} - \ddot{q}_2) - J_\phi (g - \dot{q}_2) - J_2^+ \dot{J}_2 \dot{e}_N. \tag{5.20}$$

Substituting (5.15) into (5.20) results in

$$\ddot{e}_N = \left(I_{n_2} - J_2^+ J_2\right)\dot{g} - \phi_N - J_\phi (g - \dot{q}_2) - J_2^+ \dot{J}_2 \dot{e}_N \tag{5.21}$$

where the fact that $\phi_N(t)$ exists in the null-space of $J_2(\cdot)$ and Appendix A are utilized. The auxiliary function $J_\phi(t) \in \mathbb{R}^{n_2 \times n_2}$ is based on the slave system Jacobian and defined as

$$J_\phi \triangleq \dot{J}_2^+ J_2 + J_2^+ \dot{J}_2 J_2^+ J_2. \tag{5.22}$$

The auxiliary null-space vector $\phi_N(t)$, introduced in (5.14), is designed to be

$$\phi_N \triangleq \left(I_{n_2} - J_2^+ J_2\right)(\dot{g} + k_n \dot{e}_N) - J_\phi (g - \dot{q}_2), \tag{5.23}$$

where $k_n \in \mathbb{R}$ is a positive constant. After substituting $\phi_N(t)$ into (5.21), the expres-

sion in (5.23) simplifies into

$$\ddot{e}_N = k_n \left(I_{n_2} - J_2^+ J_2 \right) \dot{e}_N - J_2^+ \dot{J}_2 \dot{e}_N. \tag{5.24}$$

The auxiliary null-space vector in (5.23) guarantees that $\dot{e}_N(t) \to 0$ as $t \to \infty$ as proven in [70].

5.4 Sub-Task Closed Loop Error System

The sub-task objective will be met if a Jacobian-type null-space matrix, $J_s(t) \in \mathbb{R}^{1 \times n_2}$ maintains full rank as shown in the condition stated in (5.32). To that end, when $J_s(t)$ (yet to be defined) loses rank, the sub-task objective will not be met. To facilitate this development, an auxiliary positive function $y_a(t) \in \mathbb{R}$ is defined as

$$y_a \triangleq \exp\left(-k_y \beta(q_2)\right), \tag{5.25}$$

where $k_y \in \mathbb{R}$ is a positive constant and $\beta(\cdot) \in \mathbb{R}$ is a sub-task dependent non-negative function.

The time derivative of (5.25) yields

$$\dot{y}_a = J_s \dot{q}_2, \tag{5.26}$$

where $J_s(t) \in \mathbb{R}^{1 \times n_2}$ is defined as

$$J_s \triangleq \frac{\partial y_a}{\partial q_2}. \tag{5.27}$$

Adding and subtracting the terms $J_s J_2^+ J_2 \dot{q}_2$ and $J_s \left(I_{n_2} - J_2^+ J_2 \right) (g - \dot{q}_2)$ respectively

to the right-hand-side of (5.26) and substituting (5.4) and (5.19) into the expression results in

$$\dot{y}_a = J_s J_2^+ \dot{x}_2 + J_s \left(I_{n_2} - J_2^+ J_2 \right) g - J_s \dot{e}_N. \tag{5.28}$$

The auxiliary null-space term $g(t)$ is designed to be

$$g = -k_s J_s^T y_a, \tag{5.29}$$

where $k_s \in \mathbb{R}$ is a positive constant. Substituting (5.29) into (5.28) and applying (**??**) results in

$$\dot{y}_a = -k_s \left\| J_s \left(I_{n_2} - J_2^+ J_2 \right) \right\|^2 y_a + J_s J_2^+ \dot{x}_2 - J_s \dot{e}_N. \tag{5.30}$$

Theorem 4 *The null-space term described in (5.29) guarantees that $y_a(t)$ is ultimately bounded by the inequality*

$$|y_a(t)| \leq \sqrt{y_a^2(t_0) \exp\left(-2\gamma t\right) + \frac{\varepsilon}{\gamma}}, \tag{5.31}$$

provided that

$$\left\| J_s \left(I_{n_2} - J_2^+ J_2 \right) \right\|^2 > \bar{\delta}, \tag{5.32}$$

$$\left\| J_s \left(J_2^+ x_2 - \dot{e}_N \right) \right\| \leq \delta_1, \tag{5.33}$$

$$k_s > \frac{1}{\bar{\delta} \delta_2}, \tag{5.34}$$

where ε, γ, $\bar{\delta}$, δ_1, $\delta_2 \in \mathbb{R}$ are positive constants.

Proof. The proof can be found in Appendix A of [71]. ■

Remark 4 *It should be noted that the sub-task objective is met only if the sufficient*

conditions described by the inequalities in (5.32)-(5.34) are satisfied. Based on the analysis in Section 5.2, the task-space tracking objective is always guaranteed and the sub-task control objective is always secondary to it. When the sub-task controller forces the end-effector of the manipulator to take a path not allowed by the task-space controller, the condition in (5.32) will not be satisfied. Hence, (5.31) will not hold. Thus, careful consideration is required in the design of the desired task-space trajectory and the sub-task control objective to meet the task-space tracking and sub-task objectives simultaneously.

5.5 Simulation Examples

A numerical simulation was performed using the MATLAB/Simulink$^{\text{TM}}$software package to highlight the performance of the controllers proposed in (5.8), (5.13), and (5.19) as well as the sub-task controller $g(t)$ described in (5.29). The simulation was run using an aggressive sinusoidal task-space trajectory for the master system end-effector whose dynamics were computed using the standard Euler-Lagrangian model described in [76]. The link lengths for the master system were nominally chosen to be $l_{1,1} = l_{1,2} = 0.6[m]$. The full dynamic model for the OctArm is developed and described by Tatlicioglu *et al.* in [41] and [42] with all manipulator properties listed and accounted for. It should be noted that Additive White Gaussian Noise with $SNR = 40$ was added into the feedback loop to simulate feedback delays or noise in sensor readings. The control gains were selected to be

$$\begin{aligned} k_1 = 3 \quad k_2 = 10 \quad k_3 = 10 \\ k_4 = 15 \quad k_y = 1 \quad k_s = 1 \quad k_n = 100. \end{aligned} \tag{5.35}$$

The desired task-space trajectory, $x_d(t) \in \mathbb{R}^2$ was chosen as

$$x_d = \begin{bmatrix} X_d \\ Z_d \end{bmatrix} = \begin{bmatrix} 0 + 0.01sin(t) \\ 1 + 0.01cos(t) \end{bmatrix}. \tag{5.36}$$

The sinusoidal component of the trajectory in (5.36) ensures that one possible configuration of the slave system is a singularity at $X_s = [0\ 1]^T$. This is because $k_1 = k_2 = k_3 = 0$ and the manipulator sections are then completely co-linear to the z-axis. This trajectory was chosen to test the nominal sub-task objective for the slave system of avoiding potential singular configurations, and, hence, decrease its manipulability. For this sub-task, $\beta(q_2)$, defined as the manipulability measure and described in [77] is chosen as

$$\beta = \sqrt{det\,[J_2 J_2^T]}, \tag{5.37}$$

where $det(\cdot)$ is the determinant of a matrix. It should be noted that the auxiliary signal $y_a(t)$ defined in (5.25) was chosen in order to exploit the useful properties of the exponential function. Thus, it can be seen that $0 < y_a(t) \leq 1$ results in $\beta(\cdot) \in \mathbb{R}^+$.

From (5.37), it can be seen that $\beta(q_2) = 0$ denotes singular configurations for the manipulator because the Jacobian J_2 will no longer be of full rank. Thus the problem is set up to ensure $\beta(\cdot) > 0$, which is achieved by keeping $y_a(t) \leq 1$.

The continuum manipulator was initially set to be at rest with the section curvatures set near 0 (almost a singular configuration) so as to maximize $y_a(t_0)$ and demonstrate that (5.31) holds for this simulation. Additionally, the desired task-space trajectory is specifically chosen to operate across tip locations consistent with the slave's singular configuration.

The controller performance is illustrated in Figures 5.1, and 5.2, and 5.4.

Figure 5.1 shows the tracking error between the desired trajectory and the non-redundant master system as described in equation (5.7). Figure 5.2 shows the task-space tracking error between the non-redundant master system and the continuum slave system as described in equation (5.12). Figure 5.3 shows the auxiliary sub-task function $y_a(t)$. Finally, Figure 5.4 shows that the ability of the controllers to avoid singularities is validated by the fact that the manipulability measure $\beta(q_2)$ hovers close to zero without actually reaching it. It can be seen that the slave system tracking error converges to zero much slower than the master system. While the continuum arm attempts to reach the desired tip location exponentially fast, the singularity repulsion function used for the manipulability measure $\beta(q_2)$ forces the manipulator to adjust its shape to an acceptable non-singular configuration.

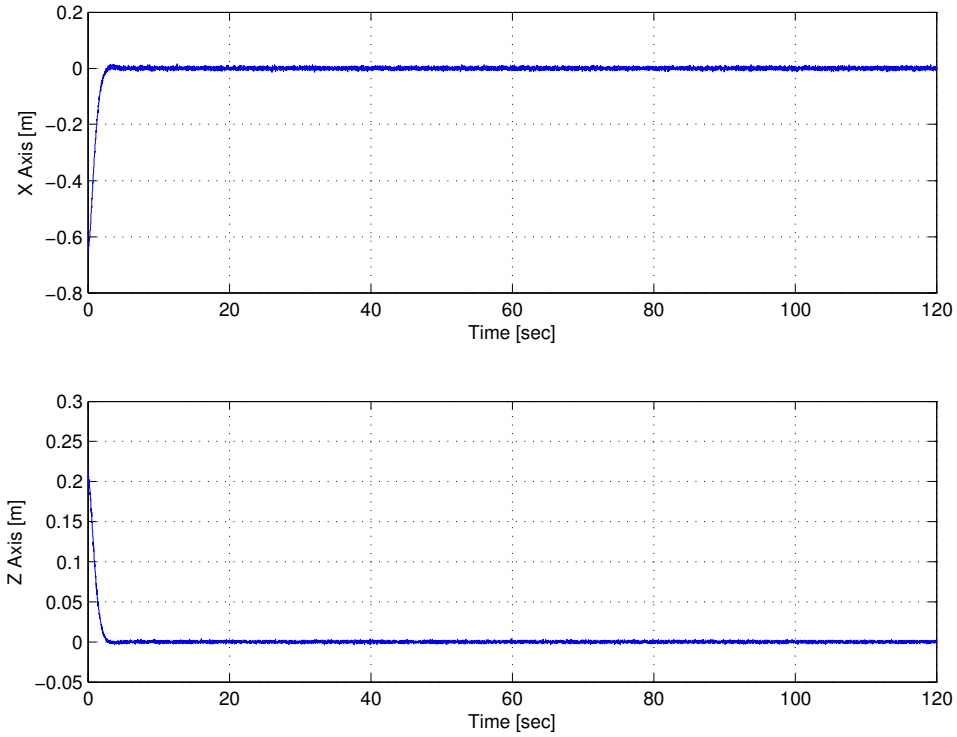

Figure 5.1: Teleoperation Simulation: Master System Tracking Error $e_1(t)$.

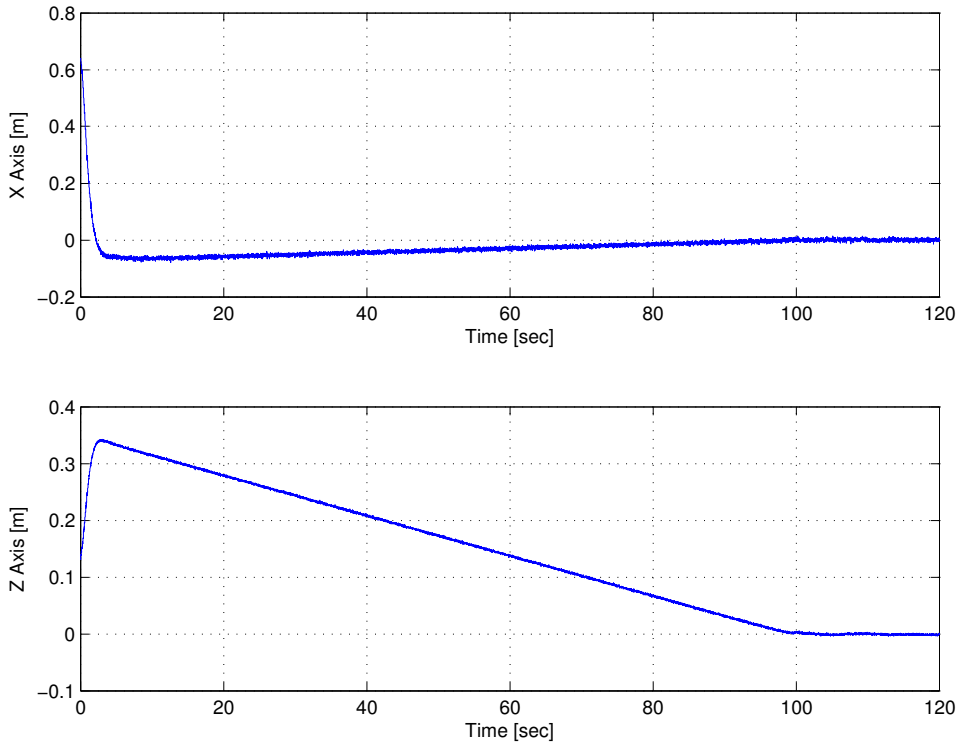

Figure 5.2: Teleoperation Simulation: Slave System Tracking Error $e_2(t)$.

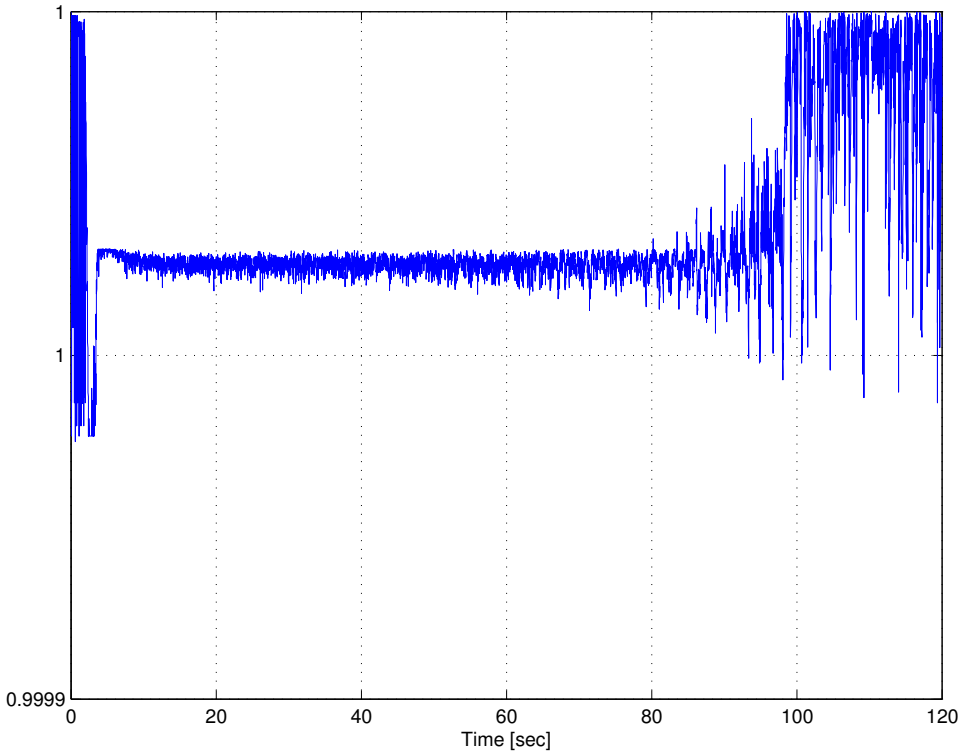

Figure 5.3: Teleoperation Simulation: Auxiliary Positive Function $y_a(t)$ for the Sub-Task Controller.

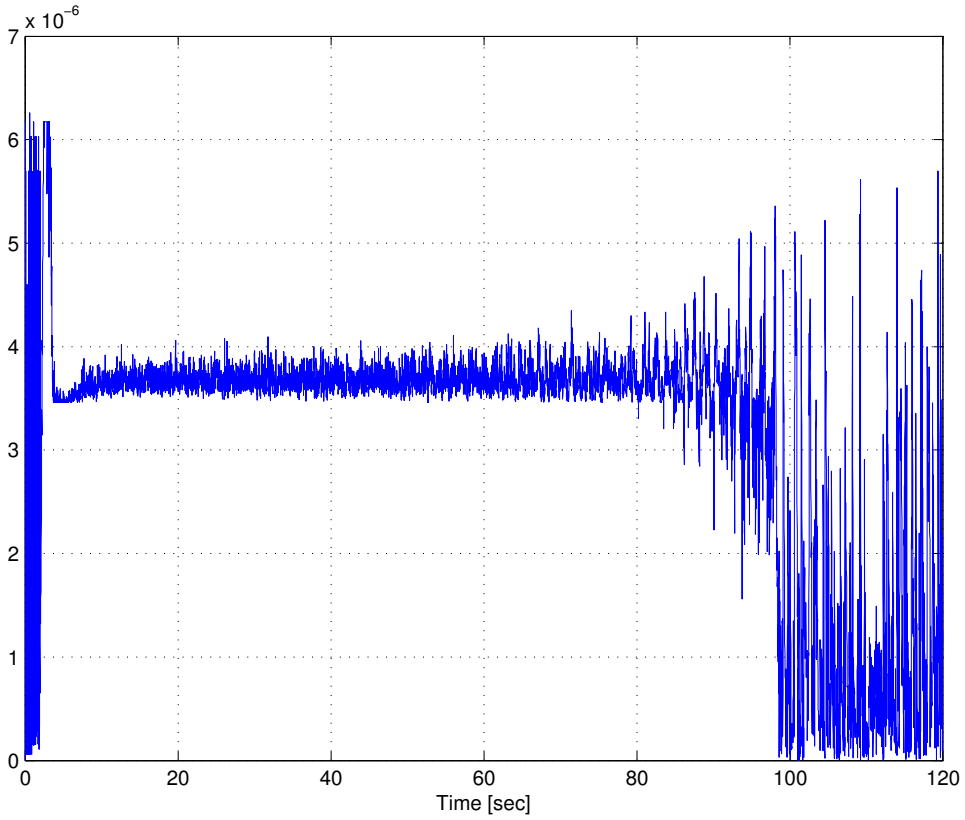

Figure 5.4: Manipulability Measure for the Continuum Arm Slave System $\beta(t)$. **Note:** Although the Measure Approaches Zero, it Never Actually Attains It.

5.6 Experimental Validation

The controller described in (5.14) was implemented on the OctArm extensible continuum manipulator. The objective of the implementation was to verify the performance of the teleoperation controller. Given that the available dynamic model developed in [41] and [42] is planar, the robot was placed on a horizontal surface. Because of this orientation, the gravitational terms in the model were unnecessary.

Similar to the simulation, the control algorithm was developed on a Dell® PC running on an Intel® i5 processor under the Windows 7® operating system. Additionally, Quanser® Q8 and Q2 data acquisition boards were used along with the QUARC® interface to connect to the OctArm hardware. The control signal from the algorithm was converted into voltages and sent to the 9 pressure regulators (one for each McKibben actuator on the OctArm) which give each section its length and curvature. The length of each actuator was measured using a string encoder from which the robot section lengths and curvatures were inferred using the conversions developed in [30] for the feedback.

As in Section 5.2, the performance of the proposed controller was measured against a task-space position which could lead to a singularity solution. Thus, the nominal desired manipulator tip location was chosen to be:

$$x_{d_{exp}} = \begin{bmatrix} X_d \\ Z_d \end{bmatrix} = \begin{bmatrix} 0.2\ [m] \\ 1.3\ [m] \end{bmatrix} \tag{5.38}$$

The teleoperation experimental results for the tip location in (5.38) can be be seen in Figures 5.5, 5.6, 5.7, and 5.8. Figures 5.5 and 5.6 show the position tracking error of the master and slave systems respectively and Figure 5.7 shows the auxiliary sub-task function $y_a(t)$. Finally, Figure 5.8 shows that the ability of the controllers

to avoid singularities is validated by the fact that the manipulability measure $\beta(q_2)$ hovers close to zero without actually reaching it. It can be seen that the slave system tracking error converges to zero much slower than the master system. While the continuum arm attempts to reach the desired tip location exponentially fast, the singularity repulsion function used for the manipulability measure $\beta(q_2)$ forces the manipulator to adjust its shape to an acceptable non-singular configuration. The slave system control voltages are shown in Figures 5.9, 5.10, and 5.11 and represent the voltage signals sent to each actuator. It should be noted that the master system aspect of the experiment was simulated due to hardware constraints and limitations with the data acquisition inputs and outputs.

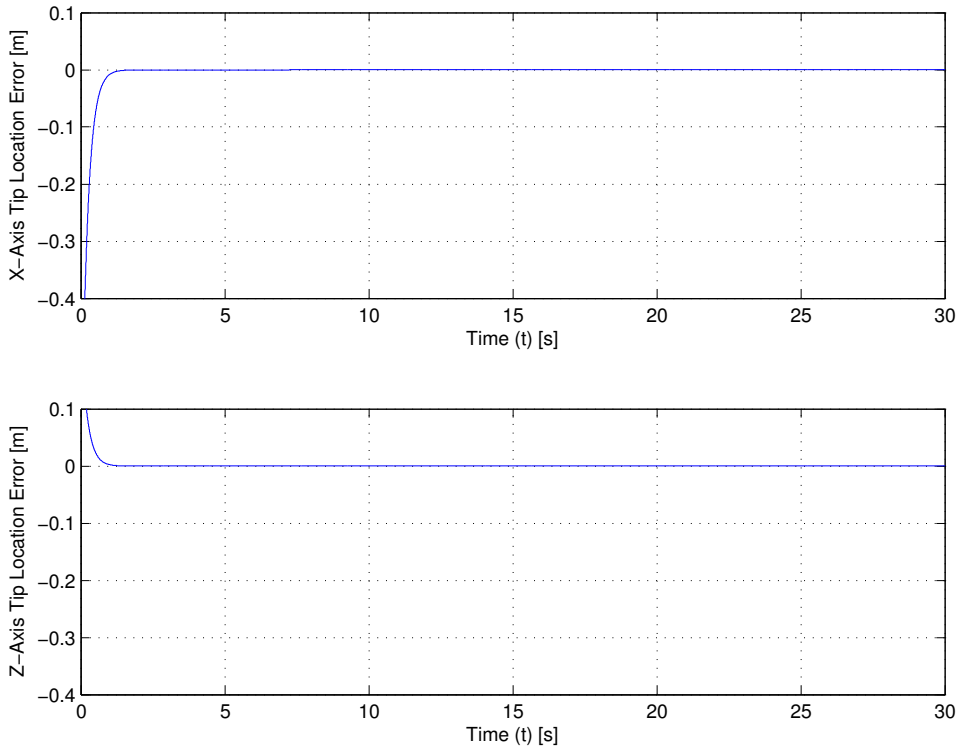

Figure 5.5: Teleoperation Experiment: Master System Tracking Error $e_1(t)$.

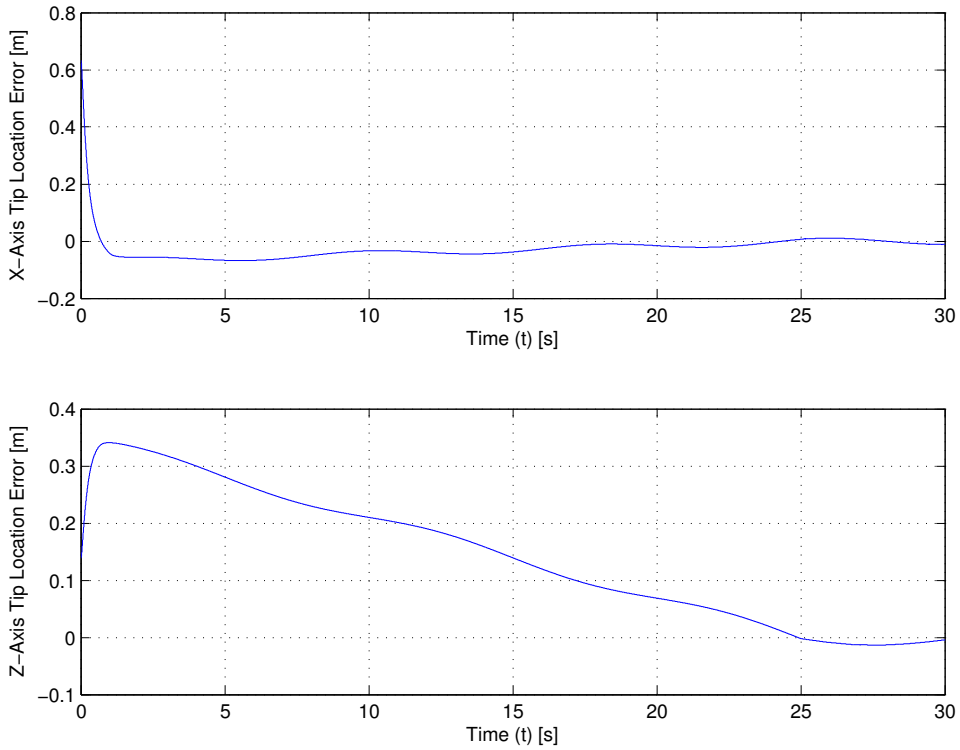

Figure 5.6: Teleoperation Experiment: Slave System Tracking Error $e_2(t)$.

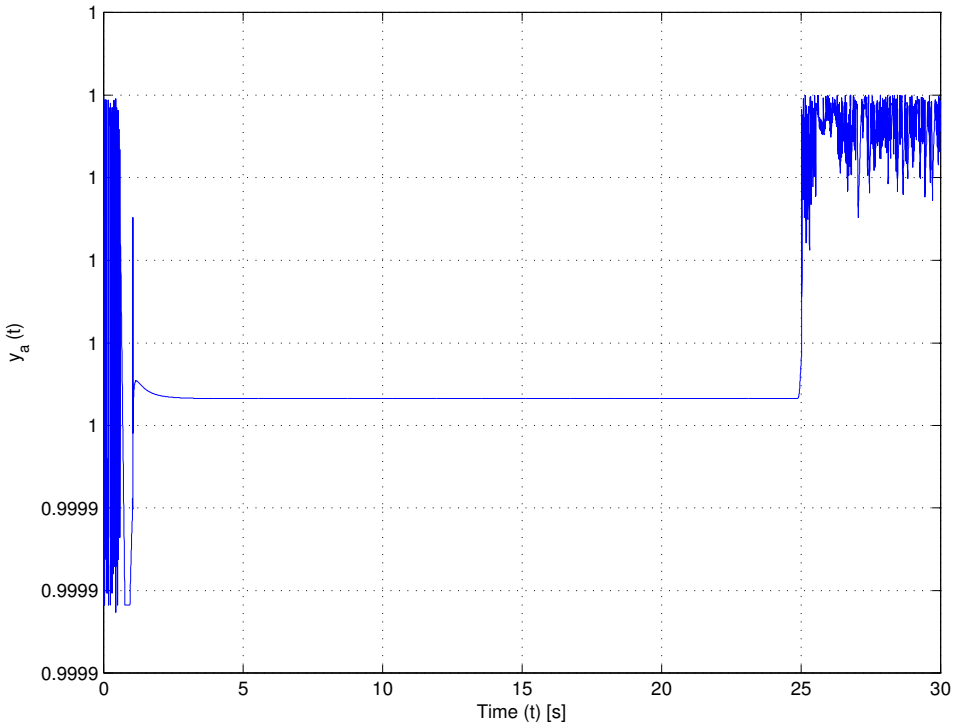

Figure 5.7: Teleoperation Experiment: Slave System Auxiliary Positive Function $y_a(t)$ for the Sub-Task Controller.

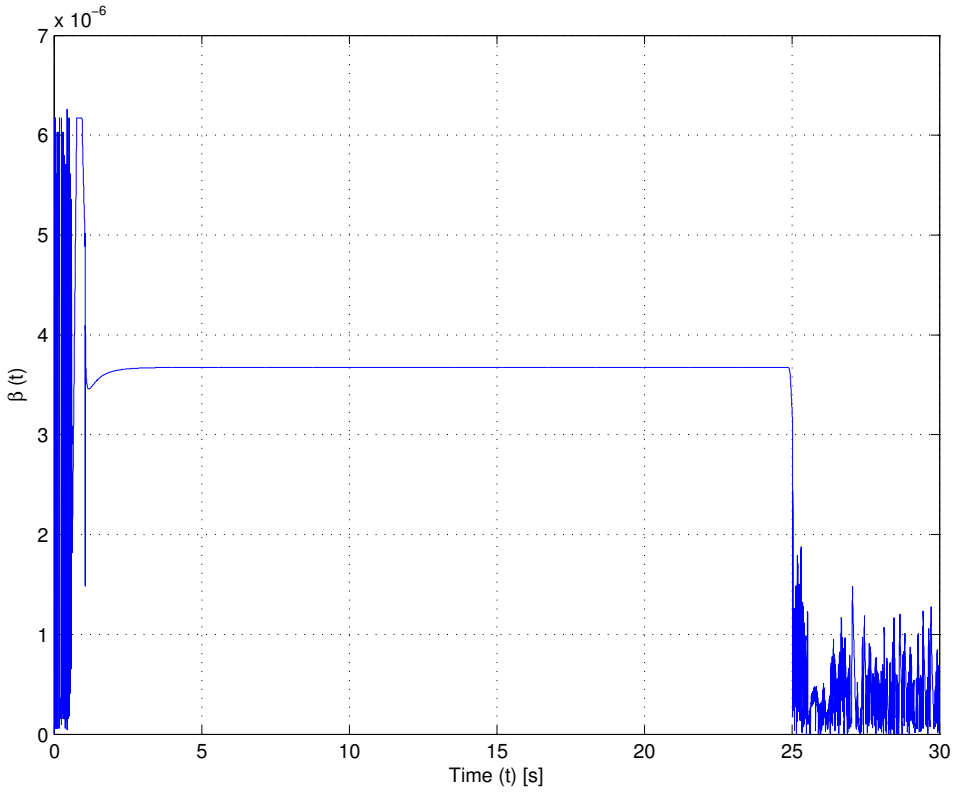

Figure 5.8: Teleoperation Experiment: Manipulability Measure for the Continuum Arm Slave System $\beta(t)$.

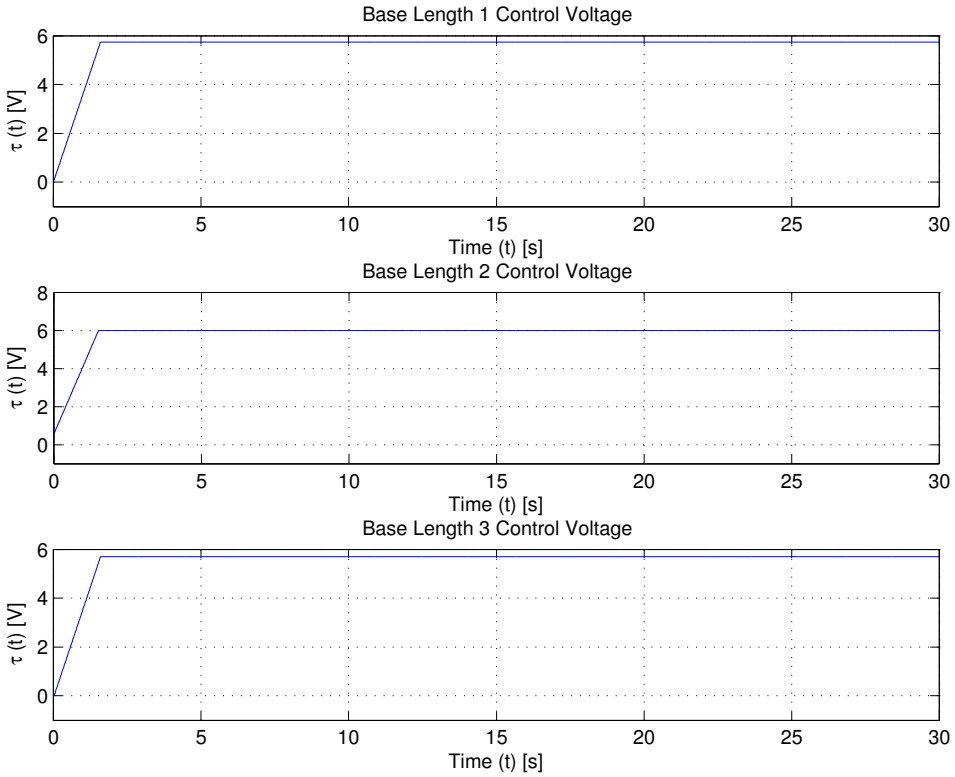

Figure 5.9: Teleoperation Experiment: Slave System Base Section Control Voltages.

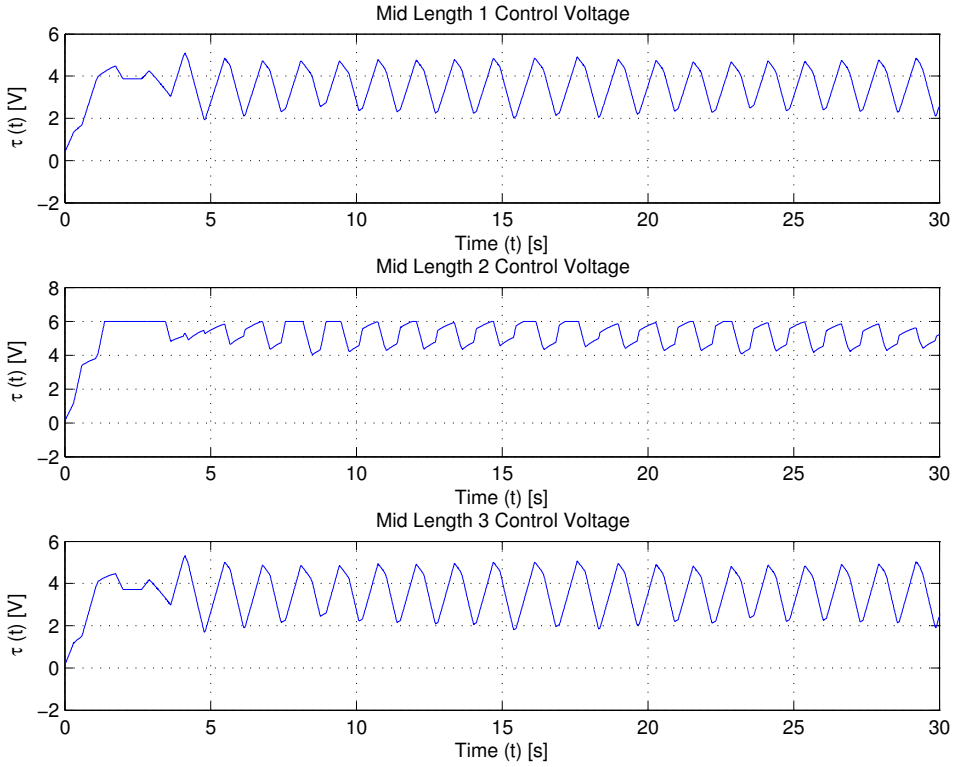

Figure 5.10: Teleoperation Experiment: Slave System Mid Section Control Voltages.

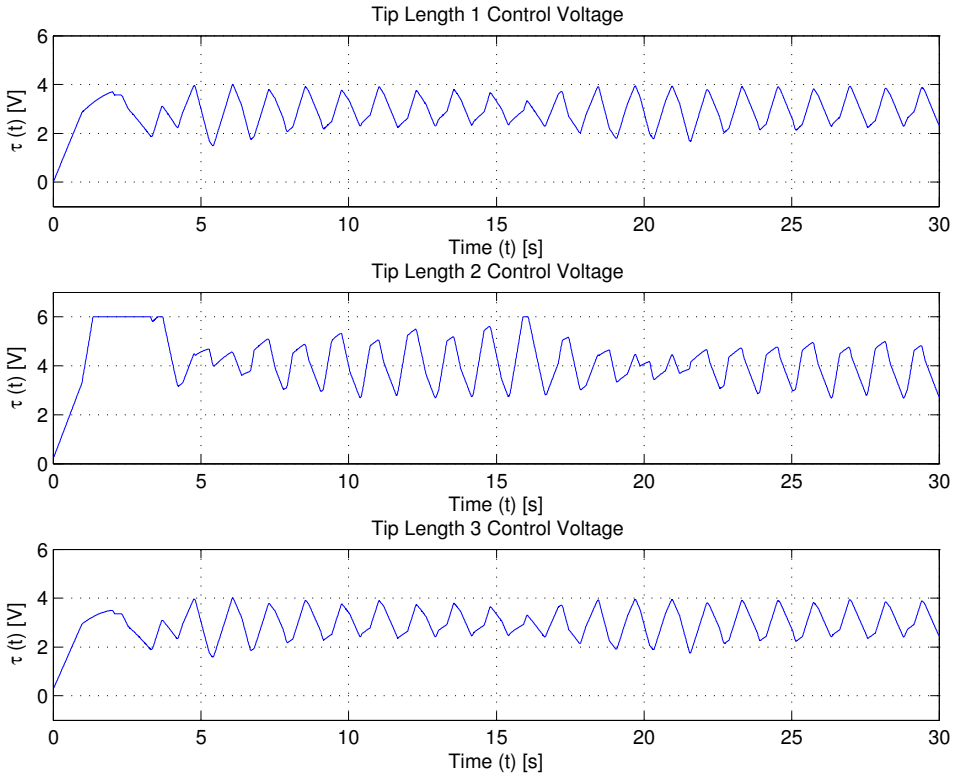

Figure 5.11: Teleoperation Experiment: Slave System Tip Section Control Voltages.

Chapter 6

Conclusion

This dissertation presents new understanding of extensible, continuous backbone ("continuum") robots utilizing a holistic approach. An kinematic model based on the manipulator measured variables was presented. Two control algorithms were proposed, one in the configuration-space and the other in the task-space, along with the first analysis of the self-motion of such manipulators.

In Chapter 2, a new set of intuitive, generalized, spatial forward kinematics for an extensible continuum manipulator was described. Previous kinematics developments utilized a rigid-link equivalent for the kinematics which were then related to the continuum manipulator variables. The new kinematics development were matched directly to the measurable variables of the 9-DOF OctArm manipulator, resulting in computationally simpler and more intuitive for determining the manipulator shape and tip position.

In Chapter 3, a new model-based nonlinear (sliding-mode) controller for continuum robots was presented. The model was based on a formulation for continuum robot dynamics recently established in the literature. By exploiting the structure inherent in these dynamics, the controller was shown to guarantee to convergence

despite inherent errors due to uncertainty in model parameters. The results are applicable to continuum robots which extend as well as bend. The designed controller was compared to a standard inverse-dynamics PD controller via simulations on a three-section extensible continuum robot operating in a plane. Experiments were also conducted on the 9-DOF OctArm whose results validated the improved effectiveness, accuracy, and speed-of-convergence of the proposed controller on a physical system.

In Chapter 4, fundamental new insight into and characterization of the self-motion properties of continuum robots showed that there was a single self-motion manifold underlying the available self-motion. Resolved-motion rate inverse kinematics based on the manipulator kinematic development of Chapter 2 were also utilized. This allowed for convenient analysis of the manipulator null-space in order to explore the self-motion characteristics of continuum manipulators. Three base self-motion cases were identified, which generated continuum manipulator behavior in the null-space. The practical implications of the findings along with the applications in each case and examples in nature were also discussed and these results were supported empirically on the 9-DOF OctArm.

In Chapter 5, the regulation of the continuum robot tip position (task-space control) teleoperated by a rigid-link, non-redundant, and kinematically dissimilar master robot was discussed. Due to the kinematic dissimilarities between the two systems, feedback linearizing task-space controllers were proposed with additional sub-task terms for the slave system to allow for varied objectives in its null-space and independent of the primary master system task-space tracking objective. Numerical simulations and experimental results on the 9-DOF OctArm highlighted the effectiveness of the controllers along with the singularity avoidance sub-task objective for the slave system.

Appendices

Appendix A Pseudoinverse Properties

For the development of the task-space controller, the pseudoinverse, $J^+(\psi)$, of the Jacobian $J(\psi)$ is defined as

$$J^+ \triangleq J^T \left(JJ^T\right)^{-1}, \tag{1}$$

resulting in the property

$$JJ^+ = I_m \tag{2}$$

where $I_m \in \mathbb{R}^{m\times m}$ is the standard identity matrix. As described in [78], the pseudoinverse defined in (1) satisfies the following Moore-Penrose properties

$$\begin{aligned} JJ^+J &= J \\ J^+JJ^+ &= J^+ \\ \left(J^+J\right)^T &= J^+J \\ \left(JJ^+\right)^T &= JJ^+. \end{aligned} \tag{3}$$

In addition to these properties listed above, the matrix $(I_n - J^+J)$ also satisfies the following useful properties

$$\begin{aligned} \left(I_n - J^+J\right)\left(I_n - J^+J\right) &= I_n - J^+J \\ \left(I_n - J^+J\right)^T &= I_n - J^+J \\ J\left(I_n - J^+J\right) &= 0_{n\times m} \\ \left(I_n - J^+J\right)J^+ &= 0_{n\times m}. \end{aligned} \tag{4}$$

Appendix B The Velocity Jacobian

The elements of (4.3) are:

$$\begin{gathered}\frac{\partial X}{\partial s_1} = sin\theta_1 cos\phi_1 - \frac{k_1}{k_2} sin\theta_1 cos\phi_1 cos\phi_2 \\ + \frac{k_1}{k_2} sin\theta_1 cos\theta_2 cos\phi_1 cos\phi_2 + \frac{k_1}{k_2} cos\theta_1 sin\theta_2 cos\phi_1,\end{gathered} \tag{5}$$

$$\begin{gathered}\frac{\partial X}{\partial k_1} = -\frac{1}{k_1^2} cos\phi_1 + \frac{s_1}{k_1} sin\theta_1 cos\phi_1 \\ + \frac{1}{k_1^2} cos\theta_1 cos\phi_1 - \frac{s_1}{k_2} sin\theta_1 cos\phi_1 cos\phi_2 \\ + \frac{s_1}{k_2} sin\theta_1 cos\theta_2 cos\phi_1 cos\phi_2 + \frac{s_1}{k_2} cos\theta_1 sin\theta_2 cos\phi_1,\end{gathered} \tag{6}$$

$$\begin{gathered}\frac{\partial X}{\partial \phi_1} = -\frac{1}{k_1} sin\phi_1 + \frac{1}{k_1} cos\theta_1 sin\phi_1 \\ + \frac{1}{k_2} cos\theta_1 sin\phi_1 cos\phi_2 + \frac{1}{k_2} cos\theta_1 cos\theta_2 sin\phi_1 cos\phi_2 \\ - \frac{1}{k_2} sin\theta_1 sin\theta_2 \sin\phi_1 - \frac{1}{k_2} cos\phi_1 sin\phi_2 +\end{gathered} \tag{7}$$

$$\begin{gathered}\frac{\partial X}{\partial s_2} = cos\theta_1 sin\theta_2 cos\phi_1 cos\phi_2 + sin\theta_1 cos\theta_2 cos\phi_1 \\ - sin\theta_2 sin\phi_1 sin\phi_2,\end{gathered} \tag{8}$$

$$\begin{gathered}\frac{\partial X}{\partial k_2} = -\frac{1}{k_2^2} cos\theta_1 cos\phi_1 cos\phi 2 \\ + \frac{1}{k_2} cos\theta_1 sin\theta_2 cos\phi_1 cos\phi_2 \\ + \frac{1}{k_2^2} cos\theta_1 cos\theta_2 cos\phi_1 cos\phi_2 + \frac{s_2}{k_2} sin\theta_1 cos\theta_2 cos\phi_1 \\ - \frac{1}{k_2^2} \sin\theta_1 sin\theta_2 cos\phi_1 + \frac{1}{k_2^2} sin\phi_1 sin\phi_2 \\ - \frac{s_2}{k_2} sin\theta_2 sin\phi_1 sin\phi_2 - \frac{1}{k_2^2} cos\theta_2 sin\phi_1 sin\phi_2,\end{gathered} \tag{9}$$

$$\begin{gathered}\frac{\partial X}{\partial \phi_2} = -\frac{1}{k_2} cos\theta_1 cos\phi_1 cos\phi_2 \\ + \frac{1}{k_2} cos\theta_1 cos\theta_2 cos\phi_1 sin\phi_2 - \frac{1}{k_2} sin\phi_1 cos\phi_2 \\ + \frac{1}{k_2} cos\theta_2 sin\phi_1 cos\phi_2,\end{gathered} \tag{10}$$

$$\begin{aligned}\frac{\partial Y}{\partial s_1} = & sin\theta_1 sin\phi_1 - \frac{k_1}{k_2} sin\theta_1 sin\phi_1 cos\phi_2 \\ & + \frac{k_1}{k_2} sin\theta_1 cos\theta_2 sin\phi_1 cos\phi_2 \\ & + \frac{k_1}{k_2} cos\theta_1 sin\theta_2 sin\phi_1,\end{aligned} \tag{11}$$

$$\begin{aligned}\frac{\partial Y}{\partial k_1} = & -\frac{1}{k_1^2} sin\phi_1 + \frac{s_1}{k_1} sin\theta_1 sin\phi_1 \\ & + \frac{1}{k_1^2} cos\theta_1 sin\phi_1 - \frac{s_1}{k_2} sin\theta_1 sin\phi_1 cos\phi_2 \\ & + \frac{s_1}{k_2} sin\theta_1 cos\theta_2 sin\phi_1 cos\phi_2 + \frac{s_1}{k_1} cos\theta_1 sin\theta_2 sin\phi_1,\end{aligned} \tag{12}$$

$$\begin{aligned}\frac{\partial Y}{\partial \phi_1} = & \frac{1}{k_1} cos\phi_1 - \frac{1}{k_1} cos\theta_1 cos\phi_1 \\ & + \frac{1}{k_2} cos\theta_1 cos\phi_1 cos\phi_2 - \frac{1}{k_2} cos\theta_1 cos\theta_2 cos\phi_1 cos\phi_2 \\ & + \frac{1}{k_2} sin\theta_1 sin\theta_2 cos\phi_1 - \frac{1}{k_2} sin\phi_1 sin\phi_2 \\ & + \frac{1}{k_2} cos\theta_2 sin\phi_1 sin\phi_2,\end{aligned} \tag{13}$$

$$\begin{aligned}\frac{\partial Y}{\partial s_2} = & cos\theta_1 sin\theta_2 sin\phi_1 cos\phi_2 + sin\theta_1 cos\theta_2 sin\phi_1 \\ & + sin\theta_2 cos\phi_1 sin\phi_2,\end{aligned} \tag{14}$$

$$\begin{aligned}\frac{\partial Y}{\partial k_2} = & \frac{1}{k_2^2} cos\theta_1 sin\phi_1 cos\phi_2 \\ & + \frac{s_2}{k_2} cos\theta_1 sin\theta_2 sin\phi_1 cos\phi_2 \\ & + \frac{1}{k_2^2} cos\theta_1 cos\theta_2 sin\phi_1 cos\phi_2 + \frac{s_2}{k_2} sin\theta_1 cos\theta_2 sin\phi_1 \\ & - \frac{1}{k_2^2} sin\theta_1 sin\theta_2 sin\phi_1 \\ & - \frac{1}{k_2^2} cos\phi_1 cos\phi_2 + \frac{s_2}{k_2} sin\theta_2 cos\phi_1 sin\phi_2 \\ & + \frac{1}{k_2^2} cos\theta_2 cos\phi_1 sin\phi_2,\end{aligned} \tag{15}$$

$$\begin{aligned}\frac{\partial Y}{\partial \phi_2} = & \frac{1}{k_2} cos\theta_1 sin\phi_1 \sin\phi_2 \\ & + \frac{1}{k_2} cos\theta_1 cos\theta_2 sin\phi_1 sin\phi_2 + \frac{1}{k_2} cos\phi_1 cos\phi_2 \\ & - \frac{1}{k_2} cos\theta_2 cos\phi_1 cos\phi_2,\end{aligned} \tag{16}$$

$$\begin{aligned}\frac{\partial Z}{\partial s_1} &= cos\theta_1 + \frac{k_1}{k_2}cos\theta_1 cos\theta 2 cos\phi_2 \\ &-\frac{k_1}{k_2}cos\theta_1 cos\phi_2 - \frac{k_1}{k_2}sin\theta_1 sin\theta_2,\end{aligned} \tag{17}$$

$$\begin{aligned}\frac{\partial Z}{\partial k_1} &= \frac{s_1}{k_1}cos\theta_1 - \frac{1}{k_1^2}sin\theta_1 + \frac{s_1}{k_2}cos\theta_1 cos\theta_2 cos\phi_2 \\ &-\frac{s_1}{k_2}cos\theta_1 cos\phi_2 - \frac{s_1}{k_2}sin\theta_1 sin\theta_2,\end{aligned} \tag{18}$$

$$\frac{\partial Z}{\partial \phi_1} = 0, \tag{19}$$

$$\frac{\partial Z}{\partial s_2} = -sin\theta_1 sin\theta_2 cos\phi_2 + cos\theta_1 cos\theta_2, \tag{20}$$

$$\begin{aligned}\frac{\partial Z}{\partial k_2} &= -\frac{s_2}{k_2}sin\theta_1 sin\theta_2 cos\phi_2 - \frac{1}{k_2^2}sin\theta_1 cos\theta_2 cos\phi_2 \\ &+\frac{1}{k_2^2}sin\theta_1 cos\phi_2 + \frac{s_2}{k_2}cos\theta_1 cos\theta_2 - \frac{1}{k_2^2}cos\theta_1 sin\theta_2,\end{aligned} \tag{21}$$

$$\frac{\partial Z}{\partial \phi_2} = -\frac{1}{k_2}sin\theta_1 cos\theta_2 sin\phi_2 + \frac{1}{k_2}sin\theta_1 sin\phi_2. \tag{22}$$

Appendix C The Single Section 3D Jacobian

The tip coordinates of a single section extensible continuum manipulator are given in (2.15), with the resulting Jacobian having the form

$$J_{1-section} = \begin{bmatrix} \frac{\partial X}{\partial s_1} & \frac{\partial X}{\partial k_1} & \frac{\partial X}{\partial \phi_1} \\ \\ \frac{\partial Y}{\partial s_1} & \frac{\partial Y}{\partial k_1} & \frac{\partial Y}{\partial \phi_1} \\ \\ \frac{\partial Z}{\partial s_1} & \frac{\partial Z}{\partial k_1} & \frac{\partial Z}{\partial \phi_1} \end{bmatrix}. \tag{23}$$

The Jacobian $J_{1-section(t)}$ can be rewritten as $J_{1-section} = \begin{bmatrix} J_{s_1} & J_{k_1} & J_{\phi_1} \end{bmatrix}$ where

$$J_{s_1} = \begin{bmatrix} \frac{\partial X}{\partial s_1} \\ \\ \frac{\partial Y}{\partial s_1} \\ \\ \frac{\partial Z}{\partial s_1} \end{bmatrix} J_{k_1} = \begin{bmatrix} \frac{\partial X}{\partial k_1} \\ \\ \frac{\partial Y}{\partial k_1} \\ \\ \frac{\partial Z}{\partial k_1} \end{bmatrix} J_{\phi_1} = \begin{bmatrix} \frac{\partial X}{\partial \phi_1} \\ \\ \frac{\partial Y}{\partial \phi_1} \\ \\ \frac{\partial Z}{\partial \phi_1} \end{bmatrix}, \tag{24}$$

and

$$\begin{aligned} \frac{\partial X}{\partial s_1} &= sin\theta_1 cos\phi_1 \\ \frac{\partial Y}{\partial s_1} &= sin\theta_1 sin\phi_1 \\ \frac{\partial Z}{\partial s_1} &= cos\theta_1, \end{aligned} \tag{25}$$

$$\begin{aligned} \frac{\partial X}{\partial k_1} &= cos\phi_1 \left(cos\theta_1 + s_1 k_1 sin\theta_1\right) \frac{1}{k_1^2} \\ \frac{\partial Y}{\partial k_1} &= sin\phi_1 \left(cos\theta_1 + s_1 k_1 sin\theta_1\right) \frac{1}{k_1^2} \\ \frac{\partial Z}{\partial k_1} &= \left(s_1 k_1 cos\theta_1 - sin\theta_1\right) \frac{1}{k_1^2}, \end{aligned} \tag{26}$$

$$\begin{aligned} \frac{\partial X}{\partial \phi_1} &= -\frac{1}{k_1}\left(1 - cos\theta_1\right) sin\phi_1 \\ \frac{\partial Y}{\partial \phi_1} &= \frac{1}{k_1}\left(1 - cos\theta_1\right) cos\phi_1 \\ \frac{\partial Z}{\partial \phi_1} &= 0. \end{aligned} \tag{27}$$

It can further be seen that the dot products $J_{k_1} \cdot J_{\phi_1} = 0$ and $J_{s_1} \cdot J_{\phi_1} = 0$ showing that J_{k_1} is orthogonal to J_{ϕ_1} and J_{s_1} is orthogonal to J_{ϕ_1}. Given this orthogonality in both cases with the $\phi_1(t)$ term (the one required to convert 2D coordinates to 3D), it can be seen that the self-motion results found in the 2D cases are straightforward to extend to the 3D.

Appendix D 3-Section Continuum Robot Planar Dynamic Model Terms

The standard Euler-LaGrangian dynamic model for a serially-linked 3-section extensible continuum robot manipulator operating in a plane, developed in [41] and [42], is given by the equation

$$\tau = M(q)\ddot{q} + V\left(q, \dot{q}\right)\dot{q} + G(q) + B(q) + E(q), \tag{28}$$

where $M(q) \in \mathbb{R}^{6\times6}$ is the inertia matrix, $V\left(q, \dot{q}\right) \in \mathbb{R}^{6\times6}$ is the Centripetal-Coriolis Matrix, $G(q)$, $B(q)$, and $E(q) \in \mathbb{R}^6$ refers to the vectors relating the effects due to gravitational, potential energy due to bending, and potential energy due to extension. The elements of these matrices are detailed below:

D.1 Inertia Matrix Terms

The entries of the inertia matrix are defined as follows[1]

$$K_{\dot{s}_1\dot{s}_1} = \frac{m}{s\kappa_1^2} r_{20} \tag{29}$$

$$K_{\dot{s}_1\dot{s}_2} = \frac{m}{s}\left\{r_8 + r_9 - r_{23} - r_{24}\right\} \tag{30}$$

$$K_{\dot{s}_1\dot{s}_3} = \frac{m}{s}\left\{r_{16} + r_{10} - r_{25}\right\} \tag{31}$$

[1]The calculation of the these terms was done by MAPLE 9.5.

$$K_{\dot{s}_1\dot{\kappa}_1} = \frac{m}{s}\left\{-\frac{1}{\kappa_1^3}r_1 - \frac{s_1}{\kappa_2 s_3}r_{23} - \frac{s_1}{\kappa_2\left(s_2+s_3\right)}r_{24} - \frac{2}{\kappa_1^3}r_{20} - \frac{s_1}{\kappa_3 s_3}r_{25} - s_1 r_4 + \frac{s_1}{\kappa_1}\left[\frac{s_3+s_2}{\kappa_1} - \frac{s_2}{\kappa_2} - \frac{s_3}{\kappa_3}\right]\sin\left(s_1\kappa_1\right)\right\} \tag{32}$$

$$K_{\dot{s}_1\dot{\kappa}_2} = \frac{m}{s}\left\{-\frac{2}{\kappa_2}r_8 - \frac{2}{\kappa_2}r_9 - \frac{s_2}{\kappa_3 s_3}r_{25} - s_2 r_4 + \frac{1}{\kappa_2}r_{24} + \frac{s_3-s_2}{\kappa_2 s_3}r_{23} - \frac{1}{\kappa_1}s_2 s_3\left(\frac{1}{\kappa_3} - \frac{1}{\kappa_2}\right)\sin\left(s_1\kappa_1\right)\right\} \tag{33}$$

$$K_{\dot{s}_1\dot{\kappa}_3} = \frac{m}{s}\left\{-\frac{2}{\kappa_3}r_{16} - \frac{2}{\kappa_3}r_{10} + \frac{1}{\kappa_3}r_{25} - s_3 r_4\right\} \tag{34}$$

$$K_{\dot{s}_2\dot{s}_2} = \frac{m}{s\kappa_2^2}r_{21} \tag{35}$$

$$K_{\dot{s}_2\dot{s}_3} = \frac{m}{s}\left\{r_{26} - r_{11}\right\} \tag{36}$$

$$\begin{gathered} K_{\dot{s}_2\dot{\kappa}_1} = \tfrac{m}{s}\left\{\tfrac{1}{\kappa_1}r_{24} + \tfrac{s_1}{\kappa_2^3}r_5 + \tfrac{s_1}{\kappa_3 s_3}r_{26} - \tfrac{s_1}{\kappa_2}r_{13}\right\} \\ -\tfrac{m}{s}\left\{\kappa_1\kappa_2\left(\tfrac{s_1(s_1+s_2+s_3)}{\kappa_1} + \tfrac{1}{\kappa_1^2\kappa_2} - \tfrac{s_1 s_3}{\kappa_3}\right)r_8 - \tfrac{1}{\kappa_1}r_9\right\} \\ +\tfrac{m}{s}\left\{\tfrac{s_1}{\kappa_3^2}r_6 + \tfrac{s_1}{\kappa_2}\left(\tfrac{s_1}{\kappa_1} + \tfrac{s_2}{\kappa_2}\right)\sin\left(s_1\kappa_2\right)\right\} \\ -\tfrac{m}{s}\left\{\tfrac{s_1(s_1+s_2)}{\kappa_2\kappa_1}\sin\left(\left(s_1+s_2\right)\kappa_2\right)\right\} \end{gathered} \tag{37}$$

$$K_{\dot{s}_2\dot{\kappa}_2} = \frac{m}{s}\left\{\frac{s_2}{\kappa_3 s_3}r_{26} + \frac{s_2}{\kappa_3^2}r_6 - \frac{1}{\kappa_2^3}r_2 - \frac{2}{\kappa_2^3}r_{21} + s_2 s_3\kappa_1\kappa_2\left(\frac{1}{\kappa_3} - \frac{1}{\kappa_2}\right)r_8\right\} \tag{38}$$

$$K_{\dot{s}_2\dot{\kappa}_3} = \frac{m}{d\kappa_3}\left\{\frac{s_3}{\kappa_3}r_6 - r_{26} + 2r_{11}\right\} \tag{39}$$

$$K_{\dot{s}_3\dot{s}_3} = \frac{m}{s\kappa_3^2} r_{22} \tag{40}$$

$$\begin{aligned} K_{\dot{s}_3\dot{\kappa}_1} &= \tfrac{m}{s}\left\{\tfrac{s_1}{\kappa_3^3} r_7 - \tfrac{1}{\kappa_1} r_{10} - \tfrac{1}{\kappa_1} r_{16} + \tfrac{1}{\kappa_1} r_{25}\right\} \\ &+ \tfrac{m}{s}\left\{s_1\left(\tfrac{1}{\kappa_1} - \tfrac{1}{\kappa_3}\right)\left[r_{14} - \tfrac{s_3}{\kappa_3}\sin\left(\left(s_1+s_2\right)\kappa_3\right)\right]\right\} \end{aligned} \tag{41}$$

$$\begin{aligned} K_{\dot{s}_3\dot{\kappa}_2} &= \tfrac{m}{s}\left\{\tfrac{s_2}{\kappa_3^3} r_7 - \tfrac{1}{\kappa_2} r_{26} + \tfrac{1}{\kappa_2} r_{11}\right\} \\ &+ \tfrac{m}{s}\left\{s_2\left(\tfrac{1}{\kappa_2} - \tfrac{1}{\kappa_3}\right)\left[r_{14} - \tfrac{s_3}{\kappa_3}\sin\left(\left(s_1+s_2\right)\kappa_3\right)\right]\right\} \end{aligned} \tag{42}$$

$$K_{\dot{s}_3\dot{\kappa}_3} = \frac{m}{s\kappa_3^3}\left\{-r_3 - 2r_{22}\right\} \tag{43}$$

$$\begin{aligned} K_{\dot{\kappa}_1\dot{\kappa}_1} &= \tfrac{m}{s}\left\{\tfrac{s_1}{\kappa_1\kappa_2 s_3} r_{23} + \tfrac{s_1}{\kappa_1\kappa_2(s_2+s_3)} r_{24} + \tfrac{s_1}{\kappa_1\kappa_3 s_3} r_{25} + \tfrac{s_1}{\kappa_1} r_4\right\} \\ &+ \tfrac{m}{s}\left\{s_1^2\kappa_1\left(\tfrac{1}{\kappa_2} - \tfrac{1}{\kappa_1}\right) r_8 + s_1^2\kappa_1\left(\tfrac{1}{\kappa_3} - \tfrac{1}{\kappa_1}\right) r_{16} + \tfrac{1}{\kappa_1^4} r_1 + \tfrac{1}{\kappa_1^4} r_{20}\right\} \\ &+ \tfrac{m}{s}\left\{\tfrac{s_1}{\kappa_1^2}\left(\tfrac{s_2}{\kappa_2} + \tfrac{s_3}{\kappa_3} - \tfrac{s_2+s_3}{\kappa_1}\right)\sin\left(s_1\kappa_1\right)\right\} \\ &+ \tfrac{m}{s}\left\{s_1^2\left[\tfrac{s_2}{\kappa_2^2} - \tfrac{s_2}{\kappa_1\kappa_2} - \tfrac{s_3}{\kappa_1\kappa_3} + \tfrac{s_3}{\kappa_3^2} + \tfrac{s_3+s_2}{2\kappa_1^2} + \tfrac{s_1}{6\kappa_1^2}\right]\right\} \end{aligned} \tag{44}$$

$$\begin{aligned} K_{\dot{\kappa}_1\dot{\kappa}_2} &= \tfrac{m}{s}\left\{\left[\tfrac{s_2+s_3}{\kappa_1^2} + \tfrac{2s_1}{\kappa_2}\left(\tfrac{1}{\kappa_2} - \tfrac{1}{\kappa_1}\right)\right] r_{13} + \tfrac{s_2}{\kappa_1} r_4 + \tfrac{s_2}{\kappa_1\kappa_3 s_3} r_{25}\right\} \\ &+ \tfrac{m}{s}\left\{\tfrac{2s_2}{\kappa_1\kappa_2 s_3} r_{23} + \left(s_2+s_3\right) r_{17} + s_1 s_2\kappa_1\left(\tfrac{2}{\kappa_3} - \tfrac{1}{\kappa_2} - \tfrac{1}{\kappa_1}\right) r_{16} + \tfrac{2}{\kappa_1\kappa_2} r_9\right\} \\ &+ \tfrac{m}{s}\left\{\kappa_1\left[-\tfrac{s_1 s_2}{\kappa_2} + \tfrac{s_1(s_3+s_2)}{\kappa_1} - \tfrac{s_1 s_3}{\kappa_3} + \tfrac{2}{\kappa_1^2\kappa_2}\right] r_8 - \tfrac{s_1}{\kappa_2\kappa_3 s_3} r_{26} - \tfrac{s_1}{\kappa_2\kappa_3^2} r_6\right\} \\ &+ \tfrac{m}{s}\left\{\tfrac{s_1}{\kappa_2^4}\cos\left(s_2\kappa_2\right) - \tfrac{2s_1 s_2}{\kappa_2^2}\left(\tfrac{1}{\kappa_2} - \tfrac{1}{\kappa_1}\right)\sin\left(\left(s_1+s_2\right)\kappa_2\right)\right\} \\ &- \tfrac{m}{s}\left\{\tfrac{s_2 s_3}{\kappa_1^2}\left(\tfrac{1}{\kappa_2} - \tfrac{1}{\kappa_3}\right)\sin\left(s_1\kappa_1\right) - \tfrac{s_1}{\kappa_2^4} + \tfrac{s_1 s_2^2}{2\kappa_2^2}\right\} \\ &- \tfrac{m}{s}\left\{s_1 s_2 s_3\left(\tfrac{1}{\kappa_1\kappa_3} + \tfrac{1}{\kappa_2\kappa_3} - \tfrac{1}{\kappa_1\kappa_2} - \tfrac{2}{\kappa_3^2}\right)\right\} \end{aligned} \tag{45}$$

$$\begin{aligned} K_{\dot{\kappa}_1\dot{\kappa}_3} &= \frac{m}{s}\left\{\frac{2}{\kappa_1\kappa_3} r_{10} + s_3 r_{18} - s_3 r_{15} + \frac{2}{\kappa_1\kappa_3} r_{16} - \frac{s_1}{\kappa_3^4} r_7\right. \\ &\left. + s_1 s_3\left(\frac{1}{\kappa_1} - \frac{1}{\kappa_3}\right) r_{19} + \frac{2s_1}{\kappa_3}\left(\frac{1}{\kappa_3} - \frac{1}{\kappa_1}\right) r_{14} + \frac{s_1 s_3^2}{2\kappa_3^2}\right\} \end{aligned} \tag{46}$$

$$K_{\dot{\kappa}_2\dot{\kappa}_2} = \frac{m}{s}\left\{-\frac{s_2}{\kappa_2\kappa_3 s_3}r_{26} - \frac{s_2}{\kappa_2\kappa_3^2}r_6 - s_2^2\kappa_1\left(\frac{1}{\kappa_2}-\frac{1}{\kappa_3}\right)r_{16} + \frac{1}{\kappa_2^4}r_{21} + \frac{1}{\kappa_2^4}r_2\right. \quad (47)$$
$$\left. + s_2 s_3\kappa_1\left(\frac{1}{\kappa_2}-\frac{1}{\kappa_3}\right)r_8 + \frac{s_2^2\left(s_2+3s_3\right)}{6\kappa_2^2} + \frac{s_3 s_2^2}{\kappa_3}\left(\frac{1}{\kappa_3}-\frac{1}{\kappa_2}\right)\right\}$$

$$K_{\dot{\kappa}_2\dot{\kappa}_3} = \frac{m}{s}\left\{-\frac{s_2}{\kappa_3^4}r_7 - \frac{2s_2}{\kappa_3}\left(\frac{1}{\kappa_2}-\frac{1}{\kappa_3}\right)r_{14} - \frac{s_3}{\kappa_2\kappa_3^2}r_6\right. \quad (48)$$
$$\left. + \frac{1}{\kappa_2\kappa_3}r_{26} - \frac{2}{\kappa_2\kappa_3}r_{11} - s_2 s_3\left(\frac{1}{\kappa_3}-\frac{1}{\kappa_2}\right)r_{19} + \frac{s_2 s_3^2}{2\kappa_3^2}\right\}$$

$$K_{\dot{\kappa}_3\dot{\kappa}_3} = \frac{m}{s\kappa_3^2}\left\{\frac{1}{\kappa_3^2}r_3 + \frac{s_3^3}{6} + \frac{1}{\kappa_3^2}r_{22}\right\}. \quad (49)$$

The time-varying functions $r_i(t)$, $i = 1, ..., 26$, in (29)-(49) are introduced to simplify the calculations. They are defined as follows

$$r_1 = s_1\cos\left(s_1\kappa_1\right) - \frac{1}{\kappa_1}\sin\left(s_1\kappa_1\right) \quad (50)$$

$$r_2 = s_2\cos\left(s_2\kappa_2\right) - \frac{1}{\kappa_2}\sin\left(s_2\kappa_2\right) \quad (51)$$

$$r_3 = s_3\cos\left(s_3\kappa_3\right) - \frac{1}{\kappa_3}\sin\left(s_3\kappa_3\right) \quad (52)$$

$$r_4 = \frac{1}{\kappa_1\kappa_3^2}\left[\cos\left(s\kappa_3\right) - \cos\left(s_1\kappa_1 - s\kappa_3\right)\right] \quad (53)$$

$$r_5 = 1 - \cos\left(s_2\kappa_2\right) \quad (54)$$

$$r_6 = \frac{1}{\kappa_2}\left[\cos\left(\left(s_1+s_2\right)\kappa_2 - s\kappa_3\right) - \cos\left(s_1\kappa_2 - s\kappa_3\right)\right] \tag{55}$$

$$r_7 = 1 - \cos\left(s_3\kappa_3\right) \tag{56}$$

$$r_8 = \frac{1}{\kappa_1\kappa_2^2}\left[\sin\left(s_1\kappa_2\right) - \sin\left(\left(s_1+s_2\right)\kappa_2\right)\right] \tag{57}$$

$$r_9 = \frac{1}{\kappa_1\kappa_2^2}\left[\sin\left(s_1\left(\kappa_1-\kappa_2\right)\right) - \sin\left(s_1\kappa_1 - \left(s_1+s_2\right)\kappa_2\right)\right] \tag{58}$$

$$r_{10} = \frac{1}{\kappa_1\kappa_3^2}\left[\sin\left(s_1\kappa_1 - \left(s_1+s_2\right)\kappa_3\right) - \sin\left(s_1\kappa_1 - s\kappa_3\right)\right] \tag{59}$$

$$\begin{aligned} r_{11} \;=\; & \frac{1}{\kappa_2\kappa_3^2}\left[\sin\left(s_1\kappa_2 - \left(s_1+s_2\right)\kappa_3\right) - \sin\left(s_1\kappa_2 - s\kappa_3\right)\right. \\ & \left. + \sin\left(\left(s_1+s_2\right)\kappa_2 - s\kappa_3\right) - \sin\left(s_1+s_2\right)\left(\kappa_2-\kappa_3\right)\right] \end{aligned} \tag{60}$$

$$r_{12} = \frac{1}{\kappa_3^2}\left[\sin\left(\left(s_1+s_2\right)\kappa_3\right) - \sin\left(s\kappa_3\right)\right] \tag{61}$$

$$r_{13} = \frac{1}{\kappa_2^2}\left[\cos\left(s_1\kappa_2\right) - \cos\left(\left(s_1+s_2\right)\kappa_2\right)\right] \tag{62}$$

$$r_{14} = \frac{1}{\kappa_3^2}\left[\cos\left(\left(s_1+s_2\right)\kappa_3\right) - \cos\left(s\kappa_3\right)\right] \tag{63}$$

$$r_{15} = \frac{1}{\kappa_1^2\kappa_3^2}\left[\cos\left(s_1\kappa_1 - \left(s_1+s_2\right)\kappa_3\right) + \cos\left(s_1\kappa_1 - s\kappa_3\right)\right] \tag{64}$$

$$r_{16} = \frac{1}{\kappa_1 \kappa_3^2} \left[\sin\left(\left(s_1 + s_2 \right) \kappa_3 \right) - \sin\left(s \kappa_3 \right) \right] \tag{65}$$

$$r_{17} = \frac{1}{\kappa_1^2 \kappa_2^2} \left[\cos\left(\left(s_1 + s_2 \right) \kappa_2 - s_1 \kappa_1 \right) - \cos\left(s_1 \left(\kappa_2 - \kappa_1 \right) \right) \right] \tag{66}$$

$$r_{18} = \frac{1}{\kappa_1^2 \kappa_3^2} \left[\cos\left(s \kappa_3 \right) + \cos\left(\left(s_1 + s_2 \right) \kappa_3 \right) \right] \tag{67}$$

$$r_{19} = \frac{1}{\kappa_3^2} \left[\sin\left(s \kappa_3 \right) + \sin\left(\left(s_1 + s_2 \right) \kappa_3 \right) \right] \tag{68}$$

$$r_{20} = -\left(s_2 + s_3 \right) \cos\left(s_1 \kappa_1 \right) + s_1 + s_2 + s_3 - \frac{1}{\kappa_1} \sin\left(s_1 \kappa_1 \right) \tag{69}$$

$$r_{21} = -s_3 \cos\left(s_2 \kappa_2 \right) + s_2 + s_3 - \frac{1}{\kappa_2} \sin\left(s_2 \kappa_2 \right) \tag{70}$$

$$r_{22} = s_3 - \frac{1}{\kappa_3} \sin\left(s_3 \kappa_3 \right) \tag{71}$$

$$r_{23} = \frac{s_3}{\kappa_1 \kappa_2} \left[\cos\left(\left(s_1 + s_2 \right) \kappa_2 \right) - \cos\left(s_1 \kappa_1 - \left(s_1 + s_2 \right) \kappa_2 \right) \right] \tag{72}$$

$$r_{24} = \frac{s_2 + s_3}{\kappa_1 \kappa_2} \left[\cos\left(s_1 \left(\kappa_1 - \kappa_2 \right) \right) - \cos\left(s_1 \kappa_2 \right) \right] \tag{73}$$

$$r_{25} = \frac{s_3}{\kappa_1 \kappa_3} \left[\cos\left(s_1 \kappa_1 - \left(s_1 + s_2 \right) \kappa_3 \right) - \cos\left(\left(s_1 + s_2 \right) \kappa_3 \right) \right] \tag{74}$$

$$r_{26} = \frac{s_3}{\kappa_2 \kappa_3} \left[\cos\left(s_1\kappa_2 - (s_1 + s_2)\,\kappa_3\right) - \cos\left(s_1 + s_2\right)(\kappa_2 - \kappa_3) \right]. \tag{75}$$

D.2 Centripetal-Coriolis Matrix Terms

The elements of the centripetal-coriolis matrix $V(q, \dot{q})$ are defined as follows

$$V_{11} \triangleq \frac{\partial K_{\dot{s}_1\dot{s}_1}}{\partial s_1}\dot{s}_1 + \frac{\partial K_{\dot{s}_1\dot{s}_1}}{\partial s_2}\dot{s}_2 + \frac{\partial K_{\dot{s}_1\dot{s}_1}}{\partial s_3}\dot{s}_3 + \frac{\partial K_{\dot{s}_1\dot{s}_1}}{\partial \kappa_1}\dot{\kappa}_1 \tag{76}$$

$$\begin{aligned} V_{12} \triangleq\ & \frac{\partial K_{\dot{s}_1\dot{s}_2}}{\partial s_2}\dot{s}_2 - \frac{\partial K_{\dot{s}_2\dot{s}_2}}{\partial s_1}\dot{s}_2 + \frac{\partial K_{\dot{s}_1\dot{s}_1}}{\partial s_2}\dot{s}_1 + \frac{\partial K_{\dot{s}_1\dot{s}_2}}{\partial s_3}\dot{s}_3 \\ & + \frac{\partial K_{\dot{s}_1\dot{s}_2}}{\partial \kappa_1}\dot{\kappa}_1 + \frac{\partial K_{\dot{s}_1\dot{s}_2}}{\partial \kappa_2}\dot{\kappa}_2 - \frac{\partial K_{\dot{s}_2\dot{\kappa}_1}}{\partial s_1}\dot{\kappa}_1 - \frac{\partial K_{\dot{s}_2\dot{\kappa}_2}}{\partial s_1}\dot{\kappa}_2 \end{aligned} \tag{77}$$

$$\begin{aligned} V_{13} \triangleq\ & \frac{\partial K_{\dot{s}_1\dot{s}_3}}{\partial s_3}\dot{s}_3 - \frac{\partial K_{\dot{s}_3\dot{s}_3}}{\partial s_1}\dot{s}_3 + \frac{\partial K_{\dot{s}_1\dot{s}_1}}{\partial s_3}\dot{s}_1 + \frac{\partial K_{\dot{s}_1\dot{s}_3}}{\partial s_2}\dot{s}_2 \\ & - \frac{\partial K_{\dot{s}_2\dot{s}_3}}{\partial s_1}\dot{s}_2 + \frac{\partial K_{\dot{s}_1\dot{s}_3}}{\partial \kappa_1}\dot{\kappa}_1 + \frac{\partial K_{\dot{s}_1\dot{s}_3}}{\partial \kappa_3}\dot{\kappa}_3 - \frac{\partial K_{\dot{s}_3\dot{\kappa}_1}}{\partial s_1}\dot{\kappa}_1 - \frac{\partial K_{\dot{s}_3\dot{\kappa}_2}}{\partial s_1}\dot{\kappa}_2 \end{aligned} \tag{78}$$

$$\begin{aligned} V_{14} \triangleq\ & \frac{\partial K_{\dot{s}_1\dot{\kappa}_1}}{\partial \kappa_1}\dot{\kappa}_1 - \frac{\partial K_{\dot{\kappa}_1\dot{\kappa}_1}}{\partial s_1}\dot{\kappa}_1 + \frac{\partial K_{\dot{s}_1\dot{s}_1}}{\partial \kappa_1}\dot{s}_1 + \frac{\partial K_{\dot{s}_1\dot{\kappa}_1}}{\partial s_2}\dot{s}_2 \\ & + \frac{\partial K_{\dot{s}_1\dot{\kappa}_1}}{\partial s_3}\dot{s}_3 + \frac{\partial K_{\dot{s}_1\dot{\kappa}_1}}{\partial \kappa_2}\dot{\kappa}_2 + \frac{\partial K_{\dot{s}_1\dot{\kappa}_1}}{\partial \kappa_3}\dot{\kappa}_3 - \frac{\partial K_{\dot{\kappa}_1\dot{\kappa}_3}}{\partial s_1}\dot{\kappa}_3 \end{aligned} \tag{79}$$

$$\begin{aligned} V_{15} \triangleq\ & \frac{\partial K_{\dot{s}_1\dot{\kappa}_2}}{\partial \kappa_2}\dot{\kappa}_2 - \frac{\partial K_{\dot{\kappa}_2\dot{\kappa}_2}}{\partial s_1}\dot{\kappa}_2 + \frac{\partial K_{\dot{s}_1\dot{\kappa}_2}}{\partial s_2}\dot{s}_2 + \frac{\partial K_{\dot{s}_1\dot{\kappa}_2}}{\partial s_3}\dot{s}_3 \\ & + \frac{\partial K_{\dot{s}_1\dot{\kappa}_2}}{\partial \kappa_1}\dot{\kappa}_1 + \frac{\partial K_{\dot{s}_1\dot{\kappa}_2}}{\partial \kappa_3}\dot{\kappa}_3 - \frac{\partial K_{\dot{\kappa}_1\dot{\kappa}_2}}{\partial s_1}\dot{\kappa}_1 - \frac{\partial K_{\dot{\kappa}_2\dot{\kappa}_3}}{\partial s_1}\dot{\kappa}_3 \end{aligned} \tag{80}$$

$$V_{16} \triangleq \frac{\partial K_{\dot{s}_1\dot{\kappa}_3}}{\partial \kappa_3}\dot{\kappa}_3 - \frac{\partial K_{\dot{\kappa}_3\dot{\kappa}_3}}{\partial s_1}\dot{\kappa}_3 + \frac{\partial K_{\dot{s}_1\dot{\kappa}_3}}{\partial s_2}\dot{s}_2 + \frac{\partial K_{\dot{s}_1\dot{\kappa}_3}}{\partial s_3}\dot{s}_3 + \frac{\partial K_{\dot{s}_1\dot{\kappa}_3}}{\partial \kappa_1}\dot{\kappa}_1 - \frac{\partial K_{\dot{s}_2\dot{\kappa}_3}}{\partial s_1}\dot{s}_2 - \frac{\partial K_{\dot{s}_3\dot{\kappa}_3}}{\partial s_1}\dot{s}_3 \tag{81}$$

$$V_{21} \triangleq \frac{\partial K_{\dot{s}_1\dot{s}_2}}{\partial s_1}\dot{s}_1 - \frac{\partial K_{\dot{s}_1\dot{s}_1}}{\partial s_2}\dot{s}_1 + \frac{\partial K_{\dot{s}_2\dot{s}_2}}{\partial s_1}\dot{s}_2 + \frac{\partial K_{\dot{s}_2\dot{\kappa}_1}}{\partial s_1}\dot{\kappa}_1 + \frac{\partial K_{\dot{s}_2\dot{\kappa}_2}}{\partial s_1}\dot{\kappa}_2 \tag{82}$$

$$V_{22} \triangleq \frac{\partial K_{\dot{s}_2\dot{s}_2}}{\partial s_1}\dot{s}_1 + \frac{\partial K_{\dot{s}_2\dot{s}_2}}{\partial s_2}\dot{s}_2 + \frac{\partial K_{\dot{s}_2\dot{s}_2}}{\partial s_3}\dot{s}_3 + \frac{\partial K_{\dot{s}_2\dot{s}_2}}{\partial \kappa_2}\dot{\kappa}_2 \tag{83}$$

$$\begin{aligned} V_{23} \triangleq\ & \frac{\partial K_{\dot{s}_2\dot{s}_3}}{\partial s_3}\dot{s}_3 - \frac{\partial K_{\dot{s}_3\dot{s}_3}}{\partial s_2}\dot{s}_3 + \frac{\partial K_{\dot{s}_2\dot{s}_2}}{\partial s_3}\dot{s}_2 + \frac{\partial K_{\dot{s}_1\dot{s}_2}}{\partial s_3}\dot{s}_1 + \frac{\partial K_{\dot{s}_2\dot{s}_3}}{\partial s_1}\dot{s}_1 - \frac{\partial K_{\dot{s}_1\dot{s}_3}}{\partial s_2}\dot{s}_1 \\ & + \frac{\partial K_{\dot{s}_2\dot{s}_3}}{\partial \kappa_2}\dot{\kappa}_2 + \frac{\partial K_{\dot{s}_2\dot{s}_3}}{\partial \kappa_3}\dot{\kappa}_3 - \frac{\partial K_{\dot{s}_3\dot{\kappa}_1}}{\partial s_2}\dot{\kappa}_1 - \frac{\partial K_{\dot{s}_3\dot{\kappa}_2}}{\partial s_2}\dot{\kappa}_2 - \frac{\partial K_{\dot{s}_3\dot{\kappa}_3}}{\partial s_2}\dot{\kappa}_3 \end{aligned} \tag{84}$$

$$\begin{aligned} V_{24} \triangleq\ & \frac{\partial K_{\dot{s}_2\dot{\kappa}_1}}{\partial \kappa_1}\dot{\kappa}_1 - \frac{\partial K_{\dot{\kappa}_1\dot{\kappa}_1}}{\partial s_2}\dot{\kappa}_1 + \frac{\partial K_{\dot{s}_2\dot{\kappa}_1}}{\partial s_3}\dot{s}_3 + \frac{\partial K_{\dot{s}_2\dot{\kappa}_1}}{\partial \kappa_2}\dot{\kappa}_2 \\ & + \frac{\partial K_{\dot{s}_2\dot{\kappa}_1}}{\partial \kappa_3}\dot{\kappa}_3 + \frac{\partial K_{\dot{s}_1\dot{s}_2}}{\partial \kappa_1}\dot{s}_1 - \frac{\partial K_{\dot{s}_1\dot{\kappa}_1}}{\partial s_2}\dot{s}_1 - \frac{\partial K_{\dot{\kappa}_1\dot{\kappa}_2}}{\partial s_2}\dot{\kappa}_2 \end{aligned} \tag{85}$$

$$V_{25} \triangleq \frac{\partial K_{\dot{s}_2\dot{\kappa}_2}}{\partial \kappa_2}\dot{\kappa}_2 - \frac{\partial K_{\dot{\kappa}_2\dot{\kappa}_2}}{\partial s_2}\dot{\kappa}_2 + \frac{\partial K_{\dot{s}_2\dot{s}_2}}{\partial \kappa_2}\dot{s}_2 + \frac{\partial K_{\dot{s}_2\dot{\kappa}_2}}{\partial s_3}\dot{s}_3 + \frac{\partial K_{\dot{s}_2\dot{\kappa}_2}}{\partial \kappa_3}\dot{\kappa}_3 + \frac{\partial K_{\dot{s}_1\dot{s}_2}}{\partial \kappa_2}\dot{s}_1 - \frac{\partial K_{\dot{s}_1\dot{\kappa}_2}}{\partial s_2}\dot{s}_1 \tag{86}$$

$$\begin{aligned} V_{26} \triangleq\ & \frac{\partial K_{\dot{s}_2\dot{\kappa}_3}}{\partial \kappa_3}\dot{\kappa}_3 - \frac{\partial K_{\dot{\kappa}_3\dot{\kappa}_3}}{\partial s_2}\dot{\kappa}_3 + \frac{\partial K_{\dot{s}_2\dot{\kappa}_3}}{\partial s_1}\dot{s}_1 + \frac{\partial K_{\dot{s}_2\dot{\kappa}_3}}{\partial s_3}\dot{s}_3 \\ & + \frac{\partial K_{\dot{s}_2\dot{\kappa}_3}}{\partial \kappa_2}\dot{\kappa}_2 - \frac{\partial K_{\dot{s}_1\dot{\kappa}_3}}{\partial s_2}\dot{s}_1 - \frac{\partial K_{\dot{\kappa}_1\dot{\kappa}_3}}{\partial s_2}\dot{\kappa}_1 - \frac{\partial K_{\dot{\kappa}_2\dot{\kappa}_3}}{\partial s_2}\dot{\kappa}_2 \end{aligned} \tag{87}$$

$$V_{31} \triangleq \frac{\partial K_{\dot{s}_1\dot{s}_3}}{\partial s_1}\dot{s}_1 - \frac{\partial K_{\dot{s}_1\dot{s}_1}}{\partial s_3}\dot{s}_1 + \frac{\partial K_{\dot{s}_3\dot{s}_3}}{\partial s_1}\dot{s}_3 + \frac{\partial K_{\dot{s}_2\dot{s}_3}}{\partial s_1}\dot{s}_2 + \frac{\partial K_{\dot{s}_3\dot{\kappa}_1}}{\partial s_1}\dot{\kappa}_1 + \frac{\partial K_{\dot{s}_3\dot{\kappa}_2}}{\partial s_1}\dot{\kappa}_2 \quad (88)$$

$$\begin{aligned} V_{32} \triangleq\ & \frac{\partial K_{\dot{s}_2\dot{s}_3}}{\partial s_2}\dot{s}_2 - \frac{\partial K_{\dot{s}_2\dot{s}_2}}{\partial s_3}\dot{s}_2 + \frac{\partial K_{\dot{s}_3\dot{s}_3}}{\partial s_2}\dot{s}_3 + \frac{\partial K_{\dot{s}_1\dot{s}_3}}{\partial s_2}\dot{s}_1 \\ & - \frac{\partial K_{\dot{s}_1\dot{s}_2}}{\partial s_3}\dot{s}_1 + \frac{\partial K_{\dot{s}_3\dot{\kappa}_1}}{\partial s_2}\dot{\kappa}_1 + \frac{\partial K_{\dot{s}_3\dot{\kappa}_2}}{\partial s_2}\dot{\kappa}_2 + \frac{\partial K_{\dot{s}_3\dot{\kappa}_3}}{\partial s_2}\dot{\kappa}_3 \end{aligned} \quad (89)$$

$$V_{33} \triangleq \frac{\partial K_{\dot{s}_3\dot{s}_3}}{\partial s_1}\dot{s}_1 + \frac{\partial K_{\dot{s}_3\dot{s}_3}}{\partial s_2}\dot{s}_2 + \frac{\partial K_{\dot{s}_3\dot{s}_3}}{\partial s_3}\dot{s}_3 + \frac{\partial K_{\dot{s}_3\dot{s}_3}}{\partial \kappa_3}\dot{\kappa}_3 \quad (90)$$

$$V_{34} \triangleq \frac{\partial K_{\dot{s}_3\dot{\kappa}_1}}{\partial \kappa_1}\dot{\kappa}_1 - \frac{\partial K_{\dot{\kappa}_1\dot{\kappa}_1}}{\partial s_3}\dot{\kappa}_1 + \frac{\partial K_{\dot{s}_3\dot{\kappa}_1}}{\partial \kappa_3}\dot{\kappa}_3 + \frac{\partial K_{\dot{s}_1\dot{s}_3}}{\partial \kappa_1}\dot{s}_1 - \frac{\partial K_{\dot{s}_1\dot{\kappa}_1}}{\partial s_3}\dot{s}_1 - \frac{\partial K_{\dot{s}_2\dot{\kappa}_1}}{\partial s_3}\dot{s}_2 - \frac{\partial K_{\dot{\kappa}_1\dot{\kappa}_2}}{\partial s_3}\dot{\kappa}_2 \quad (91)$$

$$V_{35} \triangleq \frac{\partial K_{\dot{s}_3\dot{\kappa}_2}}{\partial \kappa_2}\dot{\kappa}_2 - \frac{\partial K_{\dot{\kappa}_2\dot{\kappa}_2}}{\partial s_3}\dot{\kappa}_2 + \frac{\partial K_{\dot{s}_3\dot{\kappa}_2}}{\partial \kappa_3}\dot{\kappa}_3 - \frac{\partial K_{\dot{s}_1\dot{\kappa}_2}}{\partial s_3}\dot{s}_1 + \frac{\partial K_{\dot{s}_2\dot{s}_3}}{\partial \kappa_2}\dot{s}_2 - \frac{\partial K_{\dot{s}_2\dot{\kappa}_2}}{\partial s_3}\dot{s}_2 - \frac{\partial K_{\dot{\kappa}_2\dot{\kappa}_3}}{\partial s_3}\dot{\kappa}_3 \quad (92)$$

$$\begin{aligned} V_{36} \triangleq\ & \frac{\partial K_{\dot{s}_3\dot{\kappa}_3}}{\partial \kappa_3}\dot{\kappa}_3 - \frac{\partial K_{\dot{\kappa}_3\dot{\kappa}_3}}{\partial s_3}\dot{\kappa}_3 + \frac{\partial K_{\dot{s}_3\dot{s}_3}}{\partial \kappa_3}\dot{s}_3 + \frac{\partial K_{\dot{s}_3\dot{\kappa}_3}}{\partial s_1}\dot{s}_1 \\ & + \frac{\partial K_{\dot{s}_1\dot{s}_3}}{\partial \kappa_3}\dot{s}_1 - \frac{\partial K_{\dot{s}_1\dot{\kappa}_3}}{\partial s_3}\dot{s}_1 + \frac{\partial K_{\dot{s}_2\dot{s}_3}}{\partial \kappa_3}\dot{s}_2 - \frac{\partial K_{\dot{s}_2\dot{\kappa}_3}}{\partial s_3}\dot{s}_2 - \frac{\partial K_{\dot{\kappa}_1\dot{\kappa}_3}}{\partial s_3}\dot{\kappa}_1 \end{aligned} \quad (93)$$

$$V_{41} \triangleq \frac{\partial K_{\dot{s}_1\dot{\kappa}_1}}{\partial s_1}\dot{s}_1 - \frac{\partial K_{\dot{s}_1\dot{s}_1}}{\partial \kappa_1}\dot{s}_1 + \frac{\partial K_{\dot{\kappa}_1\dot{\kappa}_1}}{\partial s_1}\dot{\kappa}_1 + \frac{\partial K_{\dot{\kappa}_1\dot{\kappa}_3}}{\partial s_1}\dot{\kappa}_3 \quad (94)$$

$$V_{42} \triangleq \frac{\partial K_{\dot{s}_2\dot{\kappa}_1}}{\partial s_2}\dot{s}_2 + \frac{\partial K_{\dot{\kappa}_1\dot{\kappa}_1}}{\partial s_2}\dot{\kappa}_1 - \frac{\partial K_{\dot{s}_1\dot{s}_2}}{\partial \kappa_1}\dot{s}_1 + \frac{\partial K_{\dot{s}_1\dot{\kappa}_1}}{\partial s_2}\dot{s}_1 + \frac{\partial K_{\dot{s}_2\dot{\kappa}_1}}{\partial s_1}\dot{s}_1 + \frac{\partial K_{\dot{\kappa}_1\dot{\kappa}_2}}{\partial s_2}\dot{\kappa}_2 \quad (95)$$

$$\begin{aligned} V_{43} \triangleq\ & \frac{\partial K_{\dot{s}_3\dot{\kappa}_1}}{\partial s_3}\dot{s}_3 + \frac{\partial K_{\dot{\kappa}_1\dot{\kappa}_1}}{\partial s_3}\dot{\kappa}_1 - \frac{\partial K_{\dot{s}_1\dot{s}_3}}{\partial \kappa_1}\dot{s}_1 + \frac{\partial K_{\dot{s}_1\dot{\kappa}_1}}{\partial s_3}\dot{s}_1 \\ & + \frac{\partial K_{\dot{s}_2\dot{\kappa}_1}}{\partial s_3}\dot{s}_2 + \frac{\partial K_{\dot{s}_3\dot{\kappa}_1}}{\partial s_1}\dot{s}_1 + \frac{\partial K_{\dot{s}_3\dot{\kappa}_1}}{\partial s_2}\dot{s}_2 + \frac{\partial K_{\dot{\kappa}_1\dot{\kappa}_2}}{\partial s_3}\dot{\kappa}_2 \end{aligned} \quad (96)$$

$$V_{44} \triangleq \frac{\partial K_{\dot{\kappa}_1\dot{\kappa}_1}}{\partial s_1}\dot{s}_1 + \frac{\partial K_{\dot{\kappa}_1\dot{\kappa}_1}}{\partial s_2}\dot{s}_2 + \frac{\partial K_{\dot{\kappa}_1\dot{\kappa}_1}}{\partial s_3}\dot{s}_3 + \frac{\partial K_{\dot{\kappa}_1\dot{\kappa}_1}}{\partial \kappa_1}\dot{\kappa}_1 + \frac{\partial K_{\dot{\kappa}_1\dot{\kappa}_1}}{\partial \kappa_2}\dot{\kappa}_2 + \frac{\partial K_{\dot{\kappa}_1\dot{\kappa}_1}}{\partial \kappa_3}\dot{\kappa}_3 \quad (97)$$

$$V_{45} \triangleq \frac{\partial K_{\dot{\kappa}_1\dot{\kappa}_2}}{\partial \kappa_2}\dot{\kappa}_2 + \frac{\partial K_{\dot{\kappa}_1\dot{\kappa}_1}}{\partial \kappa_2}\dot{\kappa}_1 + \frac{\partial K_{\dot{\kappa}_1\dot{\kappa}_2}}{\partial \kappa_3}\dot{\kappa}_3 + \frac{\partial K_{\dot{\kappa}_1\dot{\kappa}_2}}{\partial s_1}\dot{s}_1 + \frac{\partial K_{\dot{s}_1\dot{\kappa}_1}}{\partial \kappa_2}\dot{s}_1 - \frac{\partial K_{\dot{s}_1\dot{\kappa}_2}}{\partial \kappa_1}\dot{s}_1 + \frac{\partial K_{\dot{s}_2\dot{\kappa}_1}}{\partial \kappa_2}\dot{s}_2 \quad (98)$$

$$\begin{aligned} V_{46} \triangleq\ & \frac{\partial K_{\dot{\kappa}_1\dot{\kappa}_3}}{\partial \kappa_3}\dot{\kappa}_3 + \frac{\partial K_{\dot{\kappa}_1\dot{\kappa}_1}}{\partial \kappa_3}\dot{\kappa}_1 + \frac{\partial K_{\dot{\kappa}_1\dot{\kappa}_3}}{\partial s_2}\dot{s}_2 + \frac{\partial K_{\dot{\kappa}_1\dot{\kappa}_3}}{\partial s_3}\dot{s}_3 \\ & + \frac{\partial K_{\dot{s}_1\dot{\kappa}_1}}{\partial \kappa_3}\dot{d}_1 - \frac{\partial K_{\dot{s}_1\dot{\kappa}_3}}{\partial \kappa_1}\dot{s}_1 + \frac{\partial K_{\dot{s}_2\dot{\kappa}_1}}{\partial \kappa_3}\dot{s}_2 + \frac{\partial K_{\dot{s}_3\dot{\kappa}_1}}{\partial \kappa_3}\dot{s}_3 \end{aligned} \quad (99)$$

$$V_{51} \triangleq \frac{\partial K_{\dot{s}_1\dot{\kappa}_2}}{\partial s_1}\dot{s}_1 + \frac{\partial K_{\dot{\kappa}_2\dot{\kappa}_2}}{\partial s_1}\dot{\kappa}_2 + \frac{\partial K_{\dot{\kappa}_1\dot{\kappa}_2}}{\partial s_1}\dot{\kappa}_1 + \frac{\partial K_{\dot{\kappa}_2\dot{\kappa}_3}}{\partial s_1}\dot{\kappa}_3 \quad (100)$$

$$V_{52} \triangleq \frac{\partial K_{\dot{s}_2\dot{\kappa}_2}}{\partial s_2}\dot{s}_2 - \frac{\partial K_{\dot{s}_2\dot{s}_2}}{\partial \kappa_2}\dot{s}_2 + \frac{\partial K_{\dot{\kappa}_2\dot{\kappa}_2}}{\partial s_2}\dot{\kappa}_2 - \frac{\partial K_{\dot{s}_1\dot{s}_2}}{\partial \kappa_2}\dot{s}_1 + \frac{\partial K_{\dot{s}_1\dot{\kappa}_2}}{\partial s_2}\dot{s}_1 + \frac{\partial K_{\dot{s}_2\dot{\kappa}_2}}{\partial s_1}\dot{s}_1 \quad (101)$$

$$V_{53} \triangleq \frac{\partial K_{\dot{s}_3\dot{\kappa}_2}}{\partial s_3}\dot{s}_3 + \frac{\partial K_{\dot{\kappa}_2\dot{\kappa}_2}}{\partial s_3}\dot{\kappa}_2 + \frac{\partial K_{\dot{s}_1\dot{\kappa}_2}}{\partial s_3}\dot{s}_1 - \frac{\partial K_{\dot{s}_2\dot{s}_3}}{\partial \kappa_2}\dot{s}_2 + \frac{\partial K_{\dot{s}_2\dot{\kappa}_2}}{\partial s_3}\dot{s}_2 + \frac{\partial K_{\dot{s}_3\dot{\kappa}_2}}{\partial s_1}\dot{s}_1 + \frac{\partial K_{\dot{s}_3\dot{\kappa}_2}}{\partial s_2}\dot{s}_2 + \frac{\partial K_{\dot{\kappa}_2\dot{\kappa}_3}}{\partial s_3}\dot{\kappa}_3 \tag{102}$$

$$V_{54} \triangleq \frac{\partial K_{\dot{\kappa}_1\dot{\kappa}_2}}{\partial \kappa_1}\dot{\kappa}_1 - \frac{\partial K_{\dot{\kappa}_1\dot{\kappa}_1}}{\partial \kappa_2}\dot{\kappa}_1 - \frac{\partial K_{\dot{s}_1\dot{\kappa}_1}}{\partial \kappa_2}\dot{s}_1 + \frac{\partial K_{\dot{s}_1\dot{\kappa}_2}}{\partial \kappa_1}\dot{s}_1 - \frac{\partial K_{\dot{s}_2\dot{\kappa}_1}}{\partial \kappa_2}\dot{s}_2 + \frac{\partial K_{\dot{\kappa}_1\dot{\kappa}_2}}{\partial s_2}\dot{s}_2 + \frac{\partial K_{\dot{\kappa}_1\dot{\kappa}_2}}{\partial s_3}\dot{s}_3 \tag{103}$$

$$V_{55} \triangleq \frac{\partial K_{\dot{\kappa}_2\dot{\kappa}_2}}{\partial s_1}\dot{s}_1 + \frac{\partial K_{\dot{\kappa}_2\dot{\kappa}_2}}{\partial s_2}\dot{s}_2 + \frac{\partial K_{\dot{\kappa}_2\dot{\kappa}_2}}{\partial s_3}\dot{s}_3 + \frac{\partial K_{\dot{\kappa}_2\dot{\kappa}_2}}{\partial \kappa_2}\dot{\kappa}_2 + \frac{\partial K_{\dot{\kappa}_2\dot{\kappa}_2}}{\partial \kappa_3}\dot{\kappa}_3 \tag{104}$$

$$V_{56} \triangleq \frac{\partial K_{\dot{\kappa}_2\dot{\kappa}_3}}{\partial \kappa_3}\dot{\kappa}_3 + \frac{\partial K_{\dot{\kappa}_2\dot{\kappa}_2}}{\partial \kappa_3}\dot{\kappa}_2 + \frac{\partial K_{\dot{\kappa}_1\dot{\kappa}_2}}{\partial \kappa_3}\dot{\kappa}_1 + \frac{\partial K_{\dot{\kappa}_2\dot{\kappa}_3}}{\partial s_2}\dot{s}_2 + \frac{\partial K_{\dot{s}_1\dot{\kappa}_2}}{\partial \kappa_3}\dot{d}_1 + \frac{\partial K_{\dot{s}_2\dot{\kappa}_2}}{\partial \kappa_3}\dot{s}_2 - \frac{\partial K_{\dot{s}_2\dot{\kappa}_3}}{\partial \kappa_2}\dot{s}_2 + \frac{\partial K_{\dot{s}_3\dot{\kappa}_2}}{\partial \kappa_3}\dot{s}_3 \tag{105}$$

$$V_{61} \triangleq \frac{\partial K_{\dot{s}_1\dot{\kappa}_3}}{\partial s_1}\dot{s}_1 + \frac{\partial K_{\dot{\kappa}_3\dot{\kappa}_3}}{\partial s_1}\dot{\kappa}_3 + \frac{\partial K_{\dot{s}_2\dot{\kappa}_3}}{\partial s_1}\dot{s}_2 + \frac{\partial K_{\dot{s}_3\dot{\kappa}_3}}{\partial s_1}\dot{s}_3 \tag{106}$$

$$V_{62} \triangleq \frac{\partial K_{\dot{s}_2\dot{\kappa}_3}}{\partial s_2}\dot{s}_2 + \frac{\partial K_{\dot{\kappa}_3\dot{\kappa}_3}}{\partial s_2}\dot{\kappa}_3 + \frac{\partial K_{\dot{s}_1\dot{\kappa}_3}}{\partial s_2}\dot{s}_1 + \frac{\partial K_{\dot{\kappa}_1\dot{\kappa}_3}}{\partial s_2}\dot{\kappa}_1 + \frac{\partial K_{\dot{\kappa}_2\dot{\kappa}_3}}{\partial s_2}\dot{\kappa}_2 \tag{107}$$

$$V_{63} \triangleq \frac{\partial K_{\dot{s}_3\dot{\kappa}_3}}{\partial s_3}\dot{s}_3 - \frac{\partial K_{\dot{s}_3\dot{s}_3}}{\partial \kappa_3}\dot{s}_3 + \frac{\partial K_{\dot{\kappa}_3\dot{\kappa}_3}}{\partial s_3}\dot{\kappa}_3 - \frac{\partial K_{\dot{s}_1\dot{s}_3}}{\partial \kappa_3}\dot{s}_1 + \frac{\partial K_{\dot{s}_1\dot{\kappa}_3}}{\partial s_3}\dot{s}_1 - \frac{\partial K_{\dot{s}_2\dot{s}_3}}{\partial \kappa_3}\dot{s}_2 + \frac{\partial K_{\dot{s}_2\dot{\kappa}_3}}{\partial s_3}\dot{s}_2 + \frac{\partial K_{\dot{s}_3\dot{\kappa}_3}}{\partial s_2}\dot{s}_2 + \frac{\partial K_{\dot{\kappa}_1\dot{\kappa}_3}}{\partial s_3}\dot{\kappa}_1 \tag{108}$$

$$V_{64} \triangleq \frac{\partial K_{\dot\kappa_1\dot\kappa_3}}{\partial \kappa_1}\dot\kappa_1 - \frac{\partial K_{\dot\kappa_1\dot\kappa_1}}{\partial \kappa_3}\dot\kappa_1 - \frac{\partial K_{\dot s_1\dot\kappa_1}}{\partial \kappa_3}\dot s_1 + \frac{\partial K_{\dot s_1\dot\kappa_3}}{\partial \kappa_1}\dot s_1 - \frac{\partial K_{\dot s_2\dot\kappa_1}}{\partial \kappa_3}\dot s_2 - \frac{\partial K_{\dot s_3\dot\kappa_1}}{\partial \kappa_3}\dot s_3 + \frac{\partial K_{\dot\kappa_1\dot\kappa_3}}{\partial s_1}\dot s_1 \tag{109}$$

$$\begin{aligned} V_{65} \triangleq\ & \frac{\partial K_{\dot\kappa_2\dot\kappa_3}}{\partial \kappa_2}\dot\kappa_2 - \frac{\partial K_{\dot\kappa_2\dot\kappa_2}}{\partial \kappa_3}\dot\kappa_2 - \frac{\partial K_{\dot\kappa_1\dot\kappa_2}}{\partial \kappa_3}\dot\kappa_1 - \frac{\partial K_{\dot s_1\dot\kappa_2}}{\partial \kappa_3}\dot s_1 \\ & - \frac{\partial K_{\dot s_2\dot\kappa_2}}{\partial \kappa_3}\dot d_2 + \frac{\partial K_{\dot s_2\dot\kappa_3}}{\partial \kappa_2}\dot s_2 - \frac{\partial K_{\dot s_3\dot\kappa_2}}{\partial \kappa_3}\dot s_3 + \frac{\partial K_{\dot\kappa_2\dot\kappa_3}}{\partial s_1}\dot s_1 + \frac{\partial K_{\dot\kappa_2\dot\kappa_3}}{\partial s_3}\dot s_3 \end{aligned} \tag{110}$$

$$V_{66} \triangleq \frac{\partial K_{\dot\kappa_3\dot\kappa_3}}{\partial s_1}\dot s_1 + \frac{\partial K_{\dot\kappa_3\dot\kappa_3}}{\partial s_2}\dot s_2 + \frac{\partial K_{\dot\kappa_3\dot\kappa_3}}{\partial s_3}\dot s_3 + \frac{\partial K_{\dot\kappa_3\dot\kappa_3}}{\partial \kappa_3}\dot\kappa_3. \tag{111}$$

D.3 Gravitational Terms

The entries of $G(q)$ are given as follows

$$
\begin{aligned}
G_1 \triangleq\ & \frac{mg}{d}\left\{\frac{1}{\kappa_1}\left[\cos\left(s_1\kappa_1\right)-\cos\left(2s_1\kappa_1\right)\right]\right. \\
& +\frac{1}{\kappa_2}\left[\cos\left(\left(s_1+s_2\right)\kappa_2\right)-\cos\left(2\left(s_1+s_2\right)\kappa_2\right)\right. \\
& \left.-\cos\left(s_1\kappa_2\right)+\cos\left(2s_1\kappa_2\right)\right] \\
& +\frac{1}{\kappa_3}\left[\cos\left(\left(s_1+s_2+s_3\right)\kappa_3\right)\right. \\
& \left.-\cos\left(2\left(s_1+s_2+s_3\right)\kappa_3\right)\right. \\
& \left.\left.-\cos\left(\left(s_1+s_2\right)\kappa_3\right)+\cos\left(2\left(s_1+s_2\right)\kappa_3\right)\right]\right\} \\
& -\frac{mg}{d^2}\left\{\frac{1}{\kappa_1^2}\left[\sin\left(s_1\kappa_1\right)-\frac{1}{2}\sin\left(2s_1\kappa_1\right)\right]\right. \\
& +\frac{1}{\kappa_2^2}\left[\sin\left(\left(s_1+s_2\right)\kappa_2\right)-\frac{1}{2}\sin\left(2\left(s_1+s_2\right)\kappa_2\right)\right. \\
& \left.-\sin\left(s_1\kappa_2\right)+\frac{1}{2}\sin\left(2s_1\kappa_2\right)\right] \\
& +\frac{1}{\kappa_3^2}\left[\sin\left(\left(s_1+s_2+s_3\right)\kappa_3\right)\right. \\
& -\frac{1}{2}\sin\left(2\left(s_1+s_2+s_3\right)\kappa_3\right) \\
& \left.\left.-\sin\left(\left(s_1+s_2\right)\kappa_3\right)+\frac{1}{2}\sin\left(2\left(s_1+s_2\right)\kappa_3\right)\right]\right\}
\end{aligned}
\tag{112}
$$

$$
\begin{aligned}
G_2 \triangleq\ & \frac{mg}{d}\left\{\frac{1}{\kappa_2}\left[\cos\left(\left(s_1+s_2\right)\kappa_2\right)\right.\right. \\
& -\cos\left(2\left(s_1+s_2\right)\kappa_2\right) \\
& +\frac{1}{\kappa_3}\left[\cos\left(\left(s_1+s_2+s_3\right)\kappa_3\right)\right. \\
& -\cos\left(2\left(s_1+s_2+s_3\right)\kappa_3\right) \\
& \left.\left.-\cos\left(\left(s_1+s_2\right)\kappa_3\right)+\cos\left(2\left(s_1+s_2\right)\kappa_3\right)\right]\right\} \\
& -\frac{mg}{d^2}\left\{\frac{1}{\kappa_1^2}\left[\sin\left(s_1\kappa_1\right)-\frac{1}{2}\sin\left(2s_1\kappa_1\right)\right]\right. \\
& +\frac{1}{\kappa_2^2}\left[\sin\left(\left(s_1+s_2\right)\kappa_2\right)-\frac{1}{2}\sin\left(2\left(s_1+s_2\right)\kappa_2\right)\right. \\
& \left.-\sin\left(s_1\kappa_2\right)+\frac{1}{2}\sin\left(2s_1\kappa_2\right)\right] \\
& +\frac{1}{\kappa_3^2}\left[\sin\left(\left(s_1+s_2+s_3\right)\kappa_3\right)\right. \\
& -\frac{1}{2}\sin\left(2\left(s_1+s_2+s_3\right)\kappa_3\right) \\
& \left.\left.-\sin\left(\left(s_1+s_2\right)\kappa_3\right)+\frac{1}{2}\sin\left(2\left(s_1+s_2\right)\kappa_3\right)\right]\right\}
\end{aligned}
\tag{113}
$$

$$
\begin{aligned}
G_3 \triangleq\ & \frac{mg}{d}\frac{1}{\kappa_3}\left[\cos\left(\left(s_1+s_2+s_3\right)\kappa_3\right)\right. \\
& \left.-\cos\left(2\left(s_1+s_2+s_3\right)\kappa_3\right)\right] \\
& -\frac{mg}{d^2}\left\{\frac{1}{\kappa_1^2}\left[\sin\left(s_1\kappa_1\right)-\frac{1}{2}\sin\left(2s_1\kappa_1\right)\right]\right. \\
& +\frac{1}{\kappa_2^2}\left[\sin\left(\left(s_1+s_2\right)\kappa_2\right)-\frac{1}{2}\sin\left(2\left(s_1+s_2\right)\kappa_2\right)\right. \\
& \left.-\sin\left(s_1\kappa_2\right)+\frac{1}{2}\sin\left(2s_1\kappa_2\right)\right] \\
& +\frac{1}{\kappa_3^2}\left[\sin\left(\left(s_1+s_2+s_3\right)\kappa_3\right)\right. \\
& -\frac{1}{2}\sin\left(2\left(s_1+s_2+s_3\right)\kappa_3\right) \\
& \left.\left.-\sin\left(\left(s_1+s_2\right)\kappa_3\right)+\frac{1}{2}\sin\left(2\left(s_1+s_2\right)\kappa_3\right)\right]\right\}
\end{aligned}
\tag{114}
$$

$$G_4 \triangleq -\frac{2mg}{d\kappa_1^3}\left[\sin(s_1\kappa_1) - \frac{1}{2}\sin(2s_1\kappa_1)\right] + \frac{mgs_1}{\kappa_1^2}\left[\cos(s_1\kappa_1) - \sin(2s_1\kappa_1)\right] \tag{115}$$

$$\begin{aligned} G_5 \triangleq & -\frac{2mg}{d\kappa_2^3}\left[\sin((s_1+s_2)\kappa_2) - \frac{1}{2}\sin(2(s_1+s_2)\kappa_2)\right. \\ & \left. -\sin(s_1\kappa_2) + \frac{1}{2}\sin(2s_1\kappa_2)\right] \\ & +\frac{mg}{d\kappa_2^2}\{(s_1+s_2)[\cos((s_1+s_2)\kappa_2) \\ & -\cos(2(s_1+s_2)\kappa_2)] \\ & -s_1[\cos(s_1\kappa_2) - \cos(2s_1\kappa_2)]\} \end{aligned} \tag{116}$$

$$\begin{aligned} G_6 \triangleq & -\frac{2mg}{d\kappa_3^3}[\sin((s_1+s_2+s_3)\kappa_3) \\ & -\frac{1}{2}\sin(2(s_1+s_2+s_3)\kappa_3) \\ & -\sin((s_1+s_2)\kappa_3) + \frac{1}{2}\sin(2(s_1+s_2)\kappa_3)\Big] \\ & +\frac{mg}{d\kappa_3^2}\{(s_1+s_2+s_3)[\cos((s_1+s_2+s_3)\kappa_3) \\ & -\cos(2(s_1+s_2+s_3)\kappa_3)] \\ & -(s_1+s_2)[\cos((s_1+s_2)\kappa_3) \\ & -\cos(2(s_1+s_2)\kappa_3)]\} \end{aligned} \tag{117}$$

D.4 Bending Terms

The entries of $B(q)$ are given as follows

$$\begin{aligned} B_1 &= \frac{1}{2}k_{b1}\left(\pi - \frac{1}{2}s_1\kappa_1\right)^2 \\ &\quad + \frac{1}{2}k_{b2}\left\{\left(\pi - \frac{1}{2}\left(s_1+s_2\right)\kappa_2\right)^2 \right. \\ &\quad \left. - \left(\pi - \frac{1}{2}s_1\kappa_2\right)^2\right\} \\ &\quad + \frac{1}{2}k_{b3}\left\{\left(\pi - \frac{1}{2}\left(s_1+s_2+s_3\right)\kappa_3\right)^2 \right. \\ &\quad \left. - \left(\pi - \frac{1}{2}\left(s_1+s_2\right)\kappa_3\right)^2\right\} \end{aligned} \tag{118}$$

$$\begin{aligned} B_2 &= \frac{1}{2}k_{b2}\left(\pi - \frac{1}{2}\left(s_1+s_2\right)\kappa_2\right)^2 \\ &\quad + \frac{1}{2}k_{b3}\left\{\left(\pi - \frac{1}{2}\left(s_1+s_2+s_3\right)\kappa_3\right)^2 \right. \\ &\quad \left. - \left(\pi - \frac{1}{2}\left(s_1+s_2\right)\kappa_3\right)^2\right\} \end{aligned} \tag{119}$$

$$B_3 = \frac{1}{2}k_{b3}\left(\pi - \frac{1}{2}\left(s_1+s_2+s_3\right)\kappa_3\right)^2 \tag{120}$$

$$B_4(t) = \frac{1}{2}k_{b1}\left[-\frac{1}{2}\pi s_1^2 + \frac{1}{6}\pi s_1^3\kappa_1\right] \tag{121}$$

$$B_5(t) = \frac{1}{2}k_{b2}\left\{\left[-\frac{1}{2}\pi(s_1+s_2)^2+\frac{1}{6}\pi(s_1+s_2)^3\kappa_2\right]-\left[-\frac{1}{2}\pi s_1^2+\frac{1}{6}\pi s_1^3\kappa_2\right]\right\} \quad (122)$$

$$B_6(t) = \frac{1}{2}k_{b3}\left\{\left[-\frac{1}{2}\pi(s_1+s_2+s_3)^2+\frac{1}{6}\pi(s_1+s_2+s_3)^3\kappa_3\right]-\left[-\frac{1}{2}\pi(s_1+s_2)^2+\frac{1}{6}\pi(s_1+s_2)^3\kappa_3\right]\right\} \quad (123)$$

D.5 Extension Terms

The entries of $E(q)$ are given as follows

$$E_1 = k_{e1}(s_1(t)-s_1^*) \quad (124)$$

$$E_2 = k_{e2}(s_2(t)-s_2^*) \quad (125)$$

$$E_3 = k_{e3}(s_3(t)-s_3^*) \quad (126)$$

$$E_4 = 0,\ E_5 = 0,\ E_6 = 0 \quad (127)$$

Bibliography

[1] G. Robinson and J. Davies, "Continuum robots - a state of the art," in *Proc. IEEE Int. Conf. Robot. Autom.*, Detroit, MI, 1999, pp. 2849–2854.

[2] D. Trivedi, C. Rahn, W. Kier, and I. Walker, "Soft robotics: Biological inspiration, state of the art, and future research," *Applied Bionics and Biomechanics*, vol. 5, no. 2, pp. 99–117, Jun. 2008.

[3] R. Webster III and B. A. Jones, "Design and modeling of constant curvature continuum robots," *Int. Jour. Robots. Res.*, vol. 29, no. 13, pp. 1661–1683, Jul. 2010.

[4] M. Grissom, V. Chitrakaran, D. Dienno, M. Csencsits, M. Pritts, B. Jones, W. McMahan, D. Dawson, C. Rahn, and I. Walker, "Design and experimental testing of the octarm soft robot manipulator," in *Proc. SPIE Conf. Unmanned Sys. Tech.*, Kissimee, FL, 2006, pp. 109–114.

[5] I. Walker, D. Dawson, T. Flash, F. Grasso, R. Hanlon, B. Hochner, W. Kier, C. Pagano, C. Rahn, and Q. Zhang, "Continuum robot arms inspired by cephalopods," in *Proc. SPIE Conf. Unmanned Ground Veh. Tech.*, Orlando, FL, 2005, pp. 303–314.

[6] W. McMahan, B. Jones, and I. Walker, "Robotic manipulators inspired by cephalopod limbs," *Jour. Eng. Des. Inno.*, vol. 1, no. P, p. 01P2, Jun. 2005.

[7] M. Calisti, A. Arienti, F. Renda, G. Levi, B. Hochner, B. Mazzolai, P. Dario, and C. Laschi, "Design and development of a soft robot with crawling and grasping capabilities," in *Proc. IEEE Int. Conf. Robot. Autom.*, St. Paul, MN, 2012, pp. 4950–4955.

[8] I. Godage, T. Nanayakara, and D. Caldwell, "Locomotion with continuous limbs," in *Proc. IEEE/RSJ Int. Conf. Intel. Robot. Syst.*, Vilamoura, Portugal, 2012, pp. 293–298.

[9] R. Buckingham and A. Graham, "Snaking around a nuclear jungle," *Ind. Robot: An Int. Jour.*, vol. 32, no. 2, pp. 120–127, Feb. 2005.

[10] Y.-J. Kim, S. Cheng, S. Kim, and K. Iagnemma, "Design of a tubular snake-like manipulator with stiffening capability by layer jamming," in *Proc. IEEE/RSJ Int. Conf. Intel. Robot. Syst.*, Vilamoura, Portugal, 2012, pp. 4251–4256.

[11] H. Ohno and S. Hirose, "Design of a slim slime robot and its gait of locomotion," in *Proc. IEEE/RSJ Int. Conf. Intel. Robot. Syst.*, Maui, HI, 2001, pp. 707–715.

[12] S. Hirose, *Biologically Inspired Robots*. Oxford, UK: Oxford University Press, 1993.

[13] G. Immega and K. Antonelli, "The ksi tentacle manipulator," in *Proc. IEEE Int. Conf. Robot. Autom.*, Nagoya, Japan, 1995, pp. 3149–3154.

[14] D. Camarillo, C. Milne, C. Carlson, M. Zinn, and J. Salisbury, "Mechanics modeling of tendon-driven continuum manipulators," *IEEE Trans. Robot.*, vol. 24, no. 6, pp. 1262–1273, Dec. 2008.

[15] L. Torres, R. Webster III, and R. Alterovitz, "Task-oriented design of concentric tube robots using mechanics-based models," in *Proc. IEEE/RSJ Int. Conf. Intel. Robot. Syst.*, Vilamoura, Portugal, 2012, pp. 4449–4455.

[16] L. Lyons, R. Webster III, and R. Alterovitz, "Planning active cannula configurations through tubular anatomy," in *Proc. IEEE Int. Conf. Robot. Autom.*, Anchorage, AK, 2010, pp. 2082–2087.

[17] E. Butler, R. Hammond-Oakley, S. Chawarski, A. Gosline, P. Codd, T. Anor, J. Madsen, P. Dupont, and J. Lock, "Robotic neuro-endoscope with concentric tube augmentation," in *Proc. IEEE/RSJ Int. Conf. Intel. Robot. Syst.*, Vilamoura, Portugal, 2012, pp. 2941–2946.

[18] J. Ding, K. Xu, R. Goldman, P. Allen, D. Fowler, and N. Simaan, "Design, simulation and evaluation of kinematic alternaties for insertable robotic effectors platforms in single port access surgery," in *Proc. IEEE Int. Conf. Robot. Autom.*, Anchorage, AK, 2010, pp. 1053–1058.

[19] E. Ayvali and J. Desai, "Towards a discretely actuated steering cannula," in *Proc. IEEE Int. Conf. Robot. Autom.*, St. Paul, MN, 2012, pp. 1614–1619.

[20] N. Simaan, R. Taylor, and P. Flint, "A dextrous system for laryngeal surgery," in *Proc. IEEE Int. Conf. Robot. Autom.*, New Orleans, LA, 2004, pp. 351–357.

[21] R. Penning, J. Jung, J. Borgstadt, N. Ferrier, and M. Zinn, "Towards closed loop control of a continuum robotic manipulator for medical applications," in *Proc. IEEE Int. Conf. Robot. Autom.*, Shanghai, China, 2011, pp. 4822–4827.

[22] D. Lane, B. Davies, G. Robinson, D. O'Brien, J. Sneddon, E. Seaton, and A. Elfstrom, "Aspects of the design and development of a subsea dextrous grasping system," *IEEE Jour. Ocean. Eng.*, vol. 24, no. 1, pp. 96–111, Jan. 1999.

[23] K. Suzimori, S. Iikura, and H. Tanaka, "Development of a flexible microactuator and its applications to robotic mechanisms," in *Proc. IEEE Int. Conf. Robot. Autom.*, Sacramento, CA, 1991, pp. 1622–1627.

[24] J. Bishop-Moser, G. Krishnan, C. Kim, and S. Kota, "Design of soft robotic actuators using fluid-filled fiber-reinforced elastomeric enclosures in parallel combinations," in *Proc. IEEE/RSJ Int. Conf. Intel. Robot. Syst.*, Vilamoura, Portugal, 2012, pp. 4262–4269.

[25] A. Bajo and N. Simaan, "Finding lost wrenches: Using continuum robots for contact detection and estimation of contact location," in *Proc. IEEE Int. Conf. Robot. Autom.*, Anchorage, AK, 2010, pp. 3666–3672.

[26] M. Mahvash and P. Dupont, "Stiffness control of a continuum manipulator in contact with a soft environment," in *Proc. IEEE/RSJ Int. Conf. Intel. Robot. Syst.*, Taipei, Taiwan, 2010, pp. 863–870.

[27] J. Xiao and R. Vatcha, "Real-time adaptice motion planning for a continuum manipulator," in *Proc. IEEE/RSJ Int. Conf. Intel. Robot. Syst.*, Taipei, Taiwan, 2010, pp. 5919–5926.

[28] G. Chirikjian and J. Burdick, "A modal approach to hyper-redundant manipulator kinematics," *IEEE Trans. Robot. Autom.*, vol. 10, no. 3, pp. 343–354, Jun. 1994.

[29] G. Chen, M. Pham, and T. Redarce, "Development and kinematic analysis of a silicon rubber bending tip for colonoscopy," in *Proc. IEEE/RSJ Int. Conf. Intel. Robot. Syst.*, Beijing, China, 2006, pp. 168–173.

[30] B. Jones and I. Walker, "Kinematics of multisection continuum robots," *IEEE Trans. Robot.*, vol. 22, no. 1, pp. 43–57, Feb. 2006.

[31] M. Hannan and I. Walker, "Kinematics and the implementation of an elephant trunk manipulator and other continuum style robots," *J. Robot. Sys.*, vol. 20, no. 2, pp. 45–63, Feb. 2003.

[32] B. Jones and I. Walker, "Practical kinematics for real-time implementation of continuum robots," *IEEE Trans. Robot.*, vol. 22, no. 6, pp. 1087–1099, Dec. 2006.

[33] I. Gravagne and I. Walker, "Kinematics for constrained continuum robots using wavelet decomposition," in *Proc. Conf. and Expo. Robot. for Challenging Situ. and Environ.*, Alburquerque, NM, 2000, pp. 33–38.

[34] ——, "Kinematic transformations for remotely-actuated planar continuum robots," in *Proc. IEEE Int. Conf. Robot. Autom.*, San Francisco, CA, 2000, pp. 19–26.

[35] G. Chirikjian, "Hyper-redundant manipulator dynamics: A continuum approximation," *Adv. Robot.*, vol. 9, no. 3, pp. 217–243, Jun. 1995.

[36] G. Gallot, O. Ibrahimand, and W. Khalil, "Dynamic modeling and simulation of a 3-d eel-like robot," in *Proc. IEEE Int. Conf. Robot. Autom.*, Rome, Italy, 2007, pp. 1486–1491.

[37] G. Gallot, O. Ibrahim, and W. Khalil, "Dynamic modeling and simulation of a 3-d eel-like robot," in *Proc. IEEE Int. Conf. Robot. Autom.*, Rome, Italy, 2007, pp. 1486–1491.

[38] F. Matsuno and H. Sato, "Trajectory tracking of snake robots based on dynamic model," in *Proc. IEEE Int. Conf. Robot. Autom.*, Barcelona, Spain, 2005, pp. 3040–3045.

[39] N. Li, T. Zhao, and Y. Zhao, *The Dynamic Modeling of Snake-Like Robot Using Nominal Mechanism Method/ Intel. Robot. and Appl.* Berlin-Heidelberg, Germany: Springer-Verlag, 2008.

[40] H. Mochiyama and T. Suzuki, "Kinematics and dynamics of a cable-like hyper-flexible manipulator," in *Proc. IEEE Int. Conf. Robot. Autom.*, Taipei, Taiwan, 2003, pp. 3672–3677.

[41] E. Tatlicioglu, I. Walker, and D. Dawson, "Dynamic modeling for planar extensible continuum robot manipulators," *Int. Jour. Robot. Autom.*, vol. 24, no. 4, pp. 1087–1099, Apr. 2009.

[42] ——, "New dynamic models for planar extensible continuum robot manipulators," in *Proc. IEEE/RSJ Int. Conf. Intel. Robot. Syst.*, San Diego, CA, 2007, pp. 1485–1490.

[43] M. Ivanescu, N. Popescu, and D. Popescu, "A variable length tentacle manipulator control system," in *Proc. IEEE Int. Conf. Robot. Autom.*, Barcelona, Spain, 2005, pp. 3274–3279.

[44] M. Ivanescu and V. Stoian, "A variable structure controller for a tentacle manipulator," in *Proc. IEEE Int. Conf. Robot. Autom.*, Nagoya, Japan, 1995, pp. 3155–3160.

[45] ——, "A controller for hyper-redundant cooperative robots," in *Proc. IEEE/RSJ Int. Conf. Intel. Robot. Syst.*, Vancouver, Canada, 1998, pp. 167–172.

[46] D. Braganza, D. Dawson, I. Walker, and N. Nath, "A neural network controller for continuum robots," *IEEE Trans. Robot.*, vol. 23, no. 6, pp. 1270–1277, Dec. 2006.

[47] R. Penning, J. Jung, N. Ferrier, and M. Zinn, "An evaluation of closed-loop control options for continuum manipulators," in *Proc. IEEE Int. Conf. Robot. Autom.*, St. Paul, MN, 2012, pp. 5392–5397.

[48] J. Burdick, "On the inverse kinematics of redundant manipulators," in *Proc. IEEE Int. Conf. Robot. Autom.*, Scottsdale, AZ, 1989, pp. 264–270.

[49] T. B. Sheridan, *Telerobotics, Automation, and Human Supervisory Control*. Cambridge, MA, USA: MIT Press, 1992.

[50] P. F. Hokayem and M. W. Spong, "Bilateral teleoperation: An historical survey," *Automatica*, vol. 42, no. 12, pp. 2035–2057, 2006.

[51] K. Kim, W. K. Chung, and I. H. Suh, "Accurate force reflection for kinematically dissimilar bilateral teleoperation systems using instantaneous restriction space," in *Proc. IEEE Int. Conf. Robot. Autom.*, Orlando, FL, 2006, pp. 3257–3262.

[52] J. Herndon, W. Hamel, and D. Kuban, "Traction-drive telerobot for space manipulation," in *Proc. IEEE Int. Conf. Robot. Autom.*, Raleigh, NC, 1987, pp. 450–455.

[53] C. C. Nguyen, Z.-L. Zhou, and G. E. Mosier, "Joint-space adaptive control of a redundant telerobot manipulator," in *Proc. of Int. Symp. on Intel. Cont.*, Albany, NY, 1989, pp. 59–65.

[54] J. F. Jansen, R. L. Kress, S. M. Babcock, and W. R. Hamel, "Stiffness control of teleoperators with redundant, dissimilar kinematics," in *Proc. of Int. Conf. on System Engineering*, Pittsburgh, PA, 1990, pp. 97–100.

[55] J. F. Jansen and R. L. Kress, "Control of a teleoperator system with redundancy based on passivity condition," in *Proc. IEEE Int. Conf. Robot. Autom.*, Sacramento, CA, 1991, pp. 478–484.

[56] D.-Y. Hwang and B. Hannaford, "Teleoperation performance with a kinematically redundant slave robot," *Int. J. Robot. Res.*, vol. 17, no. 6, pp. 579–597, 1998.

[57] D. P. T. Nanayakkara, K. Kiguchi, T. Murakami, K. Watanabe, and K. Izumi, "Skillful adaptation of a 7-dof manipulator to avoid moving obstacles in a teleoperated force control task," in *Proc. of IEEE Int. Symposium on Indust. Electronics*, Pusan, Korea, 2001, pp. 1982–1987.

[58] M. Goel, A. A. Maciejewski, V. Balakrishnan, and R. W. Proctor, "Failure tolerant teleoperation of a kinematically redundant manipulator: An experimental study," *IEEE Trans. Sys. Man Cyber.*, vol. 33, no. 6, pp. 758–765, 2003.

[59] B. Stanczyk and M. Buss, "Development of a telerobotic system for exploration of hazardous environments," in *Proc. IEEE/RSJ Int. Conf. Intel. Robot. Syst.*, Sendai, Japan, 2004, pp. 2532–2537.

[60] M. Ueberle, N. Mock, and M. Buss, "Vishard10, a novel hyper-redundant haptic interface," in *Proc. IEEE Symp. Haptic Interf. for Virt. Envir. & Teleop. Sys.*, Chicago, IL, 2004, pp. 58–65.

[61] A. Peer, B. Stanczyk, and M. Buss, "Haptic telemanipulation with dissimilar kinematics," in *Proc. IEEE/RSJ Int. Conf. Intel. Robot. Syst.*, Alberta, Canada, 2005, pp. 3493–3498.

[62] Y. Komoguchi, A. Peer, and M. Buss, "Control and performance evaluation of a new redundant haptic interface," in *Proc. of the SICE Ann. Conf.*, Kagawa, Japan, 2007, pp. 2671–2676.

[63] M. Hayakawa, K. Hara, D. Sato, A. Konno, and M. Uchiyama, "Singularity avoidance by inputting angular velocity to a redundant axis during cooperative control of a teleoperated dual-arm robot," in *Proc. IEEE Int. Conf. Robot. Autom.*, Pasadena, CA, 2008, pp. 2013–2018.

[64] F. Gosselin, C. Andriot, F. Bergez, and X. Merlhiot, "Widening 6-dof haptic devices workspace with an additional degree of freedom," in *Proc. 2nd Joint EuroHaptics Conf. and Symp. Haptic Interf. for Virt. Env. & Teleop. Sys.*, Tsukuba, Japan, 2007, pp. 452–457.

[65] N. Nath, E. Tatlicioglu, and D. M. Dawson, "Teleoperation with kinematically redundant robot manipulators with sub-task objectives," in *Proc. IEEE Int. Conf. Decision and Control*, Cancun, Mexico, 2008, pp. 4320–4325.

[66] H. Das, T. B. Sheridan, and J.-J. E. Slotine, "Kinematic control and visual display of redundant teleoperators," in *Proc. of Int. Conf. on Systems, Man and Cybernetics*, Cambridge, MA, 1989, pp. 1072–1077.

[67] I. Walker, C. Carreras, R. McDonnell, and G. Grimes, "Extension versus bending for continuum robots," *Int. Jour. Adv. Robot. Sys.*, vol. 3, no. 2, pp. 171–178, Jun. 2006.

[68] A. Kapadia and I. Walker, "Self-motion analysis of extensible continuum manipulators," in *Proc. IEEE Int. Conf. Robot. Autom.*, Karlsruhe, Germany, 2013, pp. 3105–3110.

[69] D. Whitney, "Resolved motion rate control of manipulators and human prostheses," *IEEE Trans. Man. Mach. Sys.*, vol. 10, no. 2, pp. 47–53, Jun. 1969.

[70] P. Hsu, J. Hauser, and S. Sastry, "Dynamic control of redundant manipulators," *J. Robot. Sys.*, vol. 6, no. 2, pp. 133–148, 1989.

[71] E. Tatlicioglu, *Control of Nonlinear Mechatronic Systems*. Germany: VDM Verlag Dr. Mueller e.K., 2008.

[72] W. McMahan, B. Jones, and I. Walker, "Design and implementation of a multi-section continuum robot: Airoctor," in *Proc. IEEE/RSJ Int. Conf. Intel. Robot. Syst.*, Edmonton, Canada, 2005, pp. 3345–3352.

[73] A. Grzesiak, R. Becker, and A. Verl, "A bionic handling assistant - a success story of additive manufacturing," *Assembly Automation*, vol. 31, no. 4, pp. 329–333, Sep. 2011.

[74] F. L. Lewis, D. M. Dawson, and C. T. Abdallah, *Robot Manipulator Control: Theory and Practice*. New York, NY: Marcel Dekker, 2004.

[75] V. Klema and A. Laub, "The singular value decomposition: Its computation and some applications," *IEEE Trans. Autom. Cont.*, vol. 25, no. 2, pp. 164–176, Apr. 1980.

[76] M. W. Spong, S. Hutchinson, and M. Vidyasagar, *Robot Dynamics and Control*. New York, NY: John Wiley and Sons, 2005.

[77] L. Sciavicco and B. Sicilano, *Modeling and Control of Robot Manipulators*. New York, NY, USA: McGraw-Hill Co., 1996.

[78] Y. Nakamura, *Advanced Robot Redundancy and Optimization*. Reading, MA: Addison-Wesley, 1991.